Ninni Maria Unneberg

The effect of metal type in ion exchanged SAPO-34 for the direct conversion of methane to methanol

Master's thesis in MLREAL
Supervisor: Karina Mathisen
Co-supervisor: Daniel Ali and Muhammad Mohsin Azim
December 2022

Master's thesis

NTNU
Norwegian University of Science and Technology
Faculty of Natural Sciences
Department of Chemistry

NTNU
Norwegian University of
Science and Technology

Ninni Maria Unneberg

The effect of metal type in ion exchanged SAPO-34 for the direct conversion of methane to methanol

Master's thesis in MLREAL
Supervisor: Karina Mathisen
Co-supervisor: Daniel Ali and Muhammad Mohsin Azim
December 2022

Norwegian University of Science and Technology
Faculty of Natural Sciences
Department of Chemistry

NTNU
Norwegian University of
Science and Technology

The effect of metal type in ion exchanged SAPO-34 for the direct conversion of methane to methanol

Ninni Maria Unneberg
Supervisor: Karina Mathisen
Co-supervisor: Daniel Ali and Muhammad Mohsin Azim
December 2022

NTNU

Kunnskap for en bedre verden

Department of Chemistry
Faculty of Natural Sciences
Norwegian University of Science and Technology

Acknowledgements

Abstract

In this thesis, the main objective was: to functionalise the chabazite (CHA) zeo-type SAPO-34 by conventionally ion exchanging Cu, Zn, Fe, Ag and Co into the framework; investigate the effect of the ion exchange and evaluating the catalytic performance of the Me/SAPO-34 samples for the direct conversion of methane to methanol (dMtM).

The dMtM has attracted worldwide attention in the last decade and gained traction as a viable alternative pathway to the energy-intensive syngas route for conversion of methane into value-added chemicals. The metals Cu, Zn, Fe, Ag and Co that were ion exchanged by liquid ion exchange (LIE) into SAPO-34, have all been previously reported to be active for methane activation on other supports. However, despite the fact that SAPO-34 has been proposed as a promising support for the conversion, the literature on Me/SAPO-34 is scarce. Indeed, this is to the best of the authors knowledge the first report of catalytic tests of Zn/SAPO-34 and Ag/SAPO-34 for the dMtM, as only Cu- and Co-exchanged SAPO-34 have previously been reported.

Herein, the Me/SAPO-34 samples were characterised by XRD, nitrogen physisorption, ICP-MS and SEM. The materials were found to be successfully ion exchanged with Cu, Zn, Ag and Co with metal loadings ranging from 0.1-5.1 wt.%. In general, the ion exchange reduced the crystallinity, surface area and pore volume of all investigated samples. Higher metal loading appear to be a factor for the decrease, though not conclusive as the trend is not clear for all samples.

Catalytic performance tests showed that Me/SAPO-34 (Me = Cu, Zn, Ag, Co) were all active for the dMtM, revealing that it is possible to convert methane to methanol over oxygen activated metal sites in SAPO-34 in a stepwise process. The Cu containing SAPO-34 sample exhibited the highest methanol yield as expected. However, the 0.1 wt.% Co sample exhibited significantly (50 times) higher methanol yield per metal content than all other investigated samples.

Sammendrag på norsk

Formålet med denne masteroppgaven var å funksjonalisere chabazitt (CHA) zeo-typen SAPO-34 ved konvensjonell ionebytting med Cu, Zn, Fe, Ag og Co, undersøke effekten av ionebyttingen og evaluere Me/SAPO-34-prøvene for partiell oksidasjon av metan til metanol.

Den direkte konverteringen av metan til metanol (dMtM) har det siste tiåret tiltrukket oppmerksomhet som en alternativ rute for konvertering av metan til høyverdige kjemikalier i stedet for den energikrevene ruten gjennom dampreformering. Metal-lene Cu, Zn, Fe, Ag og Co ble konvensjonelt ionebyttet inn i strukturen til SAPO-34. Alle metallene har tidligere blitt rapportert som aktive katalysatorer for metanak-tivering i andre bærematerialer. Til tross for at SAPO-34 har blitt pekt på som et lovende bæremateriale for metankonvertering, er det lite publisert forskning på Me/SAPO-34 for denne reaksjonen. I denne oppgaven rapportes, så langt forfat-teren kjenner til, den første katalytiske testen av Zn/SAPO-34 og Ag/SAPO-34 for dMtM, ettersom bare Cu- og Co-ionebyttet SAPO-34 har blitt rapportert tidligere.

Me/SAPO-34-prøvene ble karakterisert med XRD, nitrogenfysisorpsjon, ICP-MS og SEM. Materialene ble funnet til å være ionebyttet med Cu, Zn, Ag og Co med metallinnhold som varierte fra 0,1 til 5,1 vekt%. Generelt reduserte ionebyttingen krystalliniteten, overflatearealet og porevolumet til alle undersøkte prøver. Høyere metallinnhold ser ut til å være en faktor for reduksjonene, men ikke alle resultater underbygger teorien.

Katalytiske ytelsestester viste at Me/SAPO-34 (Me = Cu, Zn, Ag, Co) alle var aktive for dMtM, og viste at det er mulig å konvertere metan til metanol over oksygenaktiverte metallseter i SAPO-34 i en trinnvis prosess. Cu-prøven viste aller høyest metanolproduksjon, tett fulgt av Zn. Metanolproduksjon per metallinnhold viste imidlertid at Co-prøven med kun 0,1 vekt% Co viste nesten 50 ganger høyere metanolproduksjon enn alle andre undersøkte prøver. Imidlertid viste Ag-prøven lav produksjon av metanol per metallsete, og er muligens ikke like godt egnet for dMtM i SAPO-34 som de andre undersøkte metallene.

Contents

Abbreviations

Ac	Acetate
A.U.	Arbitrary units
BAS	Brønsted Acid site
BET	Brunauer-Emmet-Teller method
BJH	Barrett-Joyner-Halanda analysis
CHA	Chabazite
CIE	Conventional ion exchange
CCAC	Climate and Clean Air Coalition
CLRTAP	Convention on Long-Range Transboundary Air Pollution
CO	Carbon monoxide
CO_2	Carbon dioxide
DME	Dimethyl Ether
dMtM	Direct methane to methanol conversion
GHG	Green house gas
GWP	Global warming potential
HOMO	Highest occupied molecular orbital
HTP	Heat trap potential
ICP-MS	Inductively coupled plasma - mass spectroscopy
IE	Ion exchange
IPCC	Intergovernmental Panel on Climate Change
IUPAC	Internatiol Union of Applied Chemistry
IZA	International Zeolite Association

LIE   Liquid ion exchange

LUMO   Lowest unoccupied molecular orbital

Me/SAPO-34   Metal ion exchanged SAPO-34

MFC   Mass Flow Controller

MMO   Methane monooxygenase

MO   Molecular orbital

MTO   Metanol to olefins

m/z   Mass to charge-ratio

NA   Not applicable

NTNU   Norwegian University of Science and Technology

RC   Relative crystallinity

SAPO   Silicoaluminophosphate

SCR   Selective catalytic reduction

SEM   Scanning electron microscopy

UNEP   UN Environment Programme

UNFCCC   United Nations Framework Convention on Climate Change

wt%   Weight percent

XRD   X-ray diffraction

ZRF   Zero routine flaring

Å   Ångstrøm

4MR   Four-membered ring

6MR   Six-membered ring

8MR   Eight-membered ring

1 Introduction

Methane is the second most abundant antrophogenic green house gas (GHG), with a global warming potential (GWP) of 86 over a 20 year period.[1–4] However, methane is still an important raw material for chemicals and a valuable energy source as the cleanest of the fossil fuels.[5] The recent methane leak, deemed one of the largest single releases of methane ever recorded by the United Nations Environment Programme (UNEP), caused by massive underwater blasts in september 2022 on the Nord Stream gas pipelines in the Baltic Sea, highlights the importance of the the gas.[6,7] Of particular concern is the fact that the concentration of atmospheric methane, which has remained stable for thousands of years, has reached a record high and has increased by more than 50 million tonnes the last decade due to human activity.[1,4] In fact, 60% of all global methane emissions come from antrophogenic sources, and methane alone is contributing with more than 25 per cent of the warming effect we are experiencing today.[1,8]

Global warming is rightly recognized by the environmental community as one of the greatest threats to the planet as to this day.[1] The Intergovernmental Panel on Climate Change (IPCC) has deemed a temperature increase of more than $1.5°C$ to lead to catastrophic climate changes, and warns that the current trajectory of anthrophogenic methane emissions is estimated to cause a temperature increase of more than $3°C$ before 2100.[9] In fact, the 1.5-target of the Paris Agreement cannot be achieved without reducing methane emissions by 40-45% by 2030.[4,8,9] As a consequence, stricter and stricter demands for reducing the global methane levels are put in to effect, and are absolutely necessary.[1,2,4,8–13]

A preferable solution for methane mitigation would be converting methane into value-added chemicals such as methanol, formaldehyde or aromatics.[10,14–16] The recent years the direct conversion of methane to methanol (dMtM) has gained traction as a viable recycling path for methane. Methanol is a simple organic liquid containing a high volumetric energy density, about twice that of hydrogen, which can be used as a renewable fuel source in fuel cell technology.[10] Today, most methanol production goes via the indirect route which requires the energy-intensive steam reforming step. Direct routes can potentially overcome this energy disadvantage, and is therefore a research field of the utmost worldwide interest.[14]

Possible processes for the dMtM direct are conventional catalytic processes, photo-catalysts, plasma technology, membrane technology, biological processes and super-critical water techniques.[10,12,14,17] One process that has gained scientific interest is the heterogeneous catalytic process of metal introduced zeotypes as systems mimicking methanotrophic bacteria which are able to convert methane to methanol under ambient conditions.[10,18–22] From existing research, it is clear that this process is not only plausible, but a possible breakthrough in the scientific field.[19,23–30] However, there are still unresolved issues to overcome such as over-oxidation, cleaving the strong C-H bond in methane without the use of extreme temperatures and rare noble metals.[22] Nonetheless, these processes have shown high selectivity towards methanol, which as mentioned, is a more efficiently transported and stored clean alternative fuel source, and has been described as a so called dream reaction.[10,31]

1.1 Scope of project

Accordingly, metal containing zeotypes or zeolites have emerged as a promising catalyst for the direct conversion of methane to methanol (dMtM) due to their ability to host active metal sites, and several groups are dedicated to develop this heterogeneous process.[18–20,22–28,30,32] Vora et al. have pinpointed SAPO-34 as the best option in regard to methane activation.[33] SAPO-34 is a silicoaluminophosphate (SAPO) zeotype with a chabazite (CHA) framwork, and has high techological interest as it is applied as a commercial catalyst for the methanol to olefins (MTO) reaction and also performs well for the selective catalytic reduction (SCR) of NOx-gases when loaded with copper.[19,34–36] Further, its analogous CHA-zeolite, SSZ-13, have been proven to work very well for the dMtM when introduced with metals.[37–39]

Yet, there are apparently few instances in literature where other metals than cobalt and copper introduced SAPO-34 have been catalytically tested for methane activation.[19,25] In recent years, the focus have been on investigating how the composition and structure of the metal containing zeotype or zeolite influence the reaction. Although the number on papers published on the selective oxidation of methane is increasing every year, the literature on SAPO-34 for the dMtM is particularly scarce.

In addition, Cu, Zn, Fe, Ag and Co have all been proven to activate methane, and therefore, various studies on metal ion exchanged SAPO-34 was conducted and their performance towards the selective partial oxidation of methane to methanol (Equation 1.1) in a stepwise process, using oxygen as oxidant, was evaluated.

$$CH_4 + \frac{1}{2}O_2 \rightleftharpoons CH_3OH \tag{1.1}$$

In this project, Me/SAPO-34 samples have been prepared by conventional ion exchange (CIE) into SAPO-34, and a relative catalytic study have been conducted to test their performance for methane activation. Moreover, this thesis reports, to the best of the authors knowledge, the first tests of Ag/SAPO-34 and Zn/SAPO-34 for the partial oxidation of methane to methanol.

2 Theory

In this chapter, relevant theory to the project will be presented. Firstly, the characteristics of the material SAPO-34, which has been investigated as a catalyst support, and the metal addition of active metal ions into SAPO-34 by ion exchange will be elaborated. Secondly, the characterization techniques utilised in the thesis will be accounted for. Lastly, the chemical background for the stepwise oxidation of methane to methanol, the reaction for which the performance of the Me/SAPO-34 samples will be tested, will be explained and a brief history of what has been done within this field of research will be presented.

2.1 SAPO-34 as catalyst support for metal ions

2.1.1 Zeotypes and zeolites

In general, zeotypes and zeolites have widespread applications and has been extensively used as catalysts, ion-exchangers, sorbents and molecular sieves in industry.[40,41] The significance of zeolites and zeotypes can be reflected through the annual production of more than 3000 kilotons and the fact that the global market for synthetic zeolitic materials reached 33.8 billions dollars in 2022.[42] In this subsection, the properties of zeotypes and zeolites will be accounted for.

A zeotype is an inorganic microporous crystalline material with uniform pores and cages, with a structure analogous to that of a zeolite.[5,41] While a zeolite is exclusively built up of silica (SiO_4) and alumina (AlO_4) tetrahedra, the T atoms in the TO_4-tetrahedra of a zeotype can consist of different tetrahedral framework cations, for example P, Ti, Ga, Ge and B.[5,40,41] The tetrahedra make up the primary building units, and can form secondary building blocks, such as squares, 8-rings and 6-rings, when arranged together.[5] The periodic zeolite or zeotype framework is a result of how the secondary building blocks assemble together, and are categorized into small-pore (8 tetrahedra), medium-pore (10 tetrahedra) or large-pore (12 tetrahedra) based on how many tetrahedra that make up the pore system of the framework.[43–45] Each distinct framework has been assigned a three letter code by the Structure Commission of the International Zeolite Association (IZA), and have characteristic properties.[34,46] Each framework is categorized by their dimensionality based on how many pore channels that are larger than a 6-ring. For example a two-dimensional framework has two sets of pore channels made up by secondary building block rings of more than 6 tetrahedra.[34,43]

An important group of zeotypes is silicoaluminophosphates (SAPOs) where the T atoms consist of Si, Al and P.[5,40,41] The general chemical structure of a SAPO is shown in Figure 2.3. Within this group, the structures are distinguished by numbers (n) and named SAPO-n, where n corresponds to their respective analogue zeolite framework. There are many important SAPOs like the large-pore SAPO-5 , medium-pore SAPO-11 and small-pore SAPO-34 to mention a few. For this project SAPO-34 has been investigated, and its characteristic will be further elaborated in the next subsection.[33,40]

Since zeotypes ans zeolites are microporous materials, defined by the International Union of Pure and Applied Chemistry (IUPAC) to be materials with pore diameters of less than 2 nm, their pores are in the molecular size range.[5,47,48] For that reason, they have been used as molecular sieves which are materials, usually porous solids, which separates particles of molecular dimension.[16,40,41,49,50] Therefore, zeotypes and zeolites as molecular sieves are often applied for gas separation and purification.[5,51] Furthermore, the different sized porous frameworks of zeolites and zeotypes, gives them ability to function as shape-selective catalysts.[40,44,52] Shape selectivity can be classified into three categories, namely reactant-, transition state- and product selectivity which is illustrated in Figure 2.1.[5,53] Unwanted reactants can be excluded by reactant selectivity if the reactants are larger than the pore diameter, while the smaller reactants can diffuse into the cavities and be converted over the active sites. Whereas transition state selectivity in zeotypes is when only certain reaction intermediates can be formed due to the confinement of the pores or potential cavities, allowing a greater degree of product control. Lastly, there is product selectivity which again is the restriction of products that can exit the pores or cavities in question based on the size of the pore openings.[5]
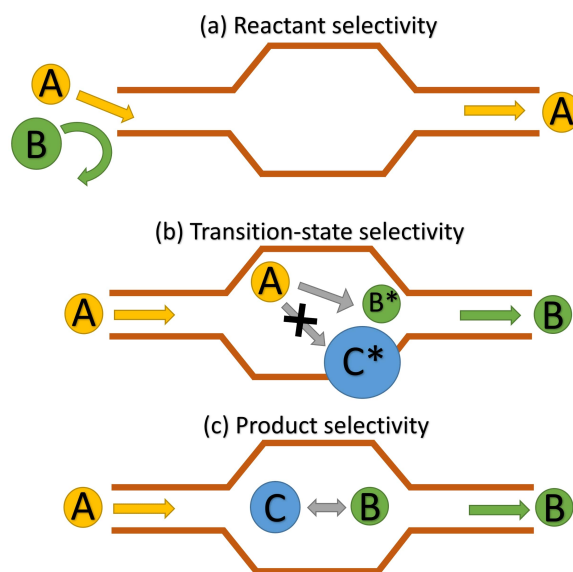
Figure 2.1: An illustation of the categories of shape selectivity in zeolites and zeotypes, namely (a) reactant, (b) transition-state and (c) product selectivity. Note that not all zeotypes and zeolites have cavities, and therefore not all categories apply for all zeolites/zeotypes. The figure is inspired by Chorkendorff and Niemantsverdriet.[5]

Another reason for which zeotypes and zeolites are applied as catalysts, is their naturally reactive surface.[5] Generally, acidic properties in zeotypes and zeolites arise from difference in the valence of the T atoms causing a net negative charge. For example, the difference between Si(IV)and Al(III) in zeolites results in a negative charge, whereas the zeotype group aluminophosphates (ALPOs) does not have acidic properties due to the charge balance between Al(III) and P(V). However, if Si replaces Al or P in the ALPO framework, the result is the mentioned SAPO framework, which will result in a valence difference and gives rise to the acidic properties

of SAPOs.[35,54,55] The acid site formed from the negative charge on the oxygen bridges can be a Brønsted acid site (BAS), a proton donor, if the cation which neutralizes the charge is a H$^+$-ion.[5] Since the cation can be exchanged, it is at these sites ion-exchange is possible in zeotypes as illustrated in Figure 2.2.[35,43] Although the acid properties of the different SAPOs varies, they are often correlated to the Si content.[56] The acid sites in zeotypes and zeolites are catalytically active for many hydrocarbon reactions such as MTO, alkene oligomerization, catalytic cracking and isomerization reactions.[5,35] In addition, the negative charge can be neutralised by other cations giving rise to ion-exchange capabilities and is the reason for which these type of materials are extensively used in detergents.[5]
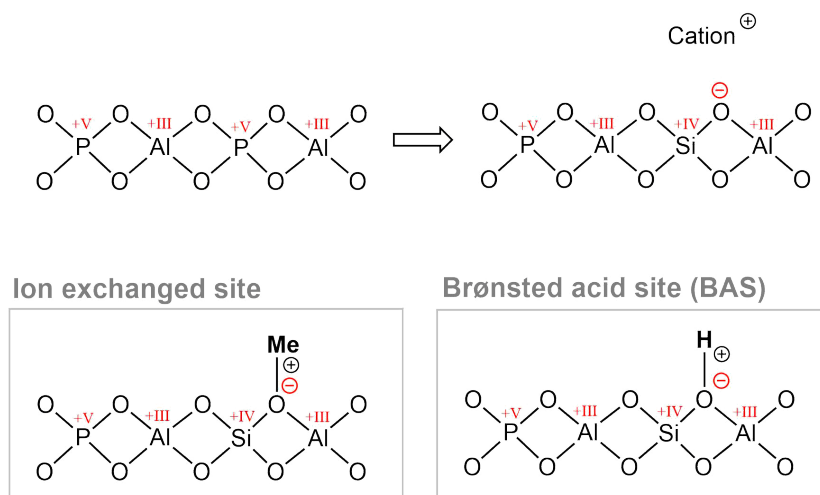
Figure 2.2: Illustration of the formation of acid sites in SAPO's by replacing a phosphorous atom with a silicon atom. The negative charge on the oxygen bridge is neutralized by a cation, and the name of the site can be distinguished by the type of cation that neutralises the negative charge.

Owing to the open and porous structure of zeotypes, they also exhibit a high specific surface area, making them suitable as both catalysts and catalyst supports.[5,43] A catalyst support is the material on which the active catalytic material is dispersed upon, and can be both inert or active for the reaction.[47,57] When the support-material contributes to the reaction, the composite catalyst can be called bifunctional.[58] An example of this can be metal containing SAPOs, where the SAPO contributes with acid sites, surface area and dispersion, while the metal in question can be active for a given reaction.[19,58–60]

Catalyst support requirements

In this thesis, the zeotype SAPO-34 is studied as a catalyst support for different metals, and there are several requirements that must be met in order to be a good support material. It is of high importance that both the support and the active material have hydrothermal, chemical and mechanic stability in catalysis since catalysts often are subject to high pressures and temperatures.[5,61] In other words, the materials must withstand such reaction conditions without decomposing. Catalyst supports are in most cases solids with high specific surface areas on which

the catalytic material, for example metal particles, can be dispersed and made accessible on the surface. Furthermore, the accessibility of the active metal is crucial for the catalytic activity, which is why supports which enable highly dispersed active species is an important factor.[62]
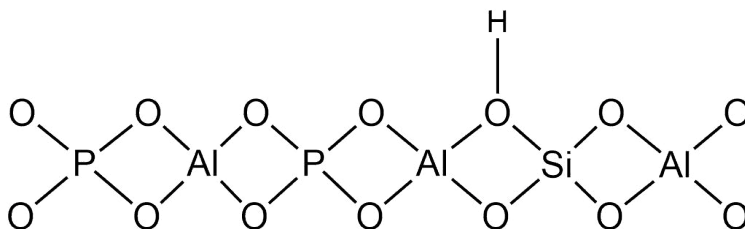
Figure 2.3: The general chemical structure of a SAPO-zeotype, where the proton is located at a Brønsted acid site.

2.1.2   Conventional SAPO-34

Among the SAPOs is SAPO-34 which has an analogous topology to the mineral chabazite (CHA). The CHA framework is built up from double six-membered rings (D6R) stacked in an ABC ABC sequence of distorted hexagonal prisms which are connected to each other by four-membered rings (4MR). The top of the hexagonal prisms and 4MR can be seen in the [001]-projection (z-direction) in Figure 2.4.[34,46] In Figure 2.5 the secondary building blocks composed of TO$_4$-tetrahedra in the CHA framework, namely 4MR, 6MR and 8MR are highlighted in red, yellow and blue, respectively.
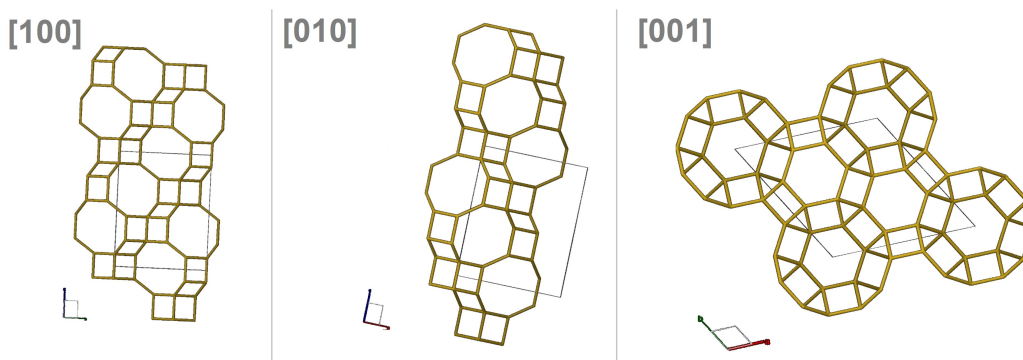
Figure 2.4: Illustration of the CHA framework along [100],[010] and [001] collected from the international database of zeolite structures.[34] Structure of SAPO-34 as seen from three different directions. The [100] shows the structure from x-direction and the [010] projection from the y-direction, and in both directions it is possible to see the ordered 8-membered rings. In the [001] projection, the structure is visualised from the z-direction where the 6-membered rings and their arrangement can be seen.

As a result of the stacking, a framework of oval cavities and pore channels is formed as can be seen in Figure 2.5. The stacking of 6MR and 4MR creates 8-membered rings (8MR) with a diameter of approximately 4 Å (3.8 x 3.8 Å). The 8MR rings makes up the pore system of SAPO-34 can be seen in the x- and y-directions in

Figure 2.4.[34,40,46] Due to the three 8MR-pore channels, the CHA framework is rendered three dimensional (3D) .[43] Furthermore, the SAPO-34 structure contains CHA cages or cavities, which can be accessed through the 8MR openings as illustrated in Figure 2.6. The cavities are ellipsoidal and measure approximately 11 X 6.7 Å and each cavity is interconnected to six other cavities [HVA HAR JEG GLEMT MED 6-ringene?].[63–65]
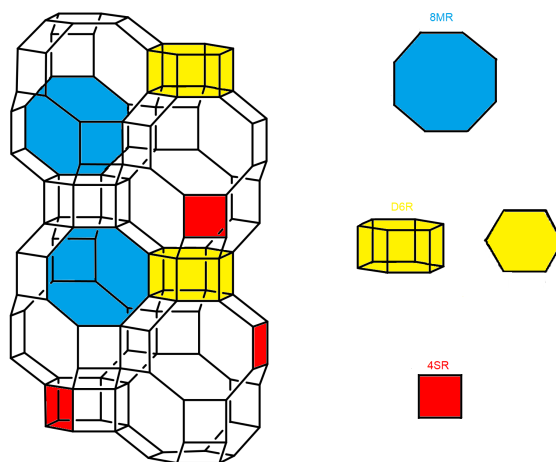
Figure 2.5: Illustration of the chabazite framework, where the 8MR, D6R and 4SR are highlighted in blue, yellow and red, respectively. The figure is adapted from the international database of zeolite structures.[46]

As mentioned, SAPO-34 is a microporous zeotype with pores and cavities of the same order of magnitude as small molecules such as methane, methanol, water and carbon dioxide.[46,48] The entrance to the cavities of SAPO-34 is through the 8MR with a diameter of 3.8 Å, which excludes larger reactants, intermediates and products, resulting in higher selectivity for smaller molecules.[46,53] For comparison, the kinetic diameter of methane and methanol is 3.8 Å and 3.7 Å respectively.[66] The smaller pore openings facilitates small linear molecules such as methanol and alkenes to diffuse through, which can induce a higher selectivity for the product in question, further explaining the commercial use of SAPO-34 for the MTO with a selectivity of 80-90% for light olefins.[35,51] However, inside the cavities larger intermediates can be be formed, and can thus be trapped inside the structure. This introduces the concern of mass transfer limitations as molecules that are not permitted to exit the cavities, can after time clog and may hence deactivate the catalyst over a certain time.[35,67,68]
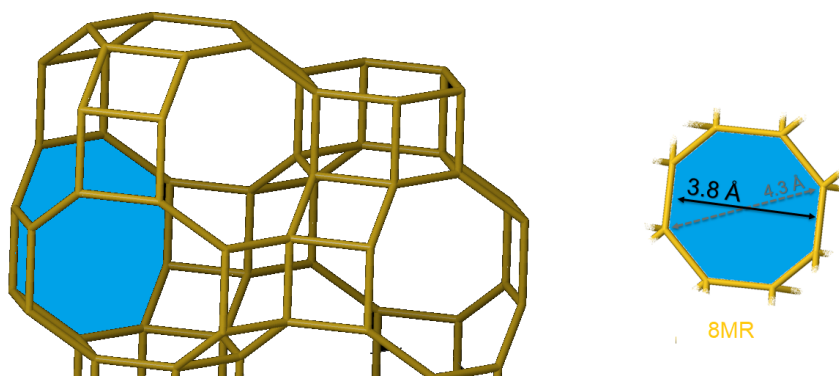
Figure 2.6: Illustration of the chabazite framework where the pore placement and size of the 8MR-ring is highlighted in blue. The original figure is collected from the international database of zeolite structures.[34]

As can be seen in Figure 2.3, the net charge of SAPO-34 and other SAPOs is not zero due to the difference in valence of Si(IV) and Al(III).[61,69] For every silicon introduced into the neutral ALPO-framework, for example by isomorphous replacement of phosphorous as illustrated in Figure 2.2, a negative charge is introduced to the oxygen bridge between the two tetrahedral atoms with difference in valence.[70] To neutralise the negative charges in the SAPO-34 framwork, cations such as Na^+, H^+ or NH_4^+ may be present.[69,71] As a result, SAPO-34 has acidic properties and ion-exchange possibilities. The cation that neutralise the negative charge can be replaced and this is called an ion exchange site and is also illustrated in Figure 2.2. In the CHA framework of SAPO-34, four unique ion exchange sites have been determined at four distinct oxygen atoms around the single crystallographically unique T-site, and among these, three of them point towards the 8MR-centre.[20,49,72]

Further, SAPO-34 exhibits several properties that make it uniquely suitable for catalytic reactions.[51] The numerous pore systems of 4-, 6- and 8-member rings in ordered composition results in a high specific surface area for SAPO-34 of around 500-600 m^2/g.[73] In comparison, SAPO-11 and SAPO-5 have specific surface areas of 100-200 and 200-300 m^2/g respectively.[74,75] In addition, SAPO-34 exhibits high thermal and hydrothermal stability and retains its crystallinity after temperatures of 400–600°C, which is necessary for catalytic applications.[40,61]

In summary, SAPO-34 exhibits a high specific surface area, thermal and hydrothermal stability, shape selective properties, ion exchange possibilities and acidic properties. These properties makes SAPO-34 suitable as a catalyst support material, but can also function as a catalyst alone.

[40,51,61] These characteristics, in addition to the ion-exchange capabilities, makes SAPO-34 attractive as a catalyst and a catalyst support material. For these reasons, SAPO-34 is employed as an industrial catalyst for the MTO and also shows potential for several applications including gas separation and water adsorption.[40,56] SAPO-34 has attracted considerable research attention in the field of heterogeneous catalysis and more recently also specifically for employment in greenhouse gas mitigation.[61] As the flexibility in the SAPO-system offers possibilities to functionalise

Table 2.1: Effective diameter of hydrated metal cations used for ion exchange in this project. [80]

Hydrated metal cation	Cu^{2+}	Zn^{2+}	Fe^{2+}	Ag^+	Co^{2+}
Effective diameter	6.8 Å	6.8 Å	6.8 Å	4.7 Å	∼6 Å

the material into having desired catalytic properties, metal containing SAPO-34 has been investigated for direct conversion of methane, the direct conversion of carbon dioxide and the selective reduction of NOx-gases. [36,61,76,77]

2.1.3   Metal introduction by liquid ion exchange into SAPO-34

One way to functionalise a zeotyoe is to introduce metal particles or ions to make it active for the reaction in question. [76] There are various deposition methods for introducing metals into zeotypes or zeolites, such as ion-exchange, impregnation and incorporation, where only the former is relevant for this master thesis. [78] The principle behind ion-exchange is to replace the proton or cation on the acidic sites with the wanted metal cation. This can be done by liquid or solid state ion-exchange (LIE or SIE, respectively), and for this thesis SIE is not relevant and will therefore not be covered. LIE is a versatile and simple technique, and will be explained in the following paragraph.

In LIE, the desired metal is introduced by suspending the solid framework in an aqueous solution of the metal cation in question where the goal is to exchange the framework ions with the ones in the metal ion solution. [5,79] The desired cation, being the metal cations Cu^{2+}, Zn^{2+}, Fe^{3+}, Ag^+ and Co^{2+} for this project, is introduced under stirring and/or under elevated temperatures to favor mass transfer. [69] The goal is to get as many as possible of the desired metal cations into the framework. In order to achieve this, the ion exchange process is often repeated several times. [69] For the metal content to be as high as possible, the amount of available acidic sites must also be satisfactory. As mentioned, four ion exchange sites have been determined in SAPO-34 and are located in the charactersitic cavity. [49,72]

On the other hand, the LIE method has some limitations. First and foremost, the inevitable weight loss throughout the repeated washing and filtration process. [79] Second, the desired cation must be soluble and fairly stable in aqueous solutions. [69] Third, the solution must be able to penetrate the pores of the zeotype. As mentioned, SAPO-34 is deemed a small pore zeolite with a pore size of around 4 Å. Consequently, liquid ion-exchange with some larger hydrated metal cations may be challenging if the pores are so small that sites may become inaccessible. [69,79] For comparison, the diameters of the hydrated metal cations relevant for this project are presented in Table 2.1.

2.2 Characterisation techniques

The theory behind the characterisation methods used in this project are presented in the following sub-chapter.

2.2.1 X-ray diffraction (XRD)

X-ray diffraction (XRD) is one of most used techniques for catalyst characterisation, and the non-destructive technique provides fingerprint information about the crystal phase or phases of the material in question.[5] In this section, the theory behind XRD and the obtained information the technique provides will be presented.

The characterisation method used in this project is powder X-ray diffraction (PXRD). In powder form different fractions of the sample will be oriented in different directions, and will thus create an image of diffraction lines when bombarded with X-rays.[5]

The crystal structure is a description of the ordered arrangements of the atoms, ions or molecules in a material. Unit cells are the smallest unit that represents the entire crystal's structure and symmetry, and the length of the principal axes of the unit cell are defined as the lattice parameters.[81] Crystalline materials are able to diffract X-rays as the wavelengths are around 0.1-100 Å, which resembles the distances between atoms in crystals. The principle behind XRD is to emit monochromatic X-rays from a cathode and focus it on a sample. The crystal lattice of the sample, as illustrated in Figure 2.7, then diffracts the x-rays which are incident with the lattice parameters.[5] Constructive and destructive interference from the X-rays that are scattered by the crystal structure of the sample, form a unique pattern of higher and lower intensities. Bragg's law, given in Equation 2.1, describes the relation between the X-ray wavelengths, λ, the distance between two planes in the crystal lattice, d, and the diffraction angle, Θ.

$$n\lambda = 2d\mathrm{sin}\Theta \tag{2.1}$$

Once the diffracted X-rays are collected, the structure of the samples can be analyzed as the distance between the planes of atoms causes different diffraction intensities. Plotting these intensities of diffracted beam against the diffraction angle creates a diffractogram.[5] The position of the intensities correlates with the lattice spacing of the crystal structure in accordance with Bragg's relation (2.1). Therefore, the diffractograms work as fingerprints for crystal phases and makes it possible to identify which ones that are present in a crystalline sample by comparing them to known diffraction patterns.[5,81]
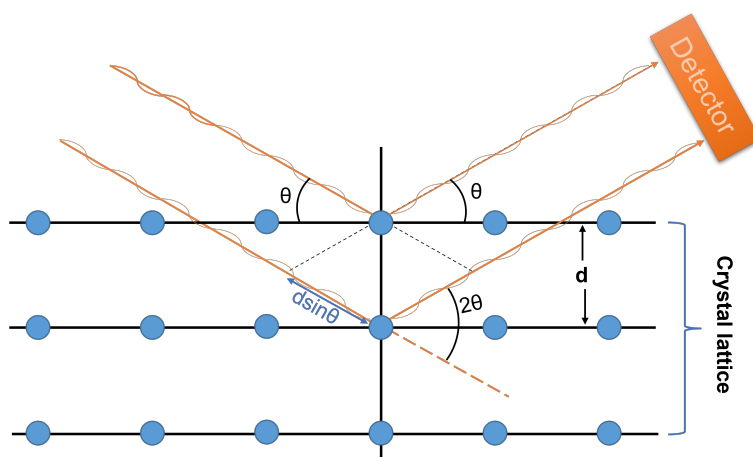
Figure 2.7: Illustration of Braggs law, where d is the distance between the crystal planes, Θ the angle between them and $d\sin\Theta$ the added path difference. In addition 2Θ is illustrated and is the angle between the incoming and the diffracted X-ray. The figure shows the scattering when X-rays hit atoms in an ordered crystal lattice, and is inspired by Chorkendorff and Niemantsverdriet[5,82]

In particular, the PXRD technique has been utilised to determine phase purity and relative crystallinity of powdered samples of Me/SAPO-34 in this project. Phase pure SAPO-34 has the same crystal structure as that of chabazite (CHA), and will have the diffractogram of the CHA structure as shown in Figure 2.8.[34,46] As long as the ion-exchanged metals have not formed impurities such as metal oxides, the same diffractogram is expected for a phase pure sample of Me/SAPO-34.[5] In addition, relative intensities can quantify changes in crystallinity. If the material has become less crystalline, the intensities in the diffractogram are smaller compared to the mother sample of conventional SAPO-34. Further, if the reflections are no longer present, then the material has become amorphous.

There are several factors which can influence the diffraction pattern. For example a higher cell lattice results in a smaller 2Θ, and both higher atomic numbers and higher crystallite sizes leads to higher intensities. In addition to identify crystal phases, the technique can be used to quantify changes in crystallite size, cell parameters and orientation.[81,83] Further, the detection limit of PXRD is particles larger than 2.5 nm or phases making up more 2-3 wt.%, which introduces an insecurity in what can appear as a phase pure sample.[5,84] In addition, since X-rays penetrate deep into the sample, information of the surface that can be of catalytic importance may be invisible.[5,81]

2.2.2   Nitrogen physisorption

To obtain knowledge on surface area, pore size and pore volume of porous samples, nitrogen physisorption is a popular technique. In gas adsorption, the principle is measuring the adsorption and desorption of an inert gas, where for nitrogen physisorption the inert gas is nitrogen. Gas adsorption on solid surfaces and in pores is a complex phenomenon which involves energy interaction, mass interaction and possibly phase transitions.[85]. In this project, the BET theory, named after
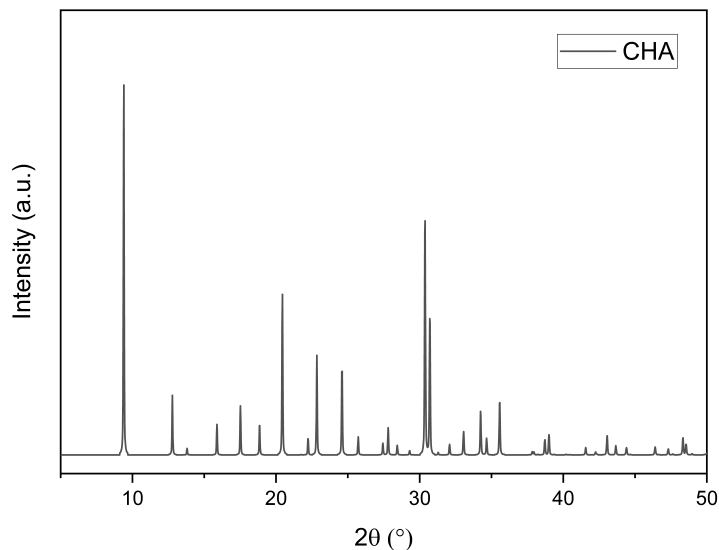
Figure 2.8: The diffractogram for the CHA structure. Data collected from IZA.[34]

Brunauer, Emmet and Teller, was utilized to provides a method to calculate the BET surface area of the solid materials. Further, the t-plot method was used to determine both external and the internal micropore area ans micropore volume of pores and cages.[86] Quantitative information of the specific surface area can be derived from the BET isotherm, as well as qualitative information on porosity.[5]

The BET theory aims to explain the adsorption of the gas to the material surface. The principle is to measure the physisorption of an inert gas, usually nitrogen, with a known adsorption area up to monolayer coverage is obtained.[85] By plotting the molar quantity of adsorbed or desorbed gas against the relative pressure at constant temperature gives an isotherm, which can be used to calculate the total surface area by using the BET isotherm.[87] Mathematically, the BET isotherm is derived from the Langmuir isotherm which again is mainly applicable for chemisorption.[44,85] The linear form of the BET isotherm gives:

$$\frac{P}{V_a(P_0 - P)} = \frac{1}{V_m C} + \frac{C-1}{V_m C}\left(\frac{P}{P_0}\right) \tag{2.2}$$

where P is the pressure, P_0 the saturation pressure, and C is another constant derived from heat values, the gas constant R and the absolute temperature T. The relative pressure, $\frac{P}{P_0}$, is the actual pressure divided by the vapor pressure of the adsorptive. The intercept, $\frac{1}{V_m C}$, and the slope, $\frac{C-1}{V_m C}$ can be used to determine the volume of one monolayer. Combining V_m in the linear region of the BET isotherm with the area occupied by a single adsorbate molecule, the surface area can be determined by assuming monolayer formation in the linear area of the isotherm. This is combined with the mean area per molecule, σ, which is 16.2 Å^2 for N$_2$- molecules.[85] When the relative pressure approaches 1, the total coverage of adsorbed gas ap-

proaches infinity and it is assumed multilayer formation on the surface.[5] Since the process is exothermic, the physisoprtion of gas on solids increases with increasing pressure and decreasing temperature. Commonly, when using nitrogen as the inert gas, the measurements are preformed at cryogenic temperature, most often at the boiling point of liquid N_2 (77 K)[85].

Yet, for the BET theory to be valid a number of conditions must be fulfilled. The fundamental assumption in the BET isotherm is that the forces active in the condensation of gases are also responsible for the binding energy in multimolecular adsorption.[85] Equal sites, negligable adsorbate interactions, hexagonal closepacking and monolayer cover in the isotherm region and continuous layer growth as on a free surface are other assumptions made in BET analysis.[88]

In fact, microporous materials such as zeolites and zeotypes does not fulfill all the assumptions of the BET isotherm, especially the assumption of multilayer formation, which introduces a challenge.[88] Adsorption is restrained by the size of micropores and limits formation of multilayers even at high pressures. The literature suggests that instead of a continuous layer growth on the surface, the adsorption fills up the pores.[5,85,88] Generally, microporous materials are not suited for BET analysis. Commonly, adsorption takes place in the smallest pores first, before filling up pores in an ascending order. Hence, the adsorption isotherms of microporous materials experience an almost vertical rise initially due to enhanced adsorption in the micropores. When the micropores are filled, the isotherm nearly levels out horizontally because almost no adsorption takes place after the micropores are filled as can be seen in Figure 2.9.[5,85,88] Yet, the surface area can be estimated and is valid under some conditions. Another limitation may be defects in the sample material, and subsequently an effect on the surface area due to blocked pores or other structure defects.[88]

In total there are six known isotherm types, categorised by IUPAC based on their shape, and these are illustrated in Figure 2.9. For the purpose of this thesis, only the Tyoe I isotherm is of relevance, and is usually associated with microporous solids.[48,85] Isotherm type IV and V have hysteresis loops, which is a result of gas being desorbed at different equilibrium pressures than it was adsorbed. This is an effect of capillary forces, and is often assosciated with mesoporous materials.[5]

Lippins, Linsen and de Boers t-plot, is a method based on BET theory, and is used to calculate the pore volumes and shows the adsorbed volume,V_m, plotted against the statistical thickness of the adsorbed layer,t.[85,86] Further, the Barret-Joyner-Halanda (BJH) adsorption method can be applied to provide information on the pore size distribution due to meniscus formation of condensed gas within pores. The BJH-method uses the Kelvin equation and a theoretic stepwise emptying of the adsorptive which has condensed in the pores.[5]

In summary, BET, BJH and t-plot can provide information on surface area, external and micropore area, pore volume and pore size distribution. Despite the typical behaviour traits of material types, it is important to keep in mind that there are large variations even within material types such as microporous materials. Conse-

quently, the isotherms may vary a lot from expected behaviour. Thus, they should be studied thoroughly in accordance with thermodynamic and kinetic principles when deriving information on pore structure and surface area from this type of analysis.[5,44,48,85] In addition, most models and theories assume cylindrical pores, so errors may result if the pore shapes vary a lot within a sample.[85]
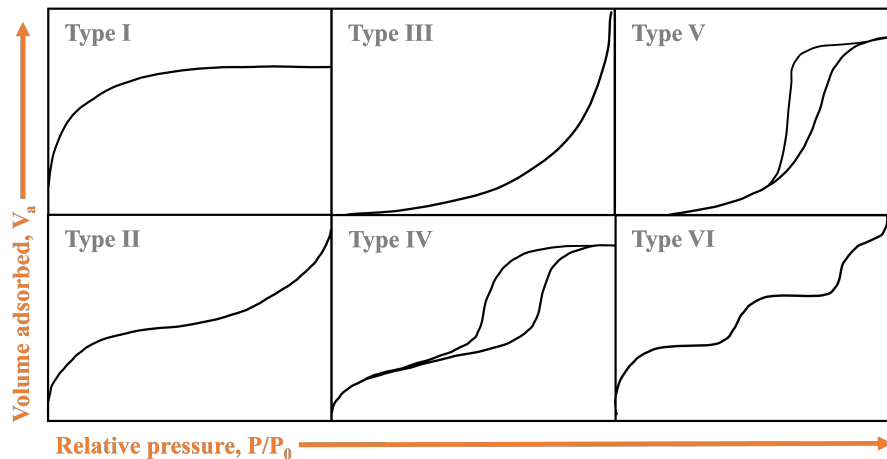
Figure 2.9: The six different types of adsorption isotherms defined by IUPAC.[47,48]

2.2.3   Scanning electron microscopy (SEM)

Scanning electron microscopy (SEM) is a technique for generating magnified images of sample surfaces and mapping microstructure morphology, and it has a broad range of fields for application.[5] To produce SEM images of a sample, the surface is scanned in a raster scan pattern with a focused and narrow electron beam, usually from a tungsten gun, with a fine spot size of about 5 nm. The energy varies from a few hundred to 50 keV, and when these electrons strike and penetrate the surface there are multiple interactions which occur and results in emission of electrons and photons from the sample.[44] By collecting the emitted electrons on a cathode ray tube (CRT), SEM images are produced by plotting the intensities of the detected signals as a function of the position of the primary electron beam.[5,44] The SEM images can achieve a resolution of up to 1 nm, and the magnification can easily be adjusted from around 10 to over 300 000.[5,44] In SEM, there are various modes differentiated on which signals are detected and subsequently imaged. This results in secondary electron (SE) images, back scattered electron (BSE) images and elemental X-ray maps, whereas SE mode is the most common.[5,44]

For the purpose of this thesis, the SE mode was the one of interest. From the images, the particle size, morphology and microstructure of the material in question can be studied and compared to previously reported images of similar materials.[5] In general, the study of zeotype morphology is especially important with respect to catalysis as it can reveal possible defects as well as particle size.

Electron gun

Condensor lenses

Scan coils

Objective lens

X-ray detector

Electron beam

Electron detector

Sample holder
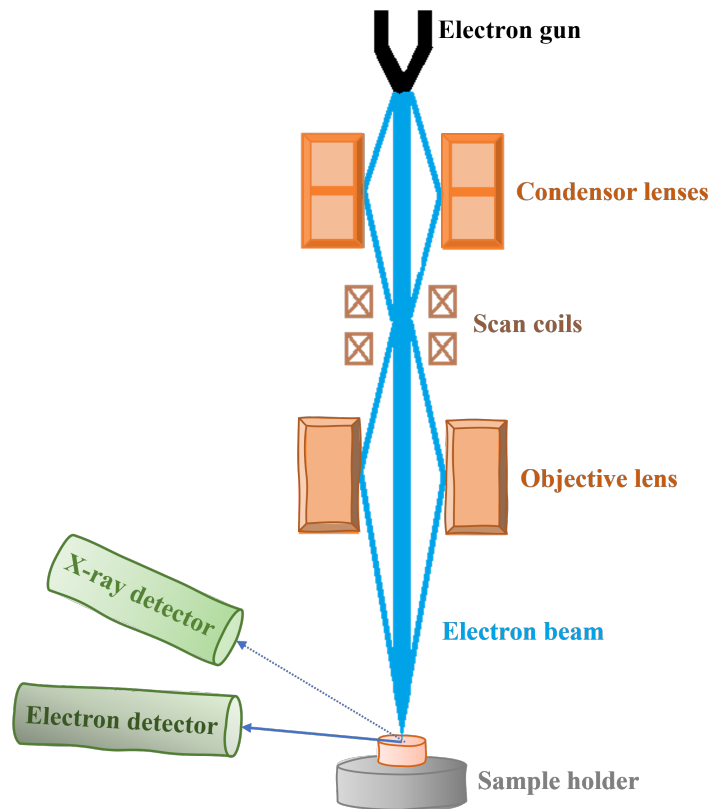
Figure 2.10: Illustration of scanning electron microscope schematic setup inspired by Chork-endorff and Niemantsverdriet.[5] When the electron beam hits the sample, numerous signals from electrons and X-rays can be detected and used to create images.

Firstly, SE mode is detecting the emittance of SE which are defined as inelastically scattered electrons with a lower energy than 50 eV.[5] This occurs as a result of a collision between the high energy primary electrons from the beam and atomic electrons, where some of the energy is transferred and the atomic electron will be emitted if that energy is high enough.[44] The orientation of the sample particles is what causes the image contrast, where the areas facing the detector appears brighter. Additionally, edges and especially corners appears lighter as a result of more SE being able to leave the surface.[44] Secondly, BSE undergoes a similar interaction, but in stead of the high energy primary electron transferring energy to atomic electrons, it collides elastically and is reflected back. Useful contrast can be developed in the image between regions in the sample which differ widely in atomic number, as the probability of BSE increases with atomic number and thus heavier atoms will appear brighter than lighter atoms.[44] BSE can travel 10-100 nm into the sample before being reflected, and can for that reason reveal compositional information.[5] Lastly, if the primary electron collides with and excites a core electron from an atom in the sample, the core electron will emit a characteristic X-ray photon or an Auger electron and decay to its ground state.[44] In addition, the latter interaction type enables SEM to be used as an indication for chemical characterisation.

However, the technique has some limitations like that the investigated samples must be electrically conductive to prevent build-up of negative charge. In the case of nonconductive samples, the sample must be sputter-coated with a thin layer of an electrically conductive materials, usually heavy metals such as carbon or gold before imaging. For better images gold is usually the preferred option, while carbon is preferred for elemental analysis. The layer must be as thin as possible, as a thicker layer could result in obscuring surface features. Another issue is sample damage, as bombarding the sample with negatively charged particles may cause charge accumulation or radiation damage such as surface rupture. Both of which will decrease the image quality, either in the form of extra bright particles or in the form of an incomplete image.

2.2.4   Inductively coupled plasma - mass spectroscopy (ICP-MS)

Inductively coupled plasma-mass spectrometry (ICP-MS) is an analytical technique for elemental analysis which is relatively fast, precise and accurate with has a detection limit as low as 0.01 ppm.[89] The principle of the technique is separating elements based on their mass-to-charge (m/z) ratio.[90]

First, the sample is prepared by dissolution in a strong acid such as hydrofluoric acid and then diluted to preferably containing less than 0.2% of the original sample. Further, the diluted sample is sent into an aerosol where an ICP-torch lits argon gas to create a plasma of around 6000-10000 K which is able to ionize the atoms in the sample.[90] Lastly, the ion beam is coupled to a mass spectrometer which can provide both qualitative and quantitative data from the sample. The signal measured in the detector is as mentioned based on each of the elements mass-to-charge ratio. The m/z-ratio is quite specific for each atom despite being post ionization, even though isotopes and other interferences during analysis must be taken into consideration.[91] From the abundance of each signal attributed to different ions, the elemental composition can be found. High resolution ICP-MS (HR-ICP-MS) is built on the same principle, but does have an additional magentic component. In other words, HR-ICP-MS has both an electrical and a magnetic unit to seperate elements, and makes it easier to differentiate between elements with mass overlap.[90] In a HR-ICP-MS the ions are accelerated by electric field, and then deflected by the magnetic field.

A disadvantage of the technique is that it is destructive, though since only small sample amounts are required this is not a major limitation. The method is suitable for most metals, but does not work well for noble gases and most halogens.

For the prospect of this thesis, the ICP-MS technique is mainly used for determining metal content in terms of weight percent (wt.%) and the T-atom relationship in the SAPO, where the Si/Al-ratio is of the highest interest. The weight percent of an element is defined as follows:

$$\text{wt.}\% = \frac{\text{Element mass}}{\text{Total sample mass}} * 100\% \tag{2.3}$$

2.3   Methane and methane conversion to methanol

Methane, CH_4, is a convenient fuel for power generation and heat, and is the cleanest alternative among the fossil fuels as it produces less carbon dioxide by combustion compared to that of oil and coal for example.[5,8,92] In industrialised and densely populated areas, methane can be readily transported and distributed through pipelines, and is not only abundant, but also an important energy source.[5] Unfortunately, methane is a strong GHG with a GWP of 86 over a 20 year period.[8,92] At present, methane is the second most abundant GHG in the world and is responsible for more than 25% of all of the warming the earth is experiencing.[8,93] Therefore, finding a commercial recycling path for methane into value-added chemicals has been a field of research of the utmost interest for over a century, though a major breakthrough is yet to come.[1,10,12,17,18,92–94] Numerous approaches for the direct conversion of methane have been investigated as can be seen in Figure 2.11.[10,14,95] Among these are the partial oxidation of methane to methanol, the coupling of methane to C2-hydrocarbons[96–98] and the coupling of methane to aromatics[99,100].
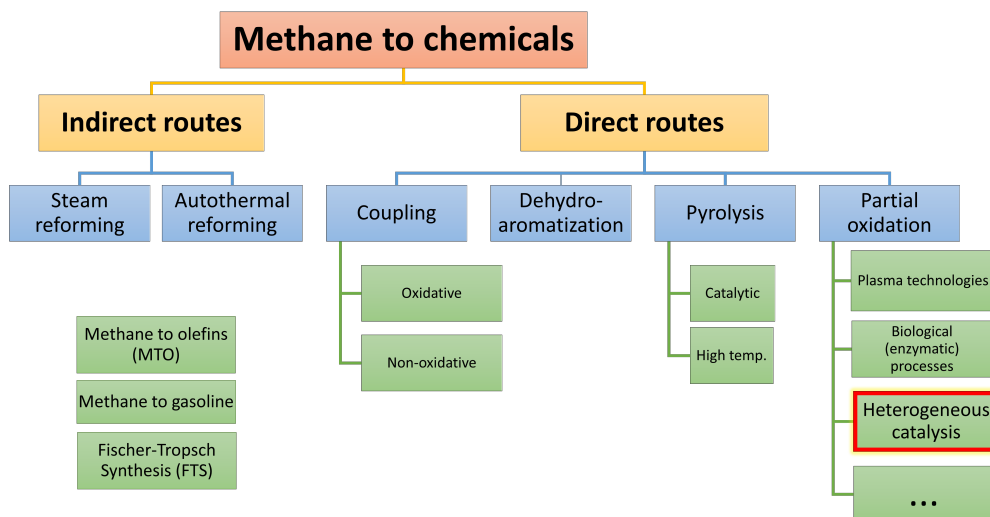
Figure 2.11: An overview of some of the routes for methane conversion to value-added chemicals inspired by Ravi et al.[10,14,18]

However, all routes suffers from the limitation arising from methane conversion versus product selectivity. For these conversions, there are two main routes, namely the indirect via synthesis gas or the direct ones such as dMtM.[1,5,18] Today, almost all commercial conversion of methane goes via the indirect route which requires the energy-intensive steam reforming step. Here the direct routes offer a promising prospect by converting methane to high-value added products like methanol, aromatics and hydrocarbons - without the economic and climate drawbacks of such high temperatures and pressures/extreme conditions that is required by the indi-

rect route. Possible processes for a direct methane to methanol (dMtM) conversion include conventional catalytic processes, photocatalytic technology, electrochemical processes, plasma technology, biological processes and supercritical water technologies.[10,12,14,17,94] In this thesis, possibilities within heterogeneous catalytic processes for the dMtM are of interest.

In this thesis, the focus will be on the direct conversion of methane to methanol which has been described by many as what can be called a dream reaction and is illustrated in Figure 2.12.[5,31] In the following subchapters, the chemistry behind methane, its climate effect and the oxidation reaction from methane to methanol will be accounted for.
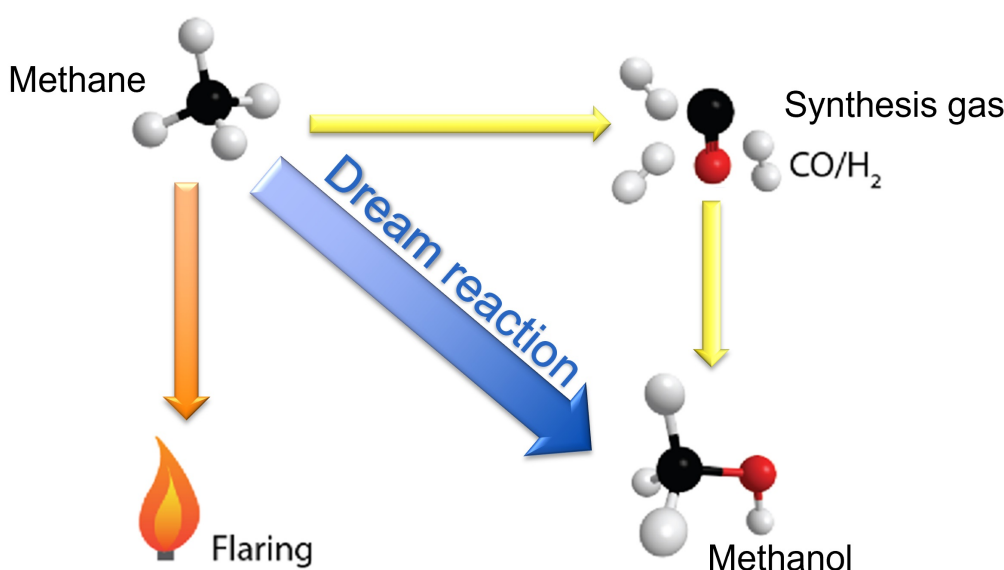
Figure 2.12: Illustration of the dream reaction of directly converting methane to methanol, avoiding flaring and the energy intensive steam-reforming step of the indirect route. Figure inspired by Tomkins et al.[31]

2.3.1 Methane emissions in a climate perspective

As mentioned, methane is the second most abundant GHG, and with a GWP 86 times that of CO_2 over a 20 year period, also a powerful one, contributing to more than 25% of all global warming.[1–4,10,92,93] The climate changes and increase of extreme weather caused by global warming is one of the planets greatest threats as to this day.[1] For that reason, the atmospheric methane emissions and the trending increase over the last decade are of utter concern for the entire global community.[1,4,12] As much as 60% of all methane emissions come from anthropogenic sources and looking at the last decade, average annual emissions have increased by around 50 million tonnes compared to the previous and is steadily increasing in the current trajectory.[2,4,92] The largest contributing sectors to these emissions are agriculture, fossil fuel operations (energy) and waste management as illustrated in Figure 2.13.[1,2,4,11,93] In addition, methane is a precursor for harmful/dangerous air pollutants such as ozone, and is responsible for 50% of tropospheric ozone formation

growth.[2,8] Further, methane gas accompanies oil recovery which often takes place at remote locations, and as methane gas is not easily transported, this provides an issue due to economically unfeasible transportation possibilities. Subsequently, methane is often flared and combusted to carbon dioxide because methane is, as mentioned, a more potent GHG.[5]
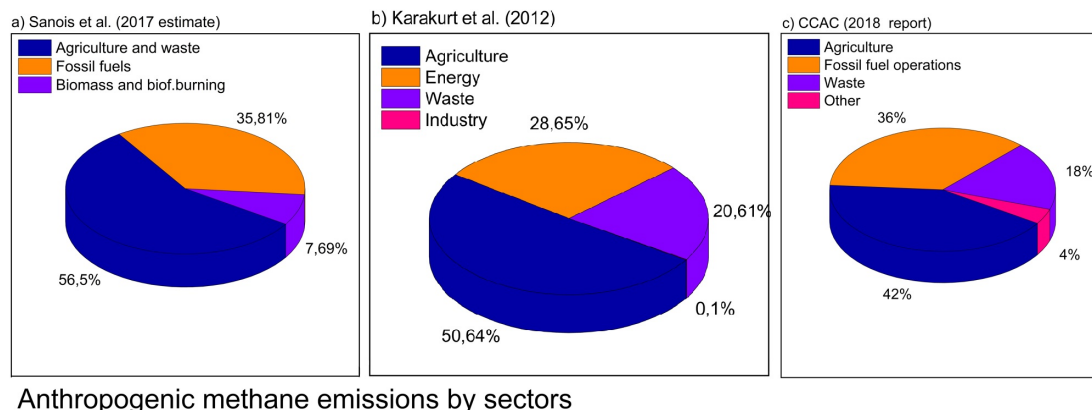
Anthropogenic methane emissions by sectors

Figure 2.13: Antrophogenic methane emission sectors as reported by a)Saunois et al.[4] b)Karakurt et al.[1] c)CCAC[11]

Naturally, the consequences of and the increase in methane emission has resulted in stricter and stricter demands for emission control.[9] Article 14 of the Paris Agreement requires participating countries to report progress in amongst others methane mitigation.[9,92] Moreover, a target has been made in the Paris Agreement that the global average temperature should not increase mote than 1.5°C since an increase of more than 2°C will cause catastrophic changes.[9] Of concern is that the Intergovernmental Panel on Climate Change (IPCC) has assessed the current trajectory of antrophogenic methane emissions to lie between the two worst scenarios, as pointed out by the Paris agreement, leading to a global temperature increase of more than 3°C before 2100. In fact, the 1.5°C-target is impossible to achieve without a 40-45% reduction of methane emissions by 2030.[3,4,8,9,11] A reduction of such a magnitude would complement long-term climate change mitigation efforts and avoid almost as much as 0.3°C warming by 2045.[11] In other words, reduction of methane emissions are crucial in the battle against global warming which is the reason for the newly launched Global Methane Pledge (COP26 - 2021) to champion methane mitigation.[8] Over 100 countries which make up 70% of the entire global economy have pledged to take actions to reduce global methane emissions by at least 30% from 2020 to 2030 and to end routine flaring by 2030.[13,101] Further, both the United Nations Framework Convention on Climate Change (UNFCCC) and the Convention on Long-Range Transboundary Air Pollution (CLRTAP) covers the importance of reducing methane emissions.[4]

For that reason, measures to reduce the atmospheric methane concentration are readily researched.[10] A preferable solution would be reducing emissions by converting methane to value added chemicals such as methanol, formaldehyde or aromatics and in that way reducing emissions.[10,14–16] As mentioned, today most chemical production with methane as raw material goes through the energy-intensive steam

reforming step and finding a direct route which can overcome that energy disadvantage would be a so-called dream reaction.[14] Simultaneously providing an economic incentive for methane mitigation and could possibly be a solution for meeting the energy need of future generations.[10] Both hydrogen and methanol could be potential clean energy sources with high energy densities which can utilise methane as a precursor. Therefore, direct methane conversion technologies are a research field of the utmost worldwide interest.

To conclude, methane management has become an increasingly prominent part of climate change mitigation and is of wide international concern[93]. The drastic increase of methane emissions, the negative impact on the climate and subsequently the stricter demands highlights the need for a viable industrial recycling path for methane.[8] As methane is a vital raw material for useful chemicals such as methanol, formaldehyde, hydrocarbons, aromatics, light olefins and hydrogen, direct conversion into the chemicals would offer an ideal solution for reducing methane emissions and alleviating the reliance on oil for chemical production, and thereby also reduce negative climate effects and contribute to achieve climate goals, whilst economically profiting from it.[5,18,93] In this master project, the direct conversion from methane to the valuable and condensable product methanol has been studied, and the theory behind the reaction will be elaborated in the next subsection.

2.3.2 Methane
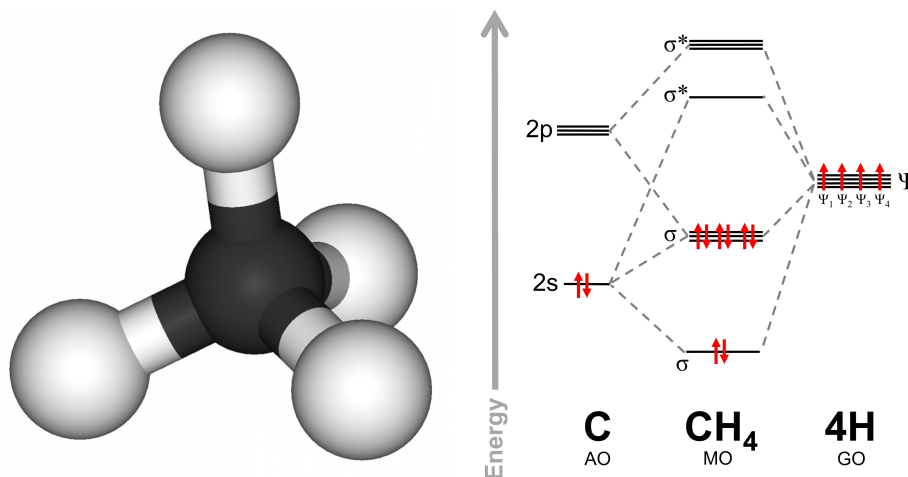
Figure 2.14: MO of the methane molecule, CH_4. Figure inspired by Shershah et al.[94]

The methane molecule has a tetrahedral molecular structure with four equivalent sp^3 hybridised C-H bonds from the C-atom, leading to a bond angle (H-C-H) of 109.5° and a C-H bond length of 1.087 Å.[66,84,94] As illustrated in Figure 2.14, these four bonding molecular orbitals (MO) are formed by the overlap of the valence orbitals of each hydrogen atom and the four from the central carbon atom.[94] The overlap between three 1s-orbitals from hydrogen and two 2p-orbitals from carbon results in triply degenerate MO's which is in fact the highest occupied MO (HOMO) and has low energy. Subsequently making it challenging to remove electrons from the

HOMO of methane. Likewise, it is challenging to add electrons to the high energy antibonding LUMO of methane. In fact, there are no electrons in antibonding MO's and no lone pairs, further contributing to the stability and chemical inertness of methane.[84,94]

Further, methane does not contain any functional group or polarity that can be used to promote a chemical reaction. Another reason for the stability of methane is the weak acidity and low proton affinity which again restricts acid or base activation of methane.[102] Owing to the chemical stability of the methane molecule, methane is not easily activated as the exceptionally strong H-CH$_3$ bond with a energy of 439.3 kJ/mol at standard conditions must be broken for a reaction to occur.[17,94,102] As a consequence of the directional orientation, the bonding sp^3-orbitals are also less prone to form new bonds in the transition state and thus creating a chemical reaction barrier.[94] In addition to the high symmetry, the difference in electronegativity between carbon (2.55) and hydrogen (2.2) results in a low polarisability makes it challenging to allow any nucleophilic or electrophilic attack on methane.[17,66,94] In addition methane remains a gas at temperatures above -162°C, making it difficult to compress and transport.[5,66]

2.3.3 Activation of methane

Nevertheless, it is possible to remove electrons from the binding σ-bonds in methane with strong electrophiles. The most facile way for methane oxidation is the homolytic cleavage of the C-H bond and formation of methyl and hydrogen radicals.[94] Since the C-H bond is weaker in the oxidation products than in methane, it is thermodynamically challenging to convert methane.[94] Subsequently, the enthalpy change of the further oxidation reactions, described in Equation 2.4, are much lower which makes the oxidation products prone to complications such as over-oxidation.[14] The values can be seen in Table 2.2. In accordance with thermodynamics, the higher the temperature, the more difficult it is to stop further oxidation of the oxygenated methane derivatives until CO$_2$ as can be seen in Equation 2.4.[103] On the other hand, methane conversion at low temperatures is kinetically challenging as the C-H bond requires a large amount of energy to be cleaved which usually is provided in the form of thermal energy.[102] Though methane oxidation is achievable at higher temperatures, it leads to intrinsic low selectivity and over-oxidation in addition to the higher cost and safety requirements caused by more extreme conditions. Therefore, to obtain the desired oxidation products such as methanol and formaldehyde, separation and kinetic or physical protection is necessary even at low temperatures. Though, this makes the oxidation even more complex which along with the other challenges is the reason behind the small number of industrial applications.[17,94]

$$CH_4 \xrightarrow{\frac{1}{2}O_2} CH_3OH \xrightarrow{\frac{1}{2}O_2} HCHO + H_2O \xrightarrow{\frac{1}{2}O_2} CO + 2H_2O \xrightarrow{\frac{1}{2}O_2} CO_2 + 2H_2O \quad (2.4)$$
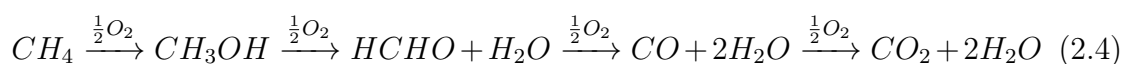
Table 2.2: Enthalpy change for the successive oxidation from methane. [94]

Molecule	Enthalpy change [kJ/mol]
CH_4	-75
Methanol	-200
Formaldehyde	-350
Carbon monoxide	-592
Carbond dioxide	-877

2.3.4   Methanol

Methanol is a simple organic liquid with a high volumetric energy density of 6.09 kWh/kg, about twice that of hydrogen (3.08 kWh/kg), which can be used as a renewable fuel source in fuel cell technology. [10,31] Further, efficient energy storage, as it does not require cryogenic handling, and low temperature reactivity are other characteristics which also make it a viable alternative fuel source. [10] In addition, methanol is a vital platform molecule and is used as a precursor for important chemicals such as dimethyl ether, formaldehyde, light olefins (MTO), hydrogen, gasoline (MTG), acetic acid and polymers. [17,31,104]

In contrast to methane, methanol has a dipole moment which facilitates activation and oxidation on the surface of a solid metal catalyst. Therefore, an addition step of extraction with a polar solvent is exploited for extracting the adsorbed methanol molecule with high desorption energy. [17,105,106]

Both methane and methanol have singlet ground states, and therefore their oxidation via O_2 is a spin prohibited reaction, which necessitates a suitable catalyst. [17] In this regard, several investigators conclude that for a fruitful dMtM an extremely selective catalyst must be exploited and for this purpose metals including Cu, Zn and Fe in zeolites and zeotypes are frequently investigated. [17,107]

2.3.5   The direct partial oxidation of methane to methanol

The dMtM (Equation 2.5) has been described as the holy grail of catalysis, and both homogeneous and heterogeneous catalyst researchers have studied the reaction intensively. [18] If a direct path to selectively oxidize methane to methanol is accomplished, it would not only be a lot more cost efficient as it doesn't require as harsh conditions as the indirect path, but it could redefine the entire petrochemical industry. [31] As mentioned, many routes have for that reason been explored for the direct conversion of methane to methanol. Unfortunately, a high methanol yield is currently elusive as of today due to over-oxidation of methanol. [31] The reaction (2.5) is exothermic at STP with an enthalpy change of -126.4 kJ/mol, but the problem is to stop the subsequent oxidation reactions to CO and CO_2 which are even more exothermic (CO: -519.5, CO_2: -792.5 kJ/mol). [94] Therefore, reported catalysts for the partial oxidation of methane suffer from the limitation of balancing between methane conversion and methanol selectivity. [97]

$$CH_4 + \frac{1}{2}O_2 \rightleftharpoons CH_3OH \tag{2.5}$$

Of particular interest is the very fact that nature itself has mastered the dMtM in the form of enzymes in methanotropic bacteria. Under ambient or physiological conditions, methane monooxygenase (MMO) enzymes are able to convert methane directly to methanol.[10,17,18] There are two types of MMO enzymes, namely sMMO which contains a dinuclear iron-centre and pMMO which contains centers of copper[21,108]. Both of which have inspired a lot of research, especially in the development of dMtM-catalysts.[10,18] Numerous research groups have investigated metal ion exchanges zeolites and zeotypes as analogous systems to MMO, and particularly copper[18,22,23,109–112] and iron[15,18,32,108,113–116] ion-exchanged zeolites and zeotypes. The reason for this is their excellent abilities as support materials in the form of high specific surface area, chemical and mechanical stability and last but not least, their pourous system which leads to shape selectivity, confinement effects and the ability to disperse active metals and hence makes the active sites accessible.[5,18,61,62] Moreover, other first row transition metals in zeolites such as cobalt[16,24,117], nickel[18] and zinc[18,26,27,29,118] have been investigated as well. Reynes et al. have published a review which investigates the role of different metal ions in zeolite frameworks for the dMtM, and includes studies which show that Co, Ni and Zn in zeolites have the ability to partially oxidize methane after activation with oxygen.[18] In additon, Kuroda et al. showed that Ag-ion exchanged HZSM-5 exhibited prominent catalytic behavior at tempperatures over 300°C for the partial oxidation of methane.[119]

It is highly desirable to develop an appropriate catalytic path to produce methanol selectively by dMtM, but as of this day, there are yet several challenges to overcome. The main issue is of course the balance between thermodynamics and kinetics to avoid over-oxidation, subsequently leading to poor selectivity or poor overall conversion rate. As methanol has a higher reactivity than methane, it favors further and total oxidation.[104] A possible solution could be forming a stable complex with the intermediate product to prevent further oxidation and CO_2 formation or separate the reactants.[23]

The stepwise process

In order to limit over-oxidation, one possibility is to make the process stepwise and thereby separate all reactants to achieve a higher selectivity, usually around 90%, to the partially oxidized products.[10,18–20,37] A drawback of this approach is that it leads to the use of excessive amounts of reactants over longer time periods and is the reason for which yields tends to be moderate. Methanol produced is therefore usually expressed as μmol per gram sample or stochiometrically in mole methanol per mole metal ions in the sample.[37] The stepwise reaction process of partial oxidation of methane usually consists of three steps. First, activation by an oxidant such as O_2 or N_2O at elevated temperatures of around 350-550°C, where the goal is to activate the metal centers. Second, the reaction temperature is set to around 100-300°C and methane is loaded upon the sample. During the contact time, the goal is that the activated metal centers in the sample cleaves the C-H bond in methane and form methyl groups.[20,37,120] Third, extraction of methanol is conducted by the use of steam or liquid ethanol or acetonitril to release methanol from the zeotype or zeolite pores.[16,20,105,119] In the case of steam, water molecules are suggested to replace the position of the methanol molecules and thereby reducing the desorption energy of methanol. In addition, this extraction should be conducted at temperatures higher than room temperatures due to the fact that the desorption energy of methanol is still too high to be desorbed by water at lower temperatures.[106]

There are several advantages of making the reaction stepwise, including drastically increasing the selectivity for partial oxidation.[20,37] The use of oxygen as the oxidant means that the reaction can proceed even at room temperature, alleviating the need for high-energy consumption and additionally few side products.[19] However, an activation step requires higher temperatures, but nonetheless not as high as the that of the steam reforming step.[10] Moreover, the aforementioned stepwise process limits over-oxidation of the chemisorbed intermediate which results in highly selective methanol yields.[10,19]

In summary, obtaining a high selectivity is challenging due to the energy needed to break the first C-H bond, and at high temperatures with high thermal energy the route to total oxidation is wide open.[97] In this regard, zeotypes and zeolites offer a promising solution due to their shape selectvity, ion-exchange possibilities, acidic properties and high surface area. Following a change of support to zeolite and zeotype materials higher methanol selectivities than thermodynamically predicted have been reported.[18]

2.3.6   Me/SAPO-34 for the reaction

In this thesis, the goal has been to directly convert methane to methanol, in a step-wise process as described in the previous section, using different metal ion-exchanged SAPO-34 zeotypes, as illustrated in Figure 2.15. SAPO-34 is a well studied, versatile and valuable material.[20,33] As elaborated in Section 2.1, its properties such as shape selectivity, acidity and high surface area results in unique catalytic properties. Therefore, SAPO-34 is used as a catalyst for the MTO on an industrial scale, and also performs well for the NH_3 assisted Selective Catalytic Reduction (SCR) of NOx-gases when loaded with copper.[35,36,40,56] In addition, the flexibility in the SAPO-system offers functionalisation possibilities for finetuning the desired catalytic properties.[76] Many metal ion exchanged zeolites and zeotypes have been tested for the dMtM, amongst others ZSM-5, MFI, MOR, beta, EMT, FER, CHA and other silica and alumina oxides, and they are in most cases exchanged with copper ions.[19,120] Despite the fact that Vora et al. concluded that SAPO-34 offers the best route for methane utilization, the literature on SAPO-34 for the dMtM is scarce.[33] Borfecchia et al. reported that copper ion exchanged CHA frameworks exhibited methanol yields of up to 125 $\mu mol_{methanol}/g$.[19,37,39,120]
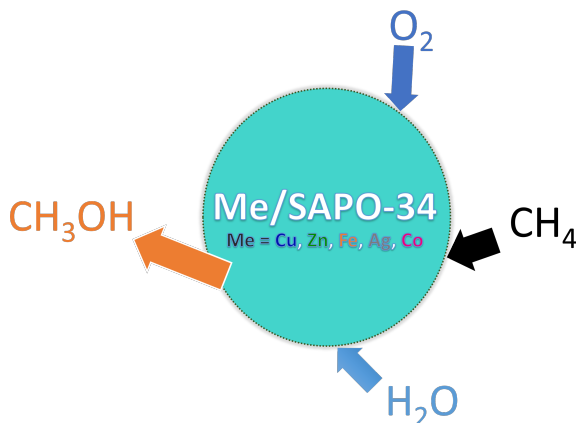
Figure 2.15: Illustration of the stepwise reaction proccess of partial oxidation of methane to methanol by metal ion exchanged SAPO-34.

As mentioned, several transition-metal ions supported on solid surfaces have been proven to activate the C–H bond in methane.[10,18,121] In order to achieve this, the metals used must form σ- or π-complexes from electron transfer between methane and the metal ions.[121] The metals investigated in this master project were copper, zinc, iron, silver and cobalt, all of which have shown promising results for the oxidation of methane.[23,24,26–28,30,32] However, despite the fact that SAPO-34 and the metals (Cu, Zn, Fe, Ag, Co) have shown promise for methane activation, there few instances where other metals than copper have been ion exchanged into SAPO-34 and tested for the dMtM reaction.[19,20,33,37,76,122]

To this day, Cu/SAPO-34 have been proven to activate methane and release methanol upon contact with steam, and the main byproducts are CO and small quantities of dimethyl ether (DME).[19,20] The reported methanol yields are 15 μmol/g (SIE with CuCl$_2$)[19] and 10-12μmol/g (LIE with CuAc$_2$)[20]. Maroni et al. (1989) reported that Co/SAPO-34 has proven to activate methane with a conversion efficiency of 15%.[25] To the extent of my knowledge, neither Ag/SAPO-34, Zn/SAPO-34 nor Fe/SAPO-34 has been tested for methane activation, but have been proven as catalytically active towards other reactions such as SCR, MTO, CO$_2$ hydrogenation, N$_2$O decomposition and others.[76,116,123–131]

An advantage of using Me/SAPO-34 for the dMtM is the fact that first row transition metals are less expensive, rare and water-sensitive than noble metals such as Pt, Ir, Ru, Rh and Pd which are frequently employed as catalysts for highly efficient methane oxidation.[31,94] In addition, it has been shown that the the metal-sites can be recovered in a relatively facile way, which means it can function in a looping cycle, prolonging the catalyst lifetime and subsequently enhance the prospect for commercial application.[19] Furthermore, the confinement within zeotypes like SAPO-34 can also help reduce the free energy of the transition state due to framework interactions such as van der Waals interations and charge stabilization.[18,33]

On the other hand, overoxidation is still a challenge even with the use of a zeotype such as SAPO-34 and a stepwise process.[10,14,18–20] Another disadvantage is the fact that the dMtM through metal sites dispersed on a support material, is not catalytic as it relies on the metal sites and their nuclearity in the material which makes the reaction stochiometric.[19] In other words, the limiting factor is not mass transfer, but the amount of metal exchanged acidic sites and how well they are dispersed.[132] However, for simplicity, the reaction will be considered catalytic.

In summary, the combination of the proposed metals with SAPO-34 as support has in few instances been tested catalytically though both have shown promise for the dMtM. The interest in dMtM shows no sign of waning, but extensive further research and understanding of it is necessary for it to be possible to commericialise.[18]

3   Experimental

3.1   Liquid ion-exchange of SAPO-34

3.1.1   Parent material: Conventional SAPO-34

The parent material of conventional SAPO-34 samples used for ion exchange, were provided by Post.Doc. Daniel Ali in the inorganic research group at the Institute for Chemistry at NTNU, and were synthesized by Dr. Joakim Tafjord. For the synthesis of SAPO-34, a modified pocedure of a BASF patent[133] with tetraethylammonium hydroxide (TEAOH) as the structure directing agent (SDA) was used. The synthesis is described in Section A.1.1 in the appendix, and the parameters for the synthesis of conventional SAPO-34, used as parent material for ion-exchange in this masters project, is listed in Table 3.1.

Table 3.1: Synthesis conditions for the parent material SAPO-34, with molar ratios of Si, Al, P, SDA and water.

Sample name	Si	Al	P	TEAOH	H_2O	Cryst. time	Cryst. temp.
SAPO-34	0.2	1	1	0.9	28	72 h	190°C

3.1.2   Liquid ion exchange

The presented methodology for liquid ion exchange is mainly based on the works of Mathisen et. al.[134] The alternations were 6 hours longer minimum drying time, pH adjustment and different concentrations for the iron ion-exchange solution as a small study of the concentration parameter was conducted.

First, aqueous ion-exchange solutions of the metal ions in question were made by slowly dissolving the corresponding metal nitrate (Cu^{2+}, Zn^{2+}, Fe^{2+}, Ag^+, Co^{2+}, 0.133 M, Sigma-Aldrich) in distilled water under stirring. Approximately 500mg - 1g zeotype of the calcined SAPO-34 support material was added to a 30 mL of the metal nitrate solution. The mixture was left to stir overnight at room temperature, then washed with 100 mL distilled water and centrifuged until clear, but at least four times. The ion-exchange procedure was repeated for a total of three times before the sample was transferred to a petri dish and dried at 80 °C for at least 18 hours.[134] The salts and the concentrations of metal nitrate solution used for the different metal ions that have been ion-exchanged in this thesis are presented in Table 3.2.

Table 3.2: Metal nitrate salts dissolved in distilled water to make metal ion exchange solutions and their respective concentrations, and the sample names for the Me/SAPO-34.

Metal ion	Salt	Concentration(s) [M]	Sample-name
Cu^{2+}	$Cu(NO_3)_2 \times 3H_2O$	0.133	Cu/S34
Zn^{2+}	$Zn(NO_3)_2 \times 6H_2O$	0.133	Zn/S34
Fe^{2+}	$Fe(NO_3)_2 \times 9H_2O$	0.133, 0.065, 0.033, 0.01	MFe/S34
Ag^+	$Ag(NO_3)$	0.133	Ag/S34
Co^{2+}	$Co(NO_3)_2 \times 6H_2O$	0.133	Co/S34
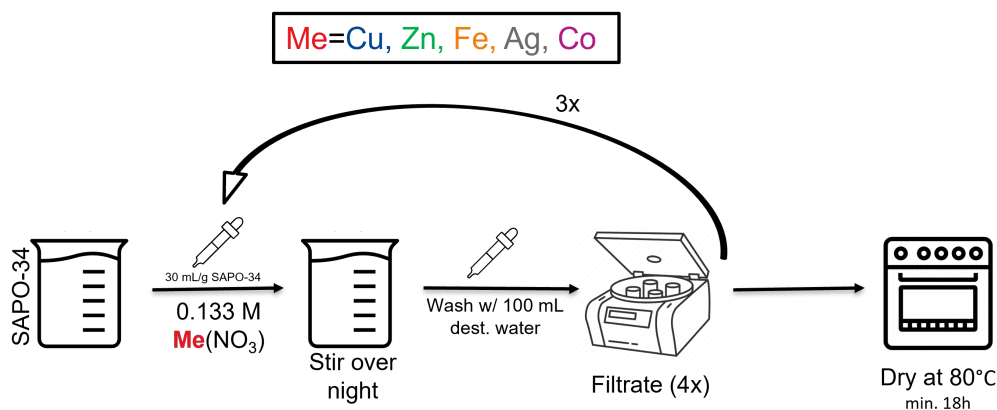
Figure 3.1: Ion exchange experimental

All samples were named Me/S34 where Me is the metal ion (Me=Cu,Zn,Fe,Ag,Co), "/" denotes ion exchanged and S34 stands for SAPO-34. For the iron samples, a small study on concentration and exposure time in the form of rounds of ion-exchange was conducted and the specific details for each solution are described in Table 3.2. Therefore, the concentration (M) of the iron nitrate solution was added to the iron sample names, and for the ones with a different number of overnight IE asterisks (*) was added to the name indicating 1 (*) and 2 (**) rounds of ion exchange.

3.2   Characterization

Several techniques were utilised for characterizing the samples to determine if they were phase pure, had sufficient surface area and other structural properties. The experimental part of these techniques are described in this subchapter.

3.2.1   XRD

To determine the samples phase purity and relative crystallinity, an XRD-analysis was performed with a Bruker D8 A25 Advance DaVinci X-ray diffractometer. In this apparatus a Cu K_α X-ray tube with wavelength 1.5046Å is combined with a lynxeye^{tm} superspeed 1D detector. The divergence slit was set to 0.1 mm and the measured 2θ-angles ranged from from 5-75° with a step size of approximately 0.013° over a 30 minute period for each sample. The conditions were the same for all samples.

Before analysis, the samples were prepared in a 10 mm Si-cavity sample holder, and after analysis the diffraction patterns were plotted by offsetting the y-values. Lastly, the obtained diffractograms of each samples were compared to that of chabazite (CHA), collected from IZA, and shown in Figure 2.8.

In this project SAPO-34 samples loaded with Cu, Zn, Fe, Ag and Co were investigated. In the case of the cobalt-containing samples, fixed slits must be used to net get a gradually increasing background with increasing 2Θ, due to the fluorescence of cobalt.

The relative crystallinity of the ion exchanged samples was calculated from the sum of the more important peaks at $2\Theta \approx 9.5$, 12.9, $20.6^{c}irc$ and relatively compared to that of the mother sample.[124]

3.2.2 Nitrogen adsorption (BET)

The surface area and pore sizes were obtained from a Micromeritics TriStar 3000 Surface Area and Porosity Analyzer. Prior to analysis the samples were weighed and degassed at 250 °C under vacuum with a VacPrep 061 Degasser to clean the surface and pores of the sample for any adsorbed contaminates. Due to low sample amounts of around 20-30 mg, filler rods were used for minimizing measuring errors. After degassing and weighing, the samples were placed in the instrument and cooled down to the liquification temperature of nitrogen (-196ΘrcC). The specific surface area was calculated from the isotherm according to the BET method, while the BJH method was applied to calculate the pore sizes and t-plot for pore volumes. In addition, the t-plot method was used for obtaining information on micropore area and external surface area.

3.2.3 Scanning Electron Microscope (SEM)

performed to determine particle size and mor- phology with a Hitachi S-3400N. A small amount of sample was scattered onto to

A Hitachi S-3400N instrument was applied for SEM imaging. For this projects, SEM analysis was performed to determine particle size and study the morphology of the ion-exchanged samples. Sample preparation was done by placing a carbon tape on a sample holder and scattering small amounts of the sample over mentioned carbon tape. Before mounting the sample into the instrument, excess grains were removed by an air baloon. Prior to turning on the electron beam, the chamber was vacuumed. Images were taken in secondary electron (SE) mode at 15 keV with a magnification of 1.90k and 8.00k.

Further, to determine the particle size, 100 particles were analysed in the ImageJ software for particle size determination.[135] The average particle size was determined by analysing 100 particles of the conventional SAPO-34 sample from the 1.90k magnified image presented in Figure A.5. For this project, the particle size was defined as the length of a side in the cubed particles.

3.2.4 Inductively Coupled Plasma Mass Spectrometry (ICP-MS)

To investigate the metal loading of the ion-exchanged samples and the molar ratio between Si and Al, ICP-MS was performed with a High Resolution Inductively Coupled Plasma ELEMENT 2 connected to an ICP-MS triple quad Agilent 8800. For sample preparation, 20-40 mg of each sample was weighed out in a Teflon tube (25 mL) and decomposed using concentrated nitric acid (HNO_3, 1.5 mL, 65%) and concentrated hydrofluoric acid (HF, 0.5 mL, 40%). The solution was then transferred to a larger Teflon canister and diluted with deionized water to a total weight of around 200-220 g. A 12 mL Teflon sample tube was then washed, first with

deionized water and then three times with the diluted solution. Lastly, the sample tube was filled with the diluted and final sample solution and lined up for ICP-MS analysis. In order to eliminate background noise, three blanks were also prepared and analysed. The ICP-MS analysis of the prepared samples were conducted by Anica Simic (IKJ, NTNU).

3.3 Experimental methane activation,

The metal ion-exchanged SAPO-34 samples with sufficient surface area and phase purity were catalytically tested for for the stepwise oxidation of methane to methanol. The experimental reaction setup is illustrated in Figure 3.2 and the temperature profile in Figure 3.3.
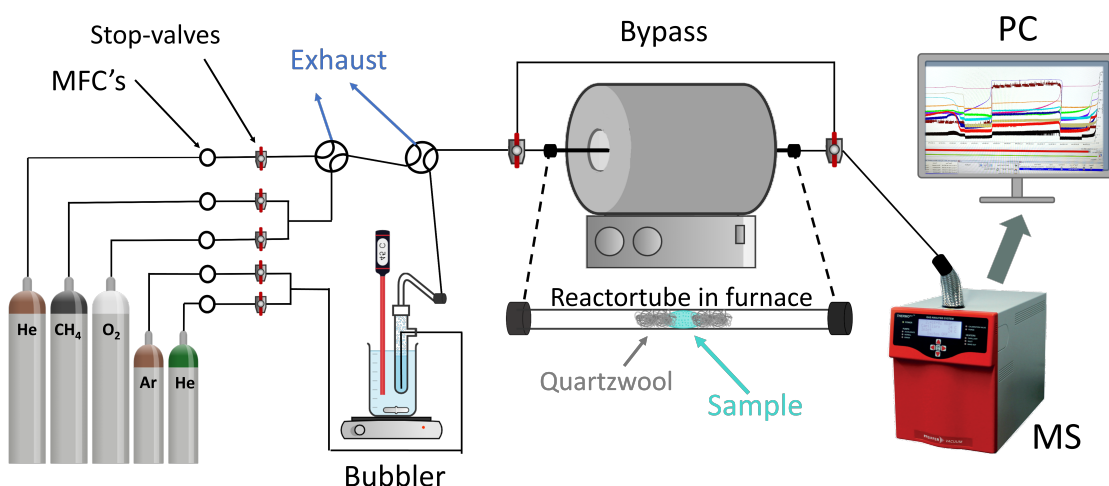
Figure 3.2: The catalytic reaction setup for the dMdM. Illustration inspired by Kvande[20] and Florence and picture in the lab, and some components are from chemix.org.

First, to control particle size distribution, 50-100 mg of the SAPO-34 samples were sieved out to achieve a particle size of 212-425 µm. Second, the particle size was packed into a glass lined stainless steel reactor with an inner diameter (ID) of 4mm and an outer diameter (OD) of 1/4". Inspired by Kvande et al. the following procedure for the catalytic study was conducted. The reactor was heated to 500°C at ramp rate of 1 °C/min in oxygen (O_2, 10% in He, 20 mL/min), and kept at 500°C for approximately 9 hours. Then the reactor was cooled to the desired reaction temperature of 300 °C with a ramp rate of 5 °C/min. Meanwhile the reactor was flushed with He (20 mL/min) to remove excess O_2 for the duration of the cool down (around 40 min), plus an additional 30 min after reaching the desired reaction temperature. Further, the catalyst was contacted with methane (CH_4, 99%, 20 mL/min) for a minimum of 3 hours. Last, an extraction of products was conducted with approximately 10% water in the stream was obtained by sending a mixture of He and Ar (20 mL/min, 10% Ar) through a H_2O-containing saturator at 45°C, corresponding to a vapor pressure of water of 9.325 kPa.[66] Argon was used as a reference gas. The extraction period tenses for about 2-3 hours, where
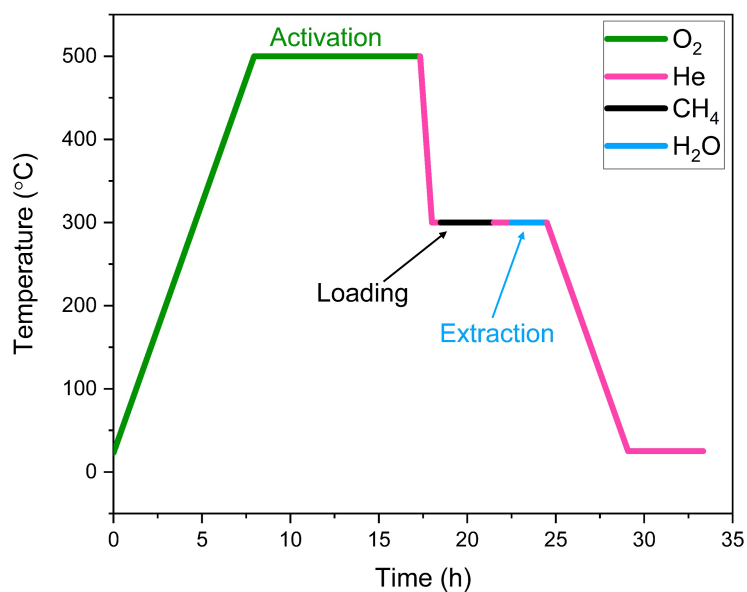
Figure 3.3: Temperature profile used for the direct conversion of methane to methanol by metal ion exchanged SAPO-34. The figure shows the temperature and the time for each step of the stepwise dMtM. All flow rates were 20 mL/min.

methanol production was continuously monitored, or until there were no products detected in the effluent.[20,136]

Methane activation was measured in terms of relative quantification of produced methanol identified with an online MS, ThermoStar GSD320, and compared to the reference of argon gas (2 mL/min).

4 Results

Results from ion exchange, characterisation techniques and performance for methane activation are presented in this chapter, and will further be discussed in the following chapter. The Me/SAPO-34 samples have been characterised by XRD, nitrogen physisorption, elemental analysis by ICP-MS and SEM. As mentioned, the samples are named Me/S34 which denotes Me for the metal ion in question and S34 for SAPO-34. Additional results are to be found in the appendix.

4.1 Observations from ion exchange

In Figure 4.1 a picture of one of each metal ion-exchanged sample is presented. From observation, a color change from white to light blue and light orange powder is observed for the Cu/S34 and Fe/S34, respectively. This can indicate the presence of metal ions in the samples.[137] Closer pictures of all samples, including the conventional SAPO-34, is to be found in Figure A.6 in the appendix.
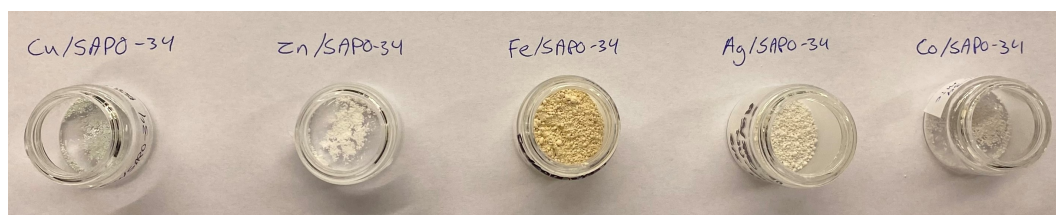
Figure 4.1: A picture of one of each of the metal ion exchanged samples of SAPO-34. From the left: Cu/S34, Zn/S34, Fe/S34, Ag/S34 and Co/S34.

The yield in the different samples after ion exchange are presented in Table 4.1, and based on the data, SAPO-34 was successfully metal ion-exchanged with metal nitrate solutions (0.133 M) of Cu, Zn, Fe, Ag and Co. A trend for the achieved yield after liquid ion exchange (LIE) with metal nitrates for SAPO-34 can appear to be in the order of Fe<Co<Zn<Cu<Ag.

Table 4.1: Yields of liquid ion exchanged samples of SAPO-34 with metal nitrate solutions.

Sample	Sample name	Yield after IE[%]	Further analysis?
Cu/SAPO-34	Cu/S34	72.9	✓
Zn/SAPO-34	Zn/S34	71.4	✓
Fe/SAPO-34	0.1Fe/S34	0	✗
Fe/SAPO-34	0.1Fe/S34**	0	✗
Fe/SAPO-34	0.1Fe/S34*	18.0	✓
Fe/SAPO-34	0.06Fe/S34	0	✗
Fe/SAPO-34	0.03Fe/S34	0	✗
Fe/SAPO-34	0.01Fe/S34	66.3	✓
Ag/SAPO-34	Ag/S34	83	✓
Co/SAPO-34	Co/S34	77.0	✓

4.1.1   Parameter study on ion exchange with iron nitrate solution

As indicated by Table 4.1, most iron samples gave a yield of 0%. The calcined SAPO-34 sample appeared to dissolve in the iron nitrate solution upon ion exchange, as it was observed that the colour of the solution went from milky orange to clear orange on the second round of ion-exchange with 0.133 M solution. Multiple attempts were conducted in order to get a viable Fe/SAPO-34 sample. First, the ion-exchange time was investigated by attempting three, two and one round(s) of overnight ion-exchange, and of the 0.1Fe/S34-samples only the one round overnight gave a positive yield of 18%. Second, the pH of the iron ion-exchange solution was measured to around 1-2, which was a highly acidic compared to that of the other metal ion solutions which were all around 4-5. Based on similar iron ion exchange procedures by Park et. al and Zhang et al, pH-control was conducted in the form of dropwise addition of ammonium.[115,116] Unfortunately, the different attempts on pH-control did not result in better yields. Third, varying the concentration of the solution, while keeping the exchange-time of three rounds overnight constant, was attempted to ameliorate the yield of iron ion exchanged SAPO-34. These samples were named 0.06Fe/S34, 0.03Fe/S34 and 0.01Fe/S34, and only the 0.01-sample gave a yield dried product of 66.3%, whereas the other were zero. The Fe/SAPO-34 samples which had not dissolved during ion-exchange, namely 0.1Fe/S34* where * indicates one round and 0.01Fe/S34, were then taken to be analysed by PXRD.

4.2 Characterization

4.2.1 XRD

Powder X-ray diffraction (PXRD) was conducted to verify phase purity, crystallinity and discover possible structure collapse. In this subsection, diffractograms of the crystalline samples obtained from the XRD-analysis are presented. First, Figure 4.2 shows the diffractogram of the parent material conventional SAPO-34 in comparison to that of chabazite (CHA), and confirms that the mother sample is phase pure.
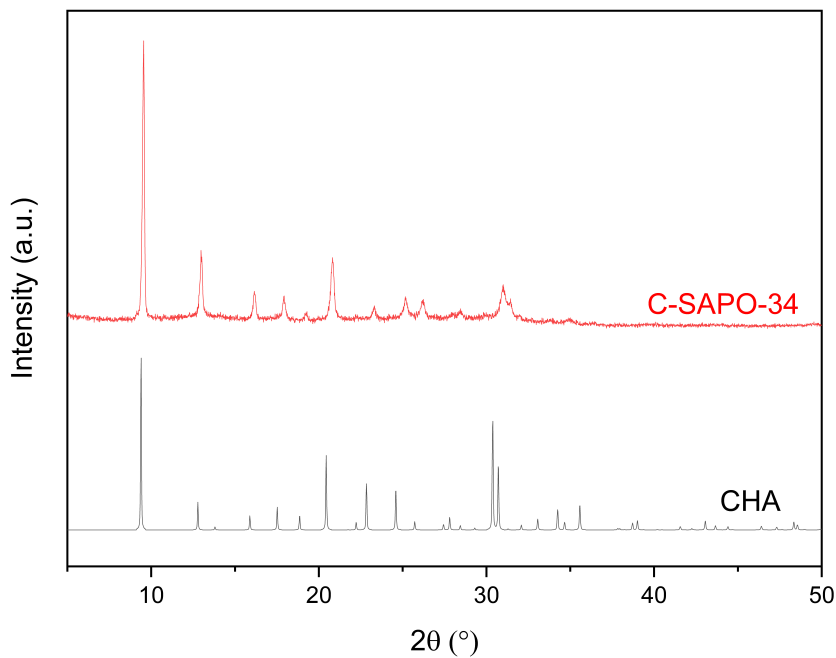
Figure 4.2: Diffractograms from 2θ=5-50° of the conventional SAPO-34 in comparison to that of chabazite. The CHA reference is from IZA.[34]

34

Second, Figure 4.3 shows the metal ion-exchanged samples, compared to the mother sample and CHA. From the XRDs, it appears that Co/S34, Ag/S34, Zn/S34 and Cu/S34 are phase pure post ion exchange with their respective metal nitrate solutions.
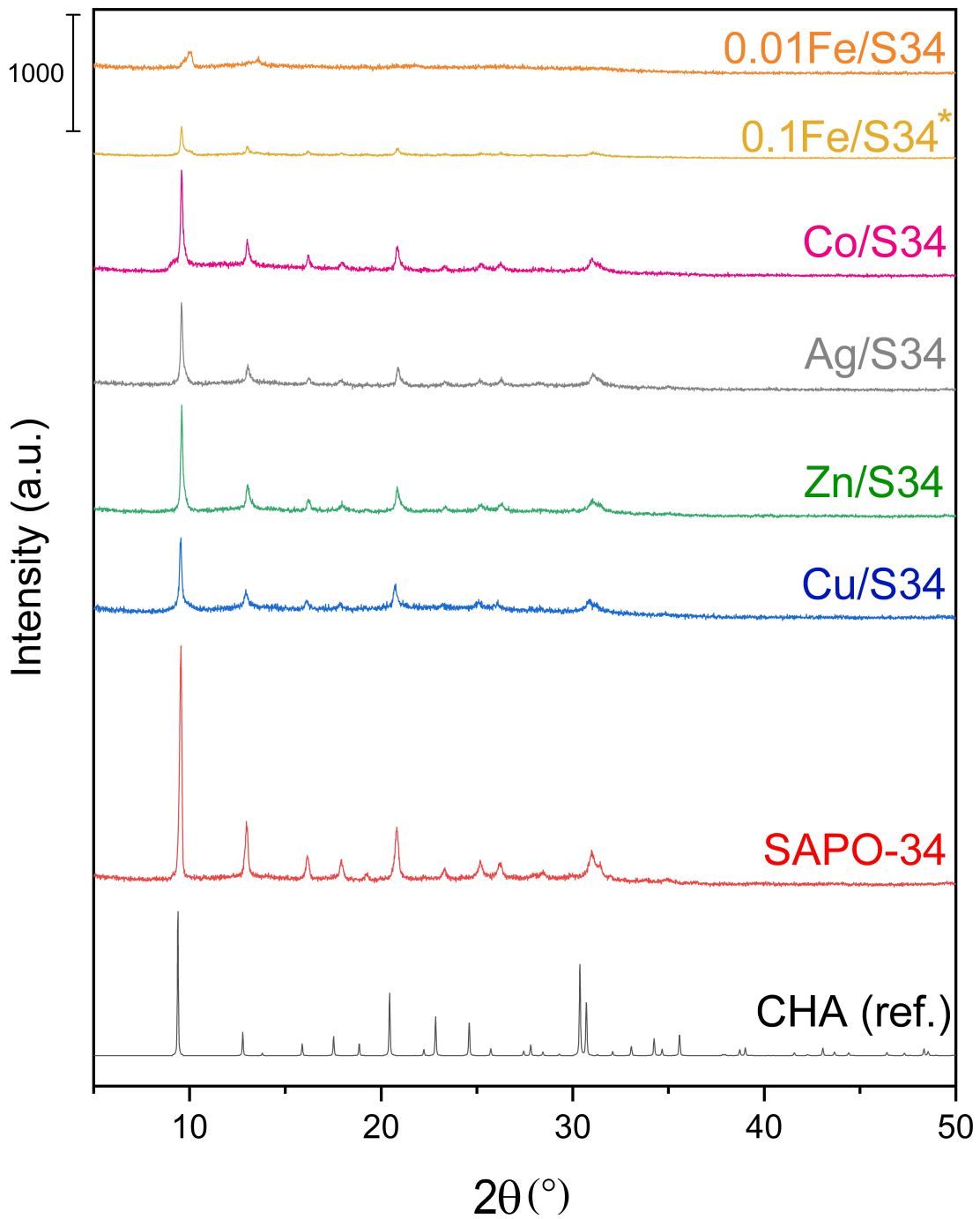
Figure 4.3: Diffractograms of the ion-exchanged samples from $2\Theta=5\text{-}50°$, in comparison to that of chabazite[34] and the conventional SAPO-34.

However, it is apparent that the ion exchanges samples have lower intensities than that of the mother sample, as expected as reduced crystallinity is common after liquid ion exchange.[138,139] Among the investigated Me/SAPO-34, Cu, Zn and Ag have been reported to obtain relative crystallinities of 19-97%.[76,124,140–142] For ion exchange with Fe, reduced crystallinity have been reported on other supports,[131,143] whereas Co/SAPO-34 have been reported to retain their crystallinity after ion exchange and an additional calcination.[128,129] It should be noted that the results in this project are obtained after drying, and without an additional heat treatment or calcination post ion-exchange.

The relative crystallinity of the ion exchanged samples was calculated as explained in section 3.2.1, and the obtained results are presented in Table 4.2.

Table 4.2: Relative crystallinities of the three important reflections (2θ=9.5, 12.9 and 20.6) compared to that of the conventional SAPO-34 sample.

Sample	Relative crystallinity [%]
SAPO-34	100
Cu/S34	42.1
Zn/S34	50.6
Ag/S34	40.6
Co/S34	50.3
Fe/S34(1.0.13)	32.6
Fe/S34(3*0.01)	12.4

From the PXRD analysis, the phase pure samples with a relative crystallinity of more than 40% were chosen for further analysis as this was deemed to be a satisfactory crystallinity. In Table 4.3 the samples chosen for further analysis are presented.

Table 4.3: Conclusion after the results from PXRD analysis of Me/SAPO-34 samples.

Sample name	XRD results	Relative crystallinity [%]	Further analysis?
Cu/S34	CHA	42.1	✓
Zn/S34	CHA	50.6	✓
0.1Fe/S34*	CHA	32.6	✗
0.01Fe/S34	amorphous	12.6	✗
Ag/S34	CHA	40.6	✓
Co/S34	CHA	50.3	✓

4.2.2 Nitrogen physisorption

Total surface area of solid catalysts is often correlated to catalytic activity as it determines the accessibility of active sites.[5,83,86] Therefore, total surface area is usually related to the catalytic activity, and it is thus highly desirable to obtain a high specific surface area. Nitrogen physisorption was used to estimate the BET surface area, micropore area and pore volume of the metal ion exchanged SAPO-34 samples and their parent material.

Table 4.4 shows the obtained results of surface area and pore volume for all samples that were phase pure and had maintained their crystallinity after ion exchange treatment. Further, the adsorption/desorption isotherms are presented in Figure 4.4 and the particle size distribution (PSD) is to be found in Figure A.1 in the Appendix. Both of which exhibit behaviours which is characteristic for microporous materials.[5,47,85]

Table 4.4: Data from N_2 adsorption analysis.

Sample name	Surface area (m^2/g)			Pore volume (cm^3/g)		
	BET	Micro	External	Total	Micro	Meso
SAPO-34	510	486	25	0.28	0.25	0.03
Cu/S34	286	266	20	0.17	0.14	0.03
Zn/S34	300	265	35	0.15	0.12	0.03
Ag/S34	228	175	54	0.13	0.09	0.04
Co/S34	326	297	30	0.18	0.15	0.03

The surface area of the parent material, SAPO-34, was within the previously reported range for conventional SAPO-34 in the literature of 450-700 m^2/g.[19,20,33,87,144] For the ion exchanged samples, the surface area ranges from 228-326 m^2/g which corresponds to a loss of surface area of 36-55%. This is within the range of what has been reported in literature for surface area loss in ion exchanged Me/SAPO-34 of 3-68%.[20,123–125,127,128,141,145,146]

The obtained surface areas increases in the order of Ag/S34 < Cu/S34 < Zn/S34 < Co/S34, while the pore volumes show an increase in the order of Ag/S34 < Zn/S34 < Cu/S34 < Co/S34.

Further, the isotherms of all samples investigated with nitrogen physisoprtion is presented in Figure 4.4, and show behaviour of Type I as expected for microporous materials.[85]
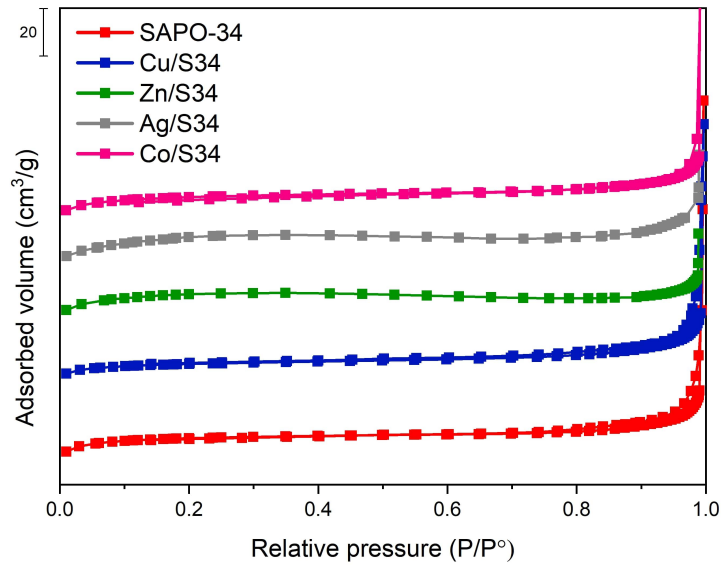
Figure 4.4: Nitrogen adsorption/desorption isotherms of SAPO-34 and Me/S34 (Me = Zn, Cu,Ag,Fe, Co).

From the results of the nitrogen physisorption analysis, it was determined that a surface area of at least 200 m^2/g was needed for further analysis and catalytic testing. The conclusion in form of which samples are chosen to be analysed furhter are presented in Table 4.5.

Table 4.5: Conclusion after the results obtained from PXRD and nitrogen physisorption of Me/SAPO-34 samples.

Sample name	XRD results	BET surface area [m^2/g]	Further analysis
Cu/S34	CHA	286	✓
Zn/S34	CHA	300	✓
Ag/S34	CHA	228	✓
Co/S34	CHA	326	✓

4.2.3 ICP-MS

Elemental analysis by ICP-MS was conducted to verify metal content, determine the metal loadings of the ion exchange samples in the form of weightpercent (wt.%) and investigate the ratio of Si/Al for all SAPO-34 samples. Table 4.6 shows the obtained results for all the ion exchanged samples and their mother sample, SAPO-34, and the detailed data is presented in Table A.2 and Figure A.2 in the appendix.

Table 4.6: Metal loadings and Si/Al ratio from ICP-MS for the ion exchanges SAPO-34 samples.

Sample	Si/Al-ratio$_{theoretical}$	Si/Al-ratio$_{experimental}$	Metal content [wt.%]
SAPO-34		0.26	-
Cu/S34		0.26	1.0
Zn/S34	0.2	0.26	0.4
Ag/S34		0.25	5.1
Co/S34		0.27	0.1

First, the Si/Al-ratio has increased from the theoretical value based on the synthesis of the parent material for all samples investigated. On the other hand, when comparing the ion exchanged samples to their parent materials Si/Al-ratio of 0.26, there are no large deviations and the ratio for the ion-exchanged samples vary from 0.25-0.27. An illustration of the Si/Al-ratio is presented in the appendix (Figure A.4). Second, Figure A.3 shows a large variation in metal load between the ion exchanged samples, varying from 0.1 wt.% for Co/S34 to 5.1 wt.% for Ag/S34. In total the trend between the different metal ions ion exchanged is as follows, in an increasing order: Co/S34 < Zn/S34 < Cu/S34 < < < Ag/S34.

Despite the large differences, this is to be expected based on what is reported for liquid ion exchange of SAPO-34 with the respective metals.[19,20,64,123,124,128,140,145,146,146]

Based on the results from the elemental analysis, the investigated samples had satisfactory metal loads to catalytically test their performance for methane activation. Before catalysis, SEM was conducted to elucidate possible changes in morphology. The conclusion after XRD, BET and ICP-MS is presented in Table 4.7.

Table 4.7: Conclusion after XRD, nitrogen physisorption and ICP-MS results.

Sample	XRD	BET surface area [m^2/g]	Me-load [wt.%]	Further analysis?
Cu/S34	CHA	286	1.0	✓
Zn/S34	CHA	300	0.4	✓
Ag/S34	CHA	228	5.1	✓
Co/S34	CHA	326	0.1	✓

4.2.4 SEM

SEM images were taken of the samples to determine particle size of the parent material, confirm the morphology of all samples and to investigate if the ion-exchanged samples had any striking differences or defects relative to the parent material. Small particles are desirable, as diffusion of reactants into porous networks have been reported to improve with smaller particle size, and the software ImageJ was utilised to determine particle size.[70,135,147]

Figure 4.5 presents the SEM images of SAPO-34 and its metal ion exchanged derivatives at a magnification of 8.00k. Additional SEM images of all samples at a magnification of 1.90k is to be found in and Figure A.5 in the appendix. From the images, it is observed that the conventional SAPO-34 and Me/SAPO-34 samples have a cubic morphology as expected for the typical CHA structure from literature.[148–150] There does not appear to be any striking differences in morphology for the ion exchanged samples.

In addition, the obtained average particle size was 1.7 μm for the conventional SAPO-34 sample, and the distribution of the analysed particles are presented in Figure A.10 in the appendix. SAPO-34 has been reported to have cubic particles in the size-range 0.6-9 μm, and the analysed sample is thus within the reported range.[70,148] Based on the SEM images of SAPO-34 and the Me/SAPO-34 samples, there does not appear to be any significant morphological change caused by the metal introduction by LIE.[125] Both the morphology and particle size is in accordance with what has been previously reported for SAPO-34 and Me/SAPO-34 with particle sizes ranging between 0.8 and 9μm.[70,125,130,146,148–150]

A summary of all the results obtained from the characterisation techniques used to investigate the Me/S34 samples are presented in Table 4.8 which lead up to the conclusion of catalytically testing Cu/S34, Zn/S34, Ag/S34 and Co/S34 for the partial oxidation of methane to methanol.

Table 4.8: Conclusion after XRD, nitrogen physisorption, ICP-MS and SEM results.

Sample	XRD	Surface area [m^2/g]	Me-load [wt.%]	SEM	To catalysis?
Cu/S34	CHA	286	1.0	✓'	✓
Zn/S34	CHA	300	0.4	✓	✓
Ag/S34	CHA	228	5.1	✓	✓
Co/S34	CHA	326	0.1	✓	✓
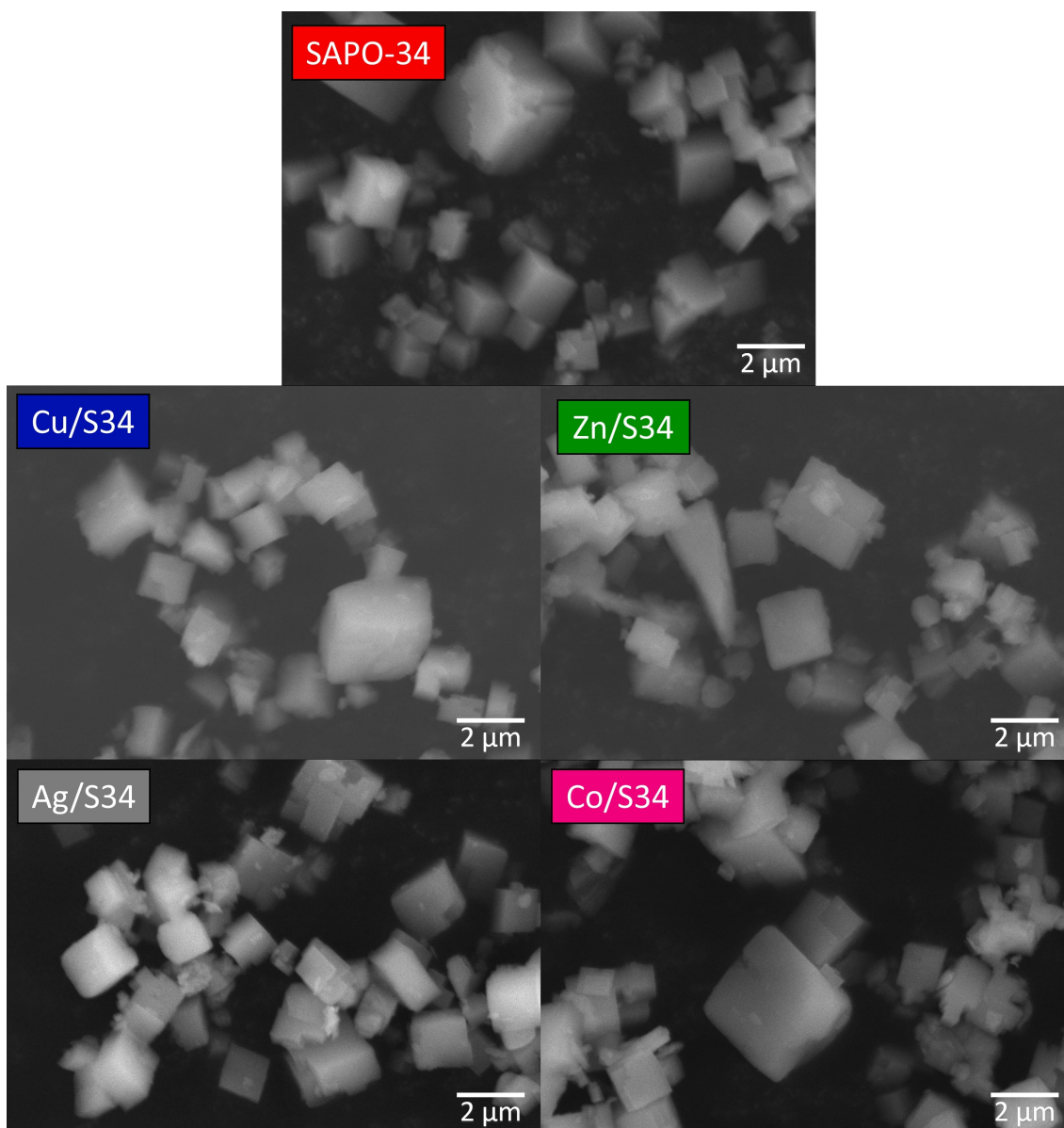
Figure 4.5: SEM images of SAPO-34 and the metal ion exchanged samples, taken in SE mode with magnification 8.0k.

4.3   Me/SAPO-34 for the partial oxidation of methane

The catalytic test of the metal ion exchanged samples for methane activation were performed as described in Chapter 3.3. Their perfomance for the partial oxidation of methane in terms of integrated MeOH signals is graphically presented in Figure 4.7 and Figure 4.8.

The metal containing samples with adequate phase purity, surface area and metal loading were tested towards the partial oxidation of methane. These were Cu/S34, Ag/S34, Co/S34 and Zn/S34. Their catalytic performance was compared relatively, and the activity of an empty reactor and the conventional SAPO-34 sample were used as reference points. Figure 4.6 shows the MeOH-signals normalised in regard to sample mass and the signal of the reference gas of argon. Cu/S34 appears the most active, as expected from literature reports.[20,111,112]
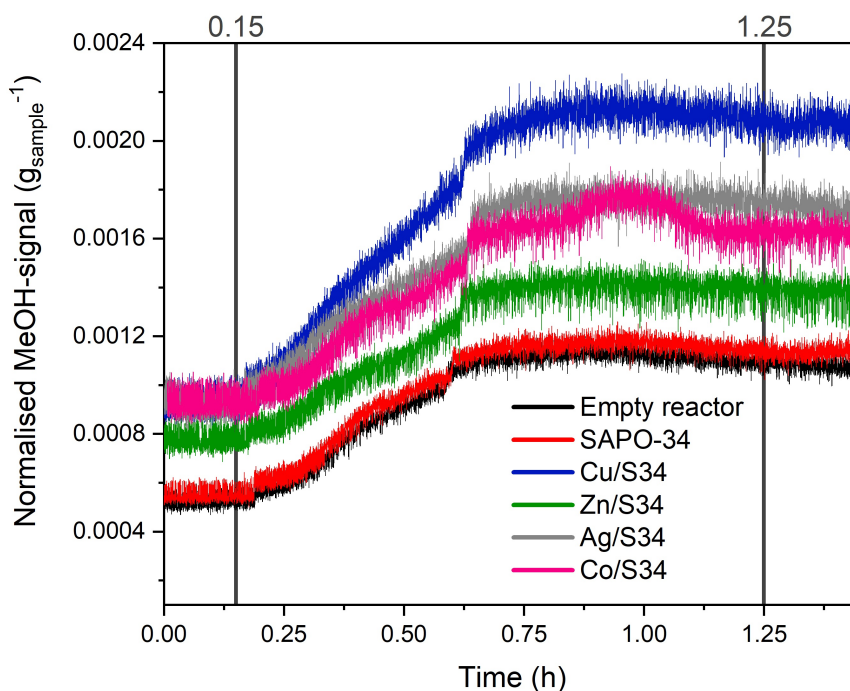
Figure 4.6: Normalised MeOH-signal for all samples. The signal is normalised with regard to the reference gas of argon, and is found by dividing the MeOH-signal with the Ar-signal. In addition, the x-values (time) are offset.

The integrated area from x=0.15 to x=1.25, marked on the x-axis (time) in Figure 4.6, of the normalised signal resulted in the areas illustrated in Figure 4.7. Further, an illustration of all integrated signals, including empty reactor and conventional SAPO-34 are to be found in Figure A.7 in the appendix, which show low values as expected, whereas the metal containing samples increased in the order of Zn/S34 < Co/S34 < Ag/S34 < Cu/S34.
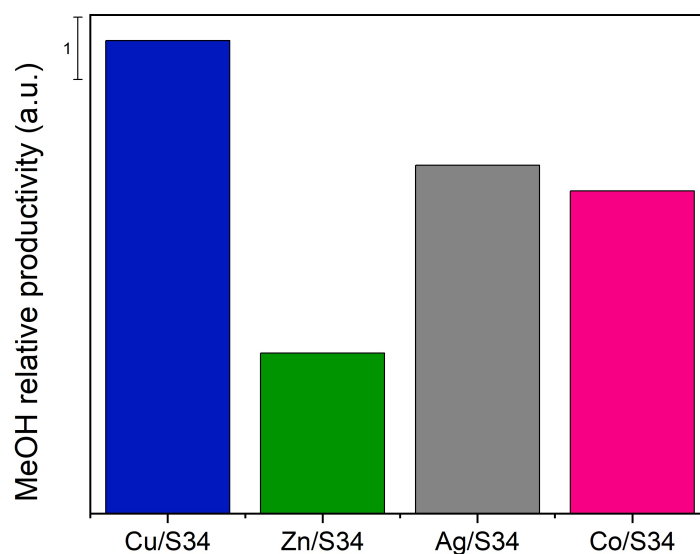
Figure 4.7: Relative MeOH productivity of Me/SAPO-34, calculated from the integrated area under the normalised MeOH signal from x=0.15 to x=1.25. Values are $*10^{-4}$.

On the other hand, when dividing the integrated area by the metal loading an entirely different trend occurs: Ag/S34 < Zn/S34 $\approx$ Cu/S34 < < < Co/S34.
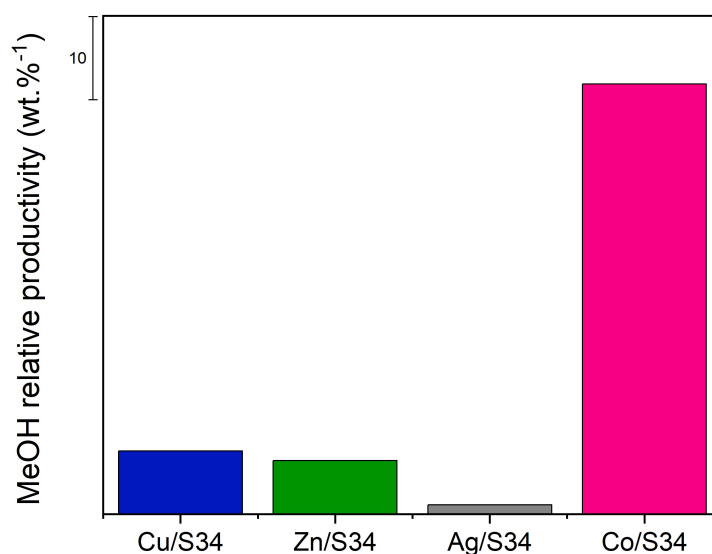
Figure 4.8: MeOH relative productivity as a function of metal wt.%, integrated from x=0.15 to x=1.25 of the normalised MeOH signals. Presented values are $*10^{-4}$.

To summarise, Cu/S34 produced the most methanol of the samples investigated as expected. However, methanol productivity relative to metal content showed that Co/S34 exhibited a particular high methanol production per metal load compared to the other samples. In this regard, Ag/S34, which had a high metal load produced, very little methanol per metal wt.%. Further, Zn/S34 produced almost the same amount of methanol as Cu/S34 when taking the metal load into consideration.

5   Discussion

The main objective in this thesis was to investigate the effect of ion exchanging Cu, Zn, Fe, Ag and Co into conventional SAPO-34, and evaluating the catalytic performance of the Me/SAPO-34 samples for the direct methane to methanol (dMtM).

First, how the ion exchange of the different metals influenced crystallinity, surface area, pore volume and metal load compared to the conventional SAPO-34 will be discussed. Since no significant morphological changes appeared from SEM imaging as all the samples displayed a similar morphology of typical cubic crystals with an average size of around 2 μm, the effect of morphology will not be discussed. Second, the catalytic properties for the partial oxidation to methanol of the chosen Me/SAPO-34 samples will be discussed in terms of which factors appear to have influenced their performance. A summary table of relevant data obtained from XRD, nitrogen physisorption, ICP-MS and catalytic methane activation of the ion exchanged samples and their parent SAPO-34 is presented in Table 5.1. In the table, relative crystallinity (RC) and loss in surface area and pore volume compared relatively to the parent SAPO-34 is also documented.

Table 5.1: Summary table of results for discussion. Phase purity (CHA), relative crystallinity (RC), surface area, pore volume, metal weight percent and relative MeOH yield (integrated area under signal normalised to sample mass). The results are obtained from a)XRD b)BET c)ICP-MS and d)Catalysis.

| Sample | XRD[a] | | Surface area[b] | | Pore volume[b] | | Metal[c] | MeOH[d] |
	CHA	RC	[m²/g][b]	Loss [%]	[cm³/g]	Loss [%]	[wt.%]	[a.u.]
SAPO-34	✓	100	510	NA	0.28	NA	NA	$11.1*10^{-4}$
Cu/S34	✓	42	286	44	0.17	39	1.0	$18.6*10^{-4}$
Zn/S34	✓	51	300	41	0.15	46	0.4	$13.6*10^{-4}$
Ag/S34	✓	41	228	55	0.13	54	5.1	$16.6*10^{-4}$
Co/S34	✓	50	326	36	0.18	36	0.1	$16.2*10^{-4}$

5.1   Evaluation of metal ion exchanged SAPO-34

The metal ion exchanged samples (Me = Cu, Zn, Fe, Ag and Co) showed noticeable differences in crystallinity, surface area, pore volume and especially metal content. In the following section, these differences in characterisation will be discussed. As the Fe/S34-samples did not exhibit sufficient phase purity and crystallinity, they will only be discussed in regard of the XRD analysis.

5.1.1   Effect of metal type on IE

Despite being metal ion exchanged by the exact same procedure, the metal loading varies from 0.1 to 5.1 wt.%. By comparison, the Ag/S34 sample had a metal wt.% more than 50 times higher than that of Co/S34 (0.1 wt.%) and approximately 5 times higher than that of Cu/S34. In literature, Ag/SAPO-34 is reported with metal

loadings of 4.2-9.0 wt.% Ag.[64,123,124] Rivera-Ramos and Hernández-Maldonado attributes this to the cation radii (1.26 Å) and relative position of Ag^+-ion.[123] As can be seen in Table 2.1 in the theory, the hydrated diameter of Ag^+ is generally lower (4.7 Å) than that of the other metals tested in this project (6-6.8 Å) which could explain why Ag more readily ion exchanged into the structure.[69,80,151] In other words, it appears that the Ag-ions can easier penetrate the small pores of the SAPO-34 framework and has higher affinity for SAPO-34 than the other metals tested, which could possibly explain the high metal content compared to the other samples.

Further, the Co/S34 exhibited the lowest metal content of all samples analysed with a 0.1 wt.% Co. In contrast to the Ag/S34 sample, this cannot be attributed to cation size as the hydrated cation of Co^{2+} is in fact slightly smaller than that of Cu^{2+} and Zn^{2+}.[80] However, lower metal loading of Co in SAPO-34 is in correspondence with what has been previously reported.[128,146] Zhong et al. reported that both Zn and Cu cations exhibit larger metal loads compared to Co cations when liquid ion exchanged under otherwise identical conditions, and ascribed the effect to differences in dissociation energy between the hydrated metal ions and the water ligands.[146] Xu et al. also experienced difficulties increasing the Co content in SAPO-34 by LIE with cobalt nitrate solution, and by extending the exchange time the maximum Co content achieved was 0.45 wt.%.[128]

Cu and Zn exhibited metal loadings of 1.0, and 0.4, respectively. Both of which is within the range for what is previously reported in literature of 0.4-3.6 wt.% Cu[19,20,140,145,146] and 0.1-1.4 wt.% Zn[64,146]. In other words, though the metal content varies a lot between the samples, all are in the range for previously reported metal contents in SAPO-34 of their respective metal ion, and thereby the results for metal content are as expected. Nonetheless, it should be noted that due to large differences in metal loadings within the sample set, it may be difficult to distinguish between the effect of metal type and the effect metal load on crystallinity and surface area measurements.

Evaluation of Si/Al-ratio

The Si/Al-ratio calculated from elemental analysis by ICP-MS of Cu/S34 and Zn/S34 are the same as for their parent SAPO-34 of 0.26, whereas Co/S34 is slightly higher (0.27) and Ag/S34 is slightly lower (0.25). A possible explanation for this can be the amount of metal introduced into the structure, since Ag/S34 and Co/S34 vary the most in metal load. However, the deviations are very small and so it does not appear to deviate from the parent material. A last note in relation to the Si-Al-ratios, is the fact that all values are higher than the theoretical value of 0.20 from the synthesis of the conventional SAPO-34.

5.1.2   Effect of IE on crystallinity
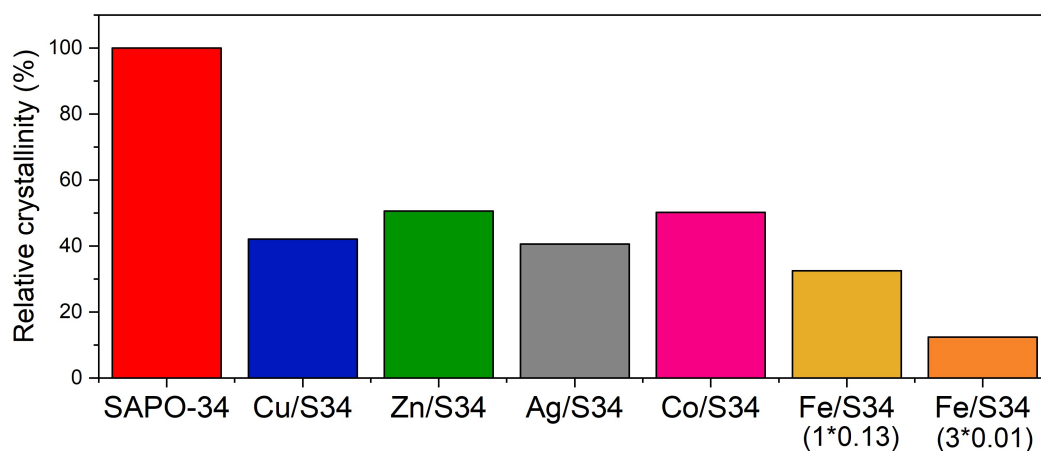
Figure 5.1: The relative intensity of the first characteristic reflection peak compared to the parent material. REMOVE IRON and/or change name

For all ion exchanged samples a decrease in crystallinity of around 50-70% compared to the parent sample was observed. Reduction in crystallinity is expected as this has been reported for Cu[140–142] and Ag[124] exchanged SAPO-34. Shalmani et al. reported Zn/SAPO-34 with 0.01-0.05 wt.% Zn to experience relative crystallinities of 19-90%, and though this was with another method for metal introduction it shows that for Zn introduced SAPO-34 the relative crystallinity may vary a lot.[76] For Fe, reduced crystallinity have been reported for aqueous ion exchange of Fe into the mordenite (MOR) zeolite and for Fe-incorporated SAPO-34.[131,143].

On the other hand, there are groups that have reported that SAPO-34 samples modified with conventional ion exchange (CIE) of Cu, Zn and Co maintained their crystallinity well.[146] Especially Co/SAPO-34 has not been reported to experience reduced crystallinity after ion exchange when additionally heat treated with a post ion exchange calcination.[128,129] The Co/S34 sample in this thesis did exhibit a relative crystallinity of 50%, similar to that of Zn/S34 and higher than the remaining samples, but this was the calculated relative crystallinity without any additional heat treatment other than drying at 80°C for 18h. Based on this, to ameliorate the relative crystallinity of the samples an additional heat treatment could be added to the ion exchange procedure for future works.

Additionally, there are no prominent signs of detectable metal oxides on the XRDs of the samples as can be seen in Figure 4.3. This suggests that the metal species are well dispersed on the SAPO-34.[128]

Nevertheless, a gradual reduction in relative crystallinity with increasing metal content in SAPO-34 have previously been reported.[125,146] The observed trend in relative crystallinity was Ag/S34 < Cu/S34 < Co/S34 < Zn/S34, which is almost the opposite trend of metal content (Co/S34 < Zn/S34 < Cu/S34 < Ag/S34) However, the difference in RC between Co/S34 and Zn/S34 is minimal (1%). At the same time, the metal load of Zn/S34 is 4 times higher than that of Co/S34, indi-

cating that the reduction in crystallinity cannot be explained by this trend alone. Therefore, there are probably other factors contributing to the loss of crystallinity in the investigated samples such as properties of different the metal types. Another possible explanation could be partial degradation or collapse of the porous structure during ion exchange, which has been reported for SAPO-34 previously.[79,145,152,153] This could be caused by irreversible hydrolysis where water molecules attached to the oxygen bridge between Si and Al in the structure and amorphous complexes are formed.[79,152,153] A possible solution to prevent this proposed by Xu et al. was using the ammonium form of SAPO-34 for structure protection during aqueous ion exchange.[153]

Of particular interest, is the fact that liquid ion exchange (LIE) with iron appeared to damage the crystal structure of SAPO-34 the most. The multiple attempts to ion exchange SAPO-34 with iron nitrate without total or severe weight loss are elaborated in Section 3.1. One possibility is that the pH of the iron nitrate solution was too low. Park et al. reports pH control in their IE procedure of Fe into ZSM-5 by adding ammonia solution, but this was attempted and did not work for the Fe/S34 samples in this project.[115] Another possibility may be that the conventional aqueous ion exchange with iron is challenging for SAPO-34 and other CHA materials because of their small pore size and the facile oxidation of Fe^{2+} into Fe^{3+}.[131] In aqueous solution hydrated Fe^{2+} and Fe^{3+} have ionic diameters of 6 Å and 9 Å, respectively.[80] A possible solution for future work to catalyitcally test Fe/SAPO-34, could be to ion exchange iron under an inert atmosphere, as this has been reported to hinder the oxidation of Fe^{2+} into Fe^{3+}.[154]

5.1.3 Effect on surface area and pore volume

Generally, the LIE procedure reduced the surface area and pore volume by 36-55% and 36-54%, respectively. The loss of surface area for metal ion exchange varies a lot in literature: for Ag/SAPO-34 surface area loss of 17-44% have been reported[123,124]; for Cu/SAPO-34 surface area loss of 1-68% have been reported[20,141,145,146]; for Zn/SAPO-34 surface area loss of 3-43% have been reported[125,146] and for Co/SAPO-34 surface area loss of 5-18% have been reported.[127,128,146] Similar trends can be seen for the pore volumes, and will therefore not be elaborated in detail.[20,123–125,127,128,141,145,146] A graphical presentation of the micropore- and external surface areas, and the micro- and meso-pore volumes is to be found in Figure 5.2.
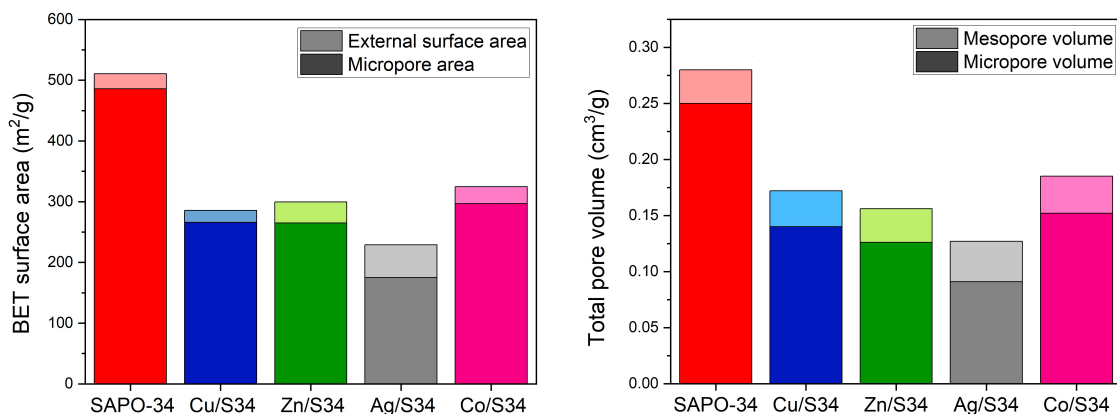
Figure 5.2: BET surface area and pore volumes of the SAPO-34 samples.

A general observation is that the smallest reported loss of surface area is a lot lower for Cu, Zn and Co compared to that of Ag, which corresponds with the samples investigated in this project. Ag/S34 experience a greater loss in surface area and pore volume than Cu/S34, Zn/S34 and Co/S34, and the reason for this may be due to the much higher metal load in Ag/S34. In lack of Ag/S34 samples with different metal load this is difficult to say for certain. Mirza et al. addressed the decrease in surface area of Ag-ion exchanged SAPO-34 to penetration of silver oxide into the pores making the pore diameter more narrow and possibly blocking some of the micropores.[124] However, this may not be the case as the XRD of at least 0.1Fe/S34 appeared to be phase pure. Supporting the theory of higher metal loadings causing greater loss of surface area is Urrutxua et al. which also reports a reduction in BET surface area with increasing metal content for Cu/SAPO-34, and attributed this to pore blockage with Cu-aggregates.[145] Since Ag-ions are known to form clusters, it is a possibility that the high metal load is responsible for the large decrease in surface area for Ag/S34.[123]

As mentioned, among the samples investigated the trend in surface areas has an inverse relationship with the trend for metal content. Subsequently, it can be deduced that higher metal loadings most likely have a negative effect on surface area. Yet, partial degradation after IE can occur as mentioned, and might be another possible explanation for the loss of surface area and pore volume in SAPO-34.[145] The trend for loss of surface area is in most cases in accordance with the trend for reduction in crystallinity. Still, it should be noted that the loss of surface area in Zn/S34 is greater than that of Co/S34, and the same trend should be observed in RC if the reason for surface area and pore volume loss is partial degradation of the porous structure. On the contrary, Co/S34 experiences a greater loss of crystallinity than Zn/SAPO-34.

To conclude, it can be deduced that both surface area and pore volume decrease after LIE and for the samples investigated in this thesis, higher metal content appears to have a negative effect on crystallinity, surface area and pore volume. There are some indications pointing towards partial degradation of the porous network or

pore blockage by metal agglomerates. However, there are observations that cannot be explained by these factors alone and following this, there are most likely other factors caused by the different metal ions which affect the surface area and pore volumes. The losses observed in the data in this thesis are in accordance with literature observations, though in the higher end of what is previously reported, could be caused by differences in the ion exchange procedure. For example, several groups report different metal containing salts (eg. acetates, chlorides, etc.), lower concentration of ion exchange solution and also an additional heat treatment post IE. Unfortunately, it is not possible to account for why the surface area decreased based on the data acquired in this work. In all cases, it should be noted that the method of nitrogen physisorption implies large uncertainties when dealing with microporous materials.

5.2   Evaluation of Me/SAPO-34 for the dMtM

The main goal for this thesis was to investigate the catalytic activity, and here, the term catalytic activity is used to relatively describe the Me/SAPO-34 samples ability to convert methane into methanol in a stepwise process. The literature of Me/SAPO-34 for the dMtM is scarce, and only Cu/SAPO-34 and Co/SAPO-34 have previously been reported. In this thesis a relative study have been conducted, and arbitrary values were 11.1 MeOH for conventional SAPO-34 and 13.6-18.6 MeOH for the Me/SAPO-34 samples. This indicated that all tested samples appeared to be active for the dMtM as the normalised MeOH signal of the ion exchanged samples were higher than that of the parent SAPO-34 and that of an empty reactor. The area of integration for the MeOH signal of the Me/SAPO-34 samples is presented in Table 5.1 together with structural characteristics of each sample.

In multifunctional Me/SAPO-34 catalysts, SAPO-34 works as a catalyst support and the metal ions act as the active material. As described in the theory, a good support has high specific surface area and chemical stability. Further, as the the active material is the metal ions exchanged into the structure of SAPO-34, a sufficient metal load is required to activate methane. Since all investigated samples have the same parent material, the stability of the support should be approximately equal. In other words, what varies between the Me/SAPO-34 samples is metal type, metal content and surface area measurements. In this section, the performance of Cu/S34, Zn/S34, Ag/S34 and Co/S34 will therefore be discussed mainly in terms of these factors.

5.2.1   Effect of metal type and metal load

All Me/SAPO-34 samples produced more methanol than that of the conventional SAPO-34. This is as expected since the metal ions are the active materials for the dMtM.[18–20] The trend for methanol yield increases in the order of Zn/S34 < Co/S34 < Ag/S34 < Cu/S34. The fact that the Cu-containing sample preforms the best for the partial oxidation of methane to methanol, is to be expected from literature.[19,20,37,122]
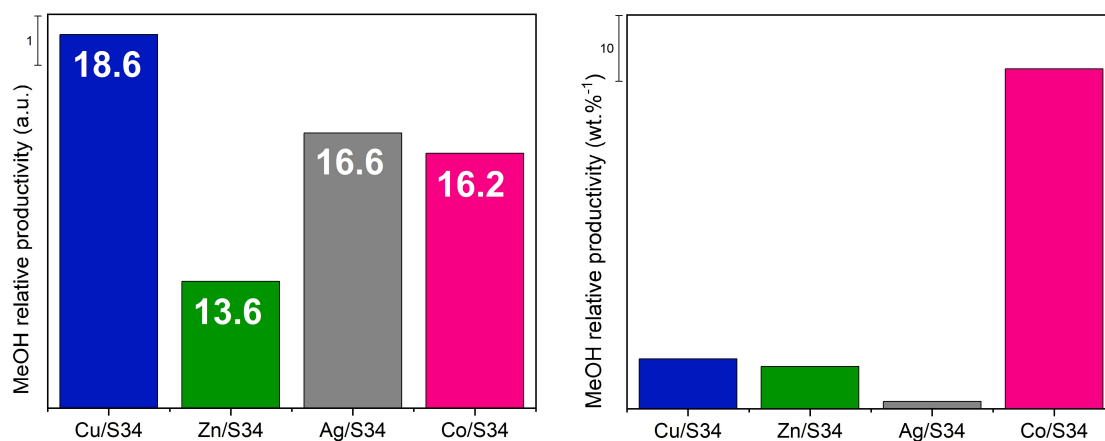
Figure 5.3: Relative yield and productivity of MeOH of all samples, where the graph to the left shows methanol yield per mass and the graph to the right is normalised per metal content as well. Presented values are $*10^{-4}$.

However, when looking at methanol productivity, the trend is completely different and increases from Ag/S34 < Zn/S34 $\approx$ Cu/S34 < < < Co/S34 as can be seen in Figure 5.3. In spite of the low metal load in Co/S34, it appears that the catalyst performs remarkably well per metal ion present in the structure. The only reported test of Co/SAPO-34 for methane activation was by Maroni et al. (1989)[25] who showed that it was active for methane activation, and is difficult to compare with as this project is a relative performance study. Further, Xu et al. (2021)[128] investigated Co^{2+} ion exchanged SAPO-34 for ethane hydrogenation and found that despite the low metal load of $\approx$0.3 wt.% Co, the catalyst exhibited a selective bond breaking between C-H and C-C and resulted in the highest and most stable selectivity. The group attributed this effect to the unique chemical state of Co^{2+}-ions.[128] In combination with the previously reported methane conversion of Maroni et al. and the significantly higher methanol production per metal content for the Co/S34 in this thesis, this highlights the need for further research on Co/SAPO-34 as a catalyst for the dMtM.

In the case of copper, a decreasing methanol production rate per metal atom with increasing metal loading amount have been reported for Cu/CHA for the partial oxidation of methane to methanol.[22] Sogukkanli et al. (2021) suggest that this found indicates that low copper loading is necessary to achieve well dispersed active copper sites which again is important for the catalytic activity.[22] In order to confirm or contradict the theory, a study with different metal loadings of each testes metal would be required, and unfortunately the data set in this thesis does not cover this and will be left for future work. Nonetheless, if comparing metal load alone to the catalytic activity, it shows an almost opposite trend where Ag/S34 with the highest metal load exhibits the lowest productivity of methanol per metal, and the lowest metal load for Co/S34 exhibits the highest, further supporting the founds of Sogukkanli et al.

On the other hand, when comparing metal content and productivity of Cu/S34 and Zn/S34 it does not appear that a higher metal content leads to lower methanol

productivity. Therefore, there are most likely other metal characteristics which influence the catalytic performance of the Me/SAPO-34, and that neither too high nor too low metal load is ideal. For example, how well the various active metal sites stabilises the adsorbed methanol, which is difficult to desorb and easily further oxidised, is a factor for the catalytic activity.[106] A further study on the effect of different metal loads within each type of the tested metals in SAPO-34 would for that reason be very interesting.

5.2.2   Effect of surface area and pore volume

There does not appear to be any trends in the methane activation in respect to surface area and pore volume, and the variations between the samples are in addition small. However, the Ag/S34 with lowest surface area and pore volume achieves the lowest MeOH productivity, and the Co/S34 with highest surface area and pore volume achieves the highest MeOH productivity per metal content. Mahyuddin et al. highlights the importance of zeotype confinement, which have been suggested to lower the C-H activation barrier in methane by increasing the energy of the HOMO, and by that higher surface areas in combination with sufficient metal loads may influence the activity.[106] Yet, for the dMtM it is more likely that the metal type has a larger impact than surface area and pore volume.[18]

Summary of methane activation

In summary, this thesis covers a relative catalytic study towards dMtM for Me/SAPO-34, where neither reaction mechanism, rate nor specific activity were taken into consideration. Based on the results however, metal type, metal content and surface area all appear to affect the conversion of methane by metal ion exchanged SAPO-34 in various degree. The most important factors are most likely metal type and metal load.

Among the tested samples, Ag and Zn ion exchanged SAPO-34 have not been reported earlier for the dMtM to the best of the authors knowledge. Herein, the Ag/S34 produced less methanol than the other samples, even though the metal loading was the highest obtained. This could indicate that silver ions are not as suited for methane activation as the others, at least in SAPO-34. Nonetheless, there are indications in the obtained results and in literature (for Cu[22]) that higher metal loads may not be be beneficial. Zn/S34 on the other hand, obtained a productivity per metal content similar to Cu/S34, although slightly inferior. Last, the productivity of Co/S34 which obtained a high methanol productivity with only 0.1 wt.% Co, and should definitely be studied further. As a final note, this was not an extensive study, where all the factors were varied, and for that reason it was not possible to draw any certain conclusions either for Me/SAPO-34 in general or within a metal type. Further studies is therefore necessary, and from the data obtained in this project cobalt ion exchanged SAPO-34 offers a promising outlook.

6 Conclusion

The main objective in this thesis was to investigate the effect of ion exchanging Cu, Zn, Fe, Ag and Co into conventional SAPO-34, and evaluating the catalytic performance of the Me/SAPO-34 samples for the direct methane to methanol (dMtM).

Cu^{2+}, Zn^{2+}, Ag^+ and Co^{2+} were conventionally ion exchanged into phase pure Me/SAPO-34 with metal loadings ranging from 0.1-5.1 wt.%. All the ion exchanged samples had a reduced crystallinity compared to the parent material, and Fe^{2+}, which also was attempted, were either amorphous or not of a satisfactory crystallinity. Further, the high metal load of Ag/S34 compared to the other samples may be due to its smaller size or higher affinity towards SAPO-34, and the low metal load of Co/S34 could possibly be ascribed to the difference in dissociation energy between metal ion and water ligands. The results could suggest that regardless of metal type, the reduction of crystallinity becomes greater with increasing metal content, but is not conclusive as there are deviations from the proposed trend. A similar trend appeared for the surface area and the pore volume, where the Me/S34 samples experience losses after ion exchange in a proportional relationship to the metal load. Subsequently, it was deduced that higher metal loading most likely has a negative effect on surface area and pore volume as well.

Furthermore, Ag/SAPO-34 and Zn/SAPO-34 have to the best of the authors knowledge not been tested for or the dMtM, and both appeared to be active. However, the Ag/S34 exhibited the lowest methanol productivity per metal load, and from this is may be concluded that silver ions might not be as suited for methane activation in SAPO-34 than the other metals investigated. Zn/S34 on the other hand performed slightly inferior to Cu/S34 which is well reported to be active for the dMtM, and may be of interest for future work. Of particular interest was the remarkable methanol production of Co/S34 in spite of its low metal load of 0.1 wt.%, and could possibly be attributed to the unique chemical state of Co^{2+}-ions. Another plausible explanation could be that methanol production decreases with higher metal loadings, which have in fact been reported for Cu. However, this trend does not apply to all tested samples, which means that there are other factors that influence the catalytic activity. Surface area and pore volume may contribute with confinement effects, but are most likely not major contributors in comparison to metal content and metal type. In conclusion, the latter two probably influence the activity of the Me/S34-samples the most.

52

7 Further work

First of all, further studies on Co/SAPO-34 as a catalyst for the direct conversion of methane to methanol (dMtM) would be intriguing based on the results obtained in this project. Particularly the chemical state of the cobalt species, and the mechanism through which Co can activate methane in SAPO-34. Since this project was intended as a screening of the catalytic performance towards the dMtM, specific activity and the kinetics should also be analysed for all the tested metals in order to obtain a better understanding of the overall performance of Me/SAPO-34. In addition, the effect of co-introduction of different metals could also be interesting for further work.

Second, catalytic tests of Fe/SAPO-34 for the dMtM should be conducted in the future. Since Fe/S34-samples in this project were not fit for catalysis and because nature in fact is able to convert methane to methanol in methanotrophic bacteria, it should be attempted again. Particular means to successfully introduce iron into SAPO-34 could be ion exchange (IE) under an inert atmosphere, change of iron precursor or pH control as mentioned. Inert atmosphere IE have been reported to work and should therefore be further investigated. Subsequently, Fe/SAPO-34 should be tested for the reaction, as this has not yet been done to the best of the authors knowledge. Additionally, studies of why the SAPO-34 samples dissolved or collapsed during IE could be of interest.

Last, some alterations to the IE process are proposed for further work. Based on the finds in this project, too high metal loadings appear to negatively affect crystallinity, surface area and catalytic activity. Therefore to investigate lower concentrations of IE solutions may be of interest. In particular if it could lead to a study with different metal loadings of each of the tested metals, and how it affected the material characteristics and the dMtM reacion. Further, liquid IE processes with additional heat treatments have been reported to obtain highly crystalline samples that experience small losses in surface areas and pore volumes. Heat treatments could for example be a post IE calcination or calcination steps between rounds of IE. Another adjustment could be to investigate the effect of metal salt, ie. metal nitrates compared to metal acetates and metal chlorides for example.

References

[1] I. Karakurt, G. Aydin, and K. Aydiner, "Sources and mitigation of methane emissions by sectors: A critical review," *Renewable Energy*, vol. 39, no. 1, pp. 40–48, 2012.

[2] The United Nations Economic Commission for Europe (UNECE), "The challenge." https://unece.org/challenge. Accessed: 20.08.22.

[3] The Intergovernmental Panel on Climate Change (IPCC), "The evidence is clear: the time for action is now. we can halve emissions by 2030.," https://www.ipcc.ch/2022/04/04/ipcc-ar6-wgiii-pressrelease/ Accessed: 29.08.22.

[4] M. Saunois, A. R. Stavert, B. Poulter, P. Bousquet, J. G. Canadell, R. B. Jackson, P. A. Raymond, E. J. Dlugokencky, S. Houweling, P. K. Patra, P. Ciais, V. K. Arora, D. Bastviken, P. Bergamaschi, D. R. Blake, G. Brailsford, L. Bruhwiler, K. M. Carlson, M. Carrol, S. Castaldi, N. Chandra, C. Crevoisier, P. M. Crill, K. Covey, C. L. Curry, G. Etiope, C. Frankenberg, N. Gedney, M. I. Hegglin, L. Höglund-Isaksson, G. Hugelius, M. Ishizawa, A. Ito, G. Janssens-Maenhout, K. M. Jensen, F. Joos, T. Kleinen, P. B. Krummel, R. L. Langenfelds, G. G. Laruelle, L. Liu, T. Machida, S. Maksyutov, K. C. McDonald, J. McNorton, P. A. Miller, J. R. Melton, I. Morino, J. Müller, F. Murguia-Flores, V. Naik, Y. Niwa, S. Noce, S. O'Doherty, R. J. Parker, C. Peng, S. Peng, G. P. Peters, C. Prigent, R. Prinn, M. Ramonet, P. Regnier, W. J. Riley, J. A. Rosentreter, A. Segers, I. J. Simpson, H. Shi, S. J. Smith, L. P. Steele, B. F. Thornton, H. Tian, Y. Tohjima, F. N. Tubiello, A. Tsuruta, N. Viovy, A. Voulgarakis, T. S. Weber, M. van Weele, G. R. van der Werf, R. F. Weiss, D. Worthy, D. Wunch, Y. Yin, Y. Yoshida, W. Zhang, Z. Zhang, Y. Zhao, B. Zheng, Q. Zhu, Q. Zhu, and Q. Zhuang, "The global methane budget 2000–2017," *Earth System Science Data*, vol. 12, pp. 1561–1623, July 2020.

[5] I. Chorkendorff and J. W. Niemantsverdriet, *Concepts of Modern Catalysis and Kinetics. 3rd edition.* Wiley, Oct. 2013.

[6] Finansavisa, "Nord stream leak: Probably the largest single release of the powerful greenhouse gas methane ever registrated." https://www.finansavisen.no/nyheter/energi/2022/10/01/7938724/nord-stream-2-er-tomt-for-gass?zephr Accessed:01.10.22.

[7] NRK, "The sabotage of the nord stream gas pipe." https://www.nrk.no/nyheter/gassrorledningen-nord-stream-1.13828304 Accessed: 18.11.22.

[8] United Nations Environment Program (UNEP), "Why is methane mitigation critical for reaching the 1.5 target?," https://www.unep.org/explore-topics/energy/facts-about-methane Accessed: 20.09.22.

[9] United Nations (UN) Treaty Collection, "Paris agreement," https://treaties.un.org/pages/ViewDetails.aspx Accessed:15.09.22.

[10] Z. Zakaria and S. Kamarudin, "Direct conversion technologies of methane to methanol: An overview," *Renewable and Sustainable Energy Reviews*, vol. 65, pp. 250–261, 2016.

[11] Climate and Clean Air Coalition (CCAC), "Methane," https://www.ccacoalition.org/en/slcps/methane Accessed: 14.10.22.

[12] R. PVL, K.-H. Kim, and H. Song, "Emerging green chemical technologies for the conversion of ch 4 to value added products," *Renewable and Sustainable Energy Reviews*, vol. 24, pp. 578–585, 08 2013.

[13] Global Methane Pledge

[14] M. Ravi, M. Ranocchiari, and J. A. vanBokhoven, "The direct catalytic oxidation of methane to methanol—a critical assessment," *Angewandte Chemie International Edition*, vol. 56, no. 52, pp. 16464–16483, 2017.

[15] P. Tan, "Active phase, catalytic activity, and induction period of fe/zeolite material in nonoxidative aromatization of methane," *Journal of Catalysis*, vol. 338, pp. 21–29, 2016.

[16] N. V. Beznis, A. N. van Laak, B. M. Weckhuysen, and J. H. Bitter, "Oxidation of methane to methanol and formaldehyde over co–zsm-5 molecular sieves: Tuning the reactivity and selectivity by alkaline and acid treatments of the zeolite zsm-5 agglomerates," *Microporous and Mesoporous Materials*, vol. 138, no. 1, pp. 176–183, 2011.

[17] R. K. Srivastava, P. K. Sarangi, L. Bhatia, A. K. Singh, and K. P. Shadangi, "Conversion of methane to methanol: technologies and future challenges," *Biomass Conversion and Biorefinery*, vol. 12, no. 5, p. 1851–1875, 2022.

[18] S. Raynes, M. A. Shah, and R. A. Taylor, "Direct conversion of methane to methanol with zeolites: towards understanding the role of extra-framework d-block metal and zeolite framework type," *Dalton Trans.*, vol. 48, pp. 10364–10384, 2019.

[19] M. J. Wulfers, S. Teketel, B. Ipek, and R. F. Lobo, "Conversion of methane to methanol on copper-containing small-pore zeolites and zeotypes," *Chemical Communications*, vol. 51, no. 21, p. 4447–4450, 2015.

[20] K. Kvande, M. Dyballa, M. Buono, M. E. B. Signorile, K. Lomachenko, B. Arstad, S. Bordiga, G. Berlier, U. Olsbye, P. Beato, and S. Svelle, "Comparing the Nature of Active Sites in Cu-loaded SAPO-34 and SSZ-13 for the Direct Conversion of Methane to Methanol," *Catalysts*, 2020. 10

[21] R. Balasubramanian and A. C. Rosenzweig, "Structural and mechanistic insights into methane oxidation by particulate methane monooxygenase," *Accounts of Chemical Research*, vol. 40, pp. 573–580, Apr. 2007.

[22] S. Sogukkanli, T. Moteki, and M. Ogura, "Selective methanol formation ivia/i CO-assisted direct partial oxidation of methane over copper-containing CHA-type zeolites prepared by one-pot synthesis," *Green Chemistry*, vol. 23, no. 5, pp. 2148–2154, 2021.

[23] S. E. Bozbag, E. M. C. Alayon, J. Pecháček, M. Nachtegaal, M. Ranocchiari, and J. A. van Bokhoven, "Methane to methanol over copper mordenite: yield improvement through multiple cycles and different synthesis techniques," *Catal. Sci. Technol.*, vol. 6, pp. 5011–5022, 2016.

[24] Y. Krisnandi, B. A. Samodro, R. Sihombing, and R. Howe, "Direct synthesis of methanol by partial oxidation of methane with oxygen over cobalt modified mesoporous h-zsm-5 catalyst," *Indonesian Journal of Chemistry*, vol. 15, pp. 263–268, 11 2015.

[25] V. A. Maroni, K. A. Willms, H. Nguyen, and L. E. Iton, "Activation of methane by transition metal-substituted aluminophosphate molecular sieves," 12 1989.

[26] J. Xu, A. Zheng, X. Wang, G. Qi, J. Su, J. Du, Z. Gan, J. Wu, W. Wang, F. Deng, and et al., "Room temperature activation of methane over zn modified h-zsm-5 zeolites: Insight from solid-state nmr and theoretical calculations," *Chemical Science*, vol. 3, no. 10, p. 2932, 2012.

[27] M. A. Shah, S. Raynes, D. C. Apperley, and R. A. Taylor, "Framework effects on activation and functionalisation of methane in zinc-exchanged zeolites," *ChemPhysChem*, vol. 21, no. 7, p. 673–679, 2020.

[28] A. A. Gabrienko, S. S. Arzumanov, I. B. Moroz, A. V. Toktarev, W. Wang, and A. G. Stepanov, "Methane activation and transformation on ag/h-zsm-5 zeolite studied with solid-state nmr," *The Journal of Physical Chemistry C*, vol. 117, no. 15, p. 7690–7702, 2013.

[29] J. Xu, A. Zheng, X. Wang, G. Qi, J. Su, J. Du, Z. Gan, J. Wu, W. Wang, and F. Deng, "Room temperature activation of methane over zn modified h-ZSM-5 zeolites: Insight from solid-state NMR and theoretical calculations," *Chemical Science*, vol. 3, no. 10, p. 2932, 2012.

[30] G. Wang, L. Huang, W. Chen, J. Zhou, and A. Zheng, "Rationally designing mixed cu–(-o)–m (m = cu, ag, zn, au) centers over zeolite materials with high catalytic activity towards methane activation," *Physical Chemistry Chemical Physics*, vol. 20, no. 41, p. 26522–26531, 2018.

[31] P. Tomkins, M. Ranocchiari, and J. A. van Bokhoven, "Direct conversion of methane to methanol under mild conditions over cu-zeolites and beyond.," *Accounts of chemical research*, vol. 50 2, pp. 418–425, 2017.

[32] B. Michalkiewicz, "Partial oxidation of methane to formaldehyde and methanol using molecular oxygen over fe-zsm-5," *Applied Catalysis A: General*, vol. 277, no. 1, pp. 147–153, 2004.

[33] B. Vora, J. Q. Chen, A. Bozzano, B. Glover, and P. Barger, "Various routes to methane utilization—sapo-34 catalysis offers the best option," *Catalysis Today*, vol. 141, no. 1, pp. 77–83, 2009. Selected Papers from the "Catalysis for future fuels" 18th National Symposium and INDO-US Seminar on Catalysis, Indian Institute of Petroleum, Dehradun, India, April 16-18, 2007.

[34] "Structure commission of the international zeolite association (IZA-SC)." Accessed: 2022-10-10.

[35] U. Olsbye, S. Svelle, M. Bjørgen, P. Beato, T. V. W. Janssens, F. Joensen, S. Bordiga, and K. P. Lillerud, "Conversion of methanol to hydrocarbons: How zeolite cavity and pore size controls product selectivity," *Angewandte Chemie International Edition*, vol. 51, pp. 5810–5831, Apr. 2012.

[36] M. Cortés-Reyes, E. Finocchio, C. Herrera, M. A. Larrubia, L. J. Alemany, and G. Busca, "A study of cu-sapo-34 catalysts for scr of nox by ammonia," *Microporous and Mesoporous Materials*, vol. 241, pp. 258–265, 2017.

[37] E. Borfecchia, P. Beato, S. Svelle, U. Olsbye, C. Lamberti, and S. Bordiga, "Cu-CHA – a model system for applied selective redox catalysis," *Chemical Society Reviews*, vol. 47, no. 22, pp. 8097–8133, 2018.

[38] H. Zhang, J. Lv, Z. Zhang, C. Du, S. Wang, J. Lin, S. Wan, Y. Wang, and H. Xiong, "Oxidation of methane to methanol by water over cu/SSZ-13: Impact of cu loading and formation of active sites," *ChemCatChem*, vol. 14, Feb. 2022.

[39] R. Oord, J. E. Schmidt, and B. M. Weckhuysen, "Methane-to-methanol conversion over zeolite cu-SSZ-13, and its comparison with the selective catalytic reduction of NOsubx/sub with NHsub3/sub," *Catalysis Science &amp Technology*, vol. 8, no. 4, pp. 1028–1038, 2018.

[40] L. Zhang, J. Bates, D. Chen, H.-Y. Nie, and Y. Huang, "Investigations of formation of molecular sieve SAPO-34," *The Journal of Physical Chemistry C*, vol. 115, pp. 22309–22319, Oct. 2011.

[41] X. Chen, G. Yang, and V. Valtchev, "Environmentally benign synthesis of crystalline nanosized molecular sieves," *Green Energy Environment*, vol. 5, no. 4, pp. 394–404, 2020. Green Catalysis and Kinetics.

[42] A. Palčić and V. Valtchev, "Analysis and control of acid sites in zeolites," *Applied Catalysis A: General*, vol. 606, p. 117795, Sept. 2020.

[43] R. Xu, W. Pang, J. Yu, Q. Huo, and J. Chen, *Chemistry of Zeolites and Related Porous Materials: Synthesis and Structure*. Wiley and sons, 2009.

[44] G. Cao and Y. Wang, *Nanostructures and Nanomaterials: Synthesis, Properties and Applications. 2nd. Edition.* World Scientific Series in Nanoscience and Nanotechnology, 2013.

[45] J. Cejka and H. van Bekkum, *Zeolites and ordered mesoporous materials:*

progress and prospects: the 1st FEZA School on Zeolites, Prague, Czech Republic. Elsevier Science, 2005.

[46] C. Baerlocher, L. B. Mccusker, D. Olson, and W. M. Meier, "Atlas of zeolite framework types," 2007.

[47] V. Gold, ed., *The IUPAC Compendium of Chemical Terminology.* International Union of Pure and Applied Chemistry (IUPAC), 2019.

[48] M. Thommes, K. Kaneko, A. V. Neimark, J. P. Olivier, F. Rodriguez-Reinoso, J. Rouquerol, and K. S. Sing, "Physisorption of gases, with special reference to the evaluation of surface area and pore size distribution (IUPAC technical report)," *Pure and Applied Chemistry*, vol. 87, pp. 1051–1069, July 2015.

[49] M. Hartmann and L. Kevan, "Transition-metal ions in aluminophosphate and silicoaluminophosphate molecular sieves: location, interaction with adsorbates and catalytic properties," *Chemical Reviews*, vol. 99, pp. 635–664, Feb. 1999.

[50] N. Najafi, S. Askari, and R. Halladj, "Hydrothermal synthesis of nanosized SAPO-34 molecular sieves by different combinations of multi templates," *Powder Technology*, vol. 254, pp. 324–330, Mar. 2014.

[51] H. Shang, Y. Li, J. Liu, X. Tang, J. Yang, and J. Li, "CH4/n2 separation on methane molecules grade diameter channel molecular sieves with a CHA-type structure," *Chinese Journal of Chemical Engineering*, vol. 27, pp. 1044–1049, May 2019.

[52] S. SVELLE, S. ARAVINTHAN, M. BJORGEN, K. LILLERUD, S. KOLBOE, I. DAHL, and U. OLSBYE, "The methyl halide to hydrocarbon reaction over h-SAPO-34," *Journal of Catalysis*, vol. 241, pp. 243–254, July 2006.

[53] S. M. Csicsery, "Shape-selective catalysis in zeolites," *Zeolites*, vol. 4, pp. 202–213, July 1984.

[54] J. Tan, Z. Liu, X. Bao, X. Liu, X. Han, C. He, and R. Zhai, "Crystallization and si incorporation mechanisms of SAPO-34," *Microporous and Mesoporous Materials*, vol. 53, pp. 97–108, June 2002.

[55] R. B. Borade and A. Clearfield, "A comparative study of acidic properties of SAPO-5, -11, -34 and -37 molecular sieves," *Journal of Molecular Catalysis*, vol. 88, pp. 249–265, Mar. 1994.

[56] Q. Zhu, J. N. Kondo, R. Ohnuma, Y. Kubota, M. Yamaguchi, and T. Tatsumi, "The study of methanol-to-olefin over proton type aluminosilicate CHA zeolites," *Microporous and Mesoporous Materials*, vol. 112, pp. 153–161, July 2008.

[57] K. Hernadi, Z. Kónya, A. Siska, J. Kiss, A. Oszkó, J. Nagy, and I. Kiricsi, "The role of zeotype catalyst support in the synthesis of carbon nanotubes by CCVD," in *Studies in Surface Science and Catalysis*, pp. 541–548, Elsevier, 2002.

[58] J. Su, D. Wang, Y. Wang, H. Zhou, C. Liu, S. Liu, C. Wang, W. Yang, Z. Xie, and M. He, "Direct conversion of syngas into light olefins over zirconium-doped indium(III) oxide and SAPO-34 bifunctional catalysts: Design of oxide component and construction of reaction network," *ChemCatChem*, vol. 10, pp. 1536–1541, Feb. 2018.

[59] S. Zhang, L. Pang, Z. Chen, S. Ming, Y. Dong, Q. Liu, P. Liu, W. Cai, and T. Li, "Cu/SSZ-13 and cu/SAPO-34 catalysts for deNOx in diesel exhaust: Current status, challenges, and future perspectives," *Applied Catalysis A: General*, vol. 607, p. 117855, Oct. 2020.

[60] D. Wang, L. Zhang, J. Li, K. Kamasamudram, and W. S. Epling, "NH3-SCR over cu/SAPO-34 – zeolite acidity and cu structure changes as a function of cu loading," *Catalysis Today*, vol. 231, pp. 64–74, Aug. 2014.

[61] M. Usman, A. S. Ghanem, S. N. A. Shah, M. D. Garba, M. Y. Khan, S. Khan, M. Humayun, and A. L. Khan, "A review on SAPO-34 zeolite materials for CO sub2/sub capture and conversion," *The Chemical Record*, vol. 22, Apr. 2022.

[62] Z. Ma and F. Zaera, "Heterogeneous catalysis by metals," Mar. 2006.

[63] P. Cnudde, R. Demuynck, S. Vandenbrande, M. Waroquier, G. Sastre, and V. V. Speybroeck, "Light olefin diffusion during the MTO process on h-SAPO-34: A complex interplay of molecular factors," *Journal of the American Chemical Society*, vol. 142, pp. 6007–6017, Mar. 2020.

[64] X. Xiang, M. Yang, B. Gao, Y. Qiao, P. Tian, S. Xu, and Z. Liu, "Direct cu^{2+} ion-exchanged into as-synthesized SAPO-34 and its catalytic application in the selective catalytic reduction of NO with NH$_3$," *RSC Advances*, vol. 6, no. 15, pp. 12544–12552, 2016.

[65] J. H. Kang, F. H. Alshafei, S. I. Zones, and M. E. Davis, "Cage-defining ring: A molecular sieve structural indicator for light olefin product distribution from the methanol-to-olefins reaction," *ACS Catalysis*, vol. 9, pp. 6012–6019, Apr. 2019.

[66] A. Blackman and L. Gahan, *Aylward and Findlay's SI Chemical Data. 7th edition.* Wiley, 2013.

[67] W. Dai, G. Wu, L. Li, N. Guan, and M. Hunger, "Mechanisms of the deactivation of SAPO-34 materials with different crystal sizes applied as MTO catalysts," *ACS Catalysis*, vol. 3, pp. 588–596, Feb. 2013.

[68] S. Peng, M. Gao, H. Li, M. Yang, M. Ye, and Z. Liu, "Control of surface barriers in mass transfer to modulate methanol-to-olefins reaction over SAPO-34 zeolites," *Angewandte Chemie*, vol. 132, pp. 22129–22132, Oct. 2020.

[69] J. Weitkamp, "Zeolites and catalysis," *Solid State Ionics*, vol. 131, pp. 175–188, June 2000.

[70] S. Wilson and P. Barger, "The characteristics of sapo-34 which influence the

conversion of methanol to light olefins," *Microporous and Mesoporous Materials*, vol. 29, no. 1, pp. 117–126, 1999.

[71] K. Kvande, *A Study of Cu-loaded SAPO-34 for the Direct Conversion of Methane to Methanol.* PhD thesis, Podunk IN, 2019.

[72] S. Nystrom, A. Hoffman, and D. Hibbitts, "Tuning brønsted acid strength by altering site proximity in CHA framework zeolites," *ACS Catalysis*, vol. 8, pp. 7842–7860, July 2018.

[73] M. Salmasi, S. Fatemi, and S. Hashemi, "MTO reaction over SAPO-34 catalysts synthesized by combination of TEAOH and morpholine templates and different silica sources," *Scientia Iranica*, vol. 19, pp. 1632–1637, Dec. 2012.

[74] D. Ali, Z. Li, M. M. Azim, H. L. Lein, and K. Mathisen, "Evaluating pore characteristics and acid site locations in hierarchical SAPO-11 by catalytic model reactions," *Microporous and Mesoporous Materials*, vol. 329, p. 111550, Jan. 2022.

[75] X.-L. Wei, X.-H. Lu, T.-J. Zhang, X. Chu, D. Zhou, R.-F. Nie, and Q.-H. Xia, "Synthesis and catalytic application of SAPO-5 by dry-gel conversion for the epoxidation of styrene with air," *Microporous and Mesoporous Materials*, vol. 214, pp. 80–87, Sept. 2015.

[76] F. M. Shalmani, R. Halladj, and S. Askari, "Physicochemical characterization to assess ni and zn incorporation into zeotype SAPO-34 nanoparticles synthesized with different mixing methods through ultrasound-promoted crystallization," *RSC Advances*, vol. 7, no. 43, pp. 26756–26769, 2017.

[77] A. Ramirez, A. D. Chowdhury, M. Caglayan, A. Rodriguez-Gomez, N. Wehbe, E. Abou-Hamad, L. Gevers, S. Ould-Chikh, and J. Gascon, "Coated sulfated zirconia/SAPO-34 for the direct conversion of COsub2/sub to light olefins," *Catalysis Science &amp Technology*, vol. 10, no. 5, pp. 1507–1517, 2020.

[78] S. Tian, S. Ji, D. Lü, B. Bai, and Q. Sun, "Preparation of modified ce-SAPO-34 catalysts and their catalytic performances of methanol to olefins," *Journal of Energy Chemistry*, vol. 22, pp. 605–609, July 2013.

[79] F. Gao, E. D. Walter, N. M. Washton, J. Szanyi, and C. H. F. Peden, "Synthesis and evaluation of cu-SAPO-34 catalysts for ammonia selective catalytic reduction. 1. aqueous solution ion exchange," *ACS Catalysis*, vol. 3, pp. 2083–2093, Aug. 2013.

[80] J. Kielland, "Individual activity coefficients of ions in aqueous solutions," *Journal of the American Chemical Society*, vol. 59, no. 9, pp. 1675–1678, 1937.

[81] "X-ray diffraction,"

[82] H. Stanjek and W. Häusler, "Basics of x-ray diffraction," *Hyperfine Interactions*, vol. 154, no. 1-4, pp. 107–119, 2004.

[83] R. J. Tilley, *Understanding solids: the science of materials.* John Wiley & Sons, 2004.

[84] M. Weller, T. Overton, F. Armstrong, and J. Rourke, *Inorganic Chemistry, 7th. edition.* Oxford University Press, 2018.

[85] P. Webb, *Analytical methods in fine particle technology.* TBD, TBD. Chapter 3 p. 53-93, Chapter 3 p.144-146, Chapter 3: Surface Area and Pore structure by Gas Adsorption

[86] S. Storck, H. Bretinger, and W. F. Maier, "Characterization of micro- and mesoporous solids by physisorption methods and pore-size analysis," *Applied Catalysis A: General*, vol. 174, pp. 137–146, Nov. 1998.

[87] K. S. W. Singh, J. Rouquerol, G. Bergeret, P. Gallezot, M. Vaarkamp, D. Koningsberger, A. K. Datye, J. W. Niemantsverdriet, T. Butz, G. Engelhardt, G. Mestl, H. Knözinger, and H. Jobic, *Characterization of Solid Catalysts.* Wiley-VHC Verlag gmbh, 1997. In Handbook of Heterogeneous Catalysis. DOI: 10.1002/9783527619474.ch3

[88] K. S. Walton and R. Q. Snurr, "Applicability of the BET method for determining surface areas of microporous metal-organic frameworks," *Journal of the American Chemical Society*, vol. 129, pp. 8552–8556, June 2007.

[89] D. Beauchemin, "Inductively coupled plasma mass spectrometry," *Analytical Chemistry*, vol. 80, pp. 4455–4486, May 2008.

[90] D. A. Skoog, D. M. West, F. J. Holler, and S. R. Crouch, *Fundamentals of Analytical Chemistry, 9th Ed.* Cengage Learning, 2014.

[91] H. Taylor, *Inductively Coupled Plasma-Mass Spectrometry.* 2001.

[92] D. H. Cusworth, A. A. Bloom, S. Ma, C. E. Miller, K. Bowman, Y. Yin, J. D. Maasakkers, Y. Zhang, T. R. Scarpelli, Z. Qu, D. J. Jacob, and J. R. Worden, "A bayesian framework for deriving sector-based methane emissions from top-down fluxes," *Communications Earth &amp Environment*, vol. 2, Nov. 2021.

[93] S. Sun, L. Ma, and Z. Li, "Methane emission estimation of oil and gas sector: A review of measurement technologies, data analysis methods and uncertainty estimation," *Sustainability*, vol. 13, p. 13895, Dec. 2021.

[94] M. S. A. S. Shah, C. Oh, H. Park, Y. J. Hwang, M. Ma, and J. H. Park, "Catalytic oxidation of methane to oxygenated products: Recent advancements and prospects for electrocatalytic and photocatalytic conversion at low temperatures," *Advanced Science*, vol. 7, p. 2001946, Oct. 2020.

[95] B. Wang, S. Albarracín-Suazo, Y. Pagán-Torres, and E. Nikolla, "Advances in methane conversion processes," *Catalysis Today*, vol. 285, pp. 147–158, May 2017.

[96] A. M. Arinaga, M. C. Ziegelski, and T. J. Marks, "Alternative oxidants for the

catalytic oxidative coupling of methane," *Angewandte Chemie International Edition*, vol. 60, pp. 10502–10515, Jan. 2021.

[97] R. Horn and R. Schlögl, "Methane activation by heterogeneous catalysis," *Catalysis Letters*, vol. 145, pp. 23–39, Nov. 2014.

[98] A. Galadima and O. Muraza, "Revisiting the oxidative coupling of methane to ethylene in the golden period of shale gas: A review," *Journal of Industrial and Engineering Chemistry*, vol. 37, pp. 1–13, May 2016.

[99] X. Guo, G. Fang, G. Li, H. Ma, H. Fan, L. Yu, C. Ma, X. Wu, D. Deng, M. Wei, D. Tan, R. Si, S. Zhang, J. Li, L. Sun, Z. Tang, X. Pan, and X. Bao, "Direct, nonoxidative conversion of methane to ethylene, aromatics, and hydrogen," *Science*, vol. 344, pp. 616–619, May 2014.

[100] S. H. Morejudo, R. Zanón, S. Escolástico, I. Yuste-Tirados, H. Malerød-Fjeld, P. K. Vestre, W. G. Coors, A. Martínez, T. Norby, J. M. Serra, and C. Kjølseth, "Direct conversion of methane to aromatics in a catalytic co-ionic membrane reactor," *Science*, vol. 353, pp. 563–566, Aug. 2016.

[101] T. W. Bank, "Zero routine flaring (zrf) by 2030," 2015.

[102] A. Holmen, "Direct conversion of methane to fuels and chemicals," *Catalysis Today*, vol. 142, pp. 2–8, Apr. 2009.

[103] M. J. Moran, H. N. Shapiro, D. D. Boettner, and M. B. Bailey, *Fundamentals of Engineering Thermodynamics, 9th edition, SI Global Edition*. Wiley, 2018.

[104] M. B. Park, E. D. Park, and W.-S. Ahn, "Recent progress in direct conversion of methane to methanol over copper-exchanged zeolites," *Frontiers in Chemistry*, vol. 7, July 2019.

[105] K. Villa, S. Murcia-López, J. R. Morante, and T. Andreu, "An insight on the role of la in mesoporous WO 3 for the photocatalytic conversion of methane into methanol," *Applied Catalysis B: Environmental*, vol. 187, pp. 30–36, June 2016.

[106] M. H. Mahyuddin, Y. Shiota, and K. Yoshizawa, "Methane selective oxidation to methanol by metal-exchanged zeolites: a review of active sites and their reactivity," *Catalysis Science &amp Technology*, vol. 9, no. 8, pp. 1744–1768, 2019.

[107] J. Yang, J. Hao, J. Wei, J. Dai, and Y. Li, "Visible-light-driven selective oxidation of methane to methanol on amorphous FeOOH coupled m-WO3," *Fuel*, vol. 266, p. 117104, Apr. 2020.

[108] E. V. Starokon, M. V. Parfenov, S. S. Arzumanov, L. V. Pirutko, A. G. Stepanov, and G. I. Panov, "Oxidation of methane to methanol on the surface of FeZSM-5 zeolite," *Journal of Catalysis*, vol. 300, pp. 47–54, Apr. 2013.

[109] M. H. Groothaert, P. J. Smeets, B. F. Sels, P. A. Jacobs, and R. A. Schoonheydt, "Selective oxidation of methane by the bis(μ-oxo)dicopper core

stabilized on ZSM-5 and mordenite zeolites," *Journal of the American Chemical Society*, vol. 127, pp. 1394–1395, Jan. 2005.

[110] H. V. Le, S. Parishan, A. Sagaltchik, H. Ahi, A. Trunschke, R. Schomäcker, and A. Thomas, "Stepwise methane-to-methanol conversion on CuO/SBA-15," *Chemistry - A European Journal*, vol. 24, pp. 12592–12599, July 2018.

[111] M. Álvarez, P. Marín, and S. Ordóñez, "Direct oxidation of methane to methanol over cu-zeolites at mild conditions," *Molecular Catalysis*, vol. 487, p. 110886, May 2020.

[112] K. Narsimhan, K. Iyoki, K. Dinh, and Y. Román-Leshkov, "Catalytic oxidation of methane into methanol over copper-exchanged zeolites with oxygen at low temperature," *ACS Central Science*, vol. 2, no. 6, p. 424–429, 2016.

[113] K. Dubkov, V. Sobolev, E. Talsi, M. Rodkin, N. Watkins, A. Shteinman, and G. Panov, "Kinetic isotope effects and mechanism of biomimetic oxidation of methane and benzene on FeZSM-5 zeolite," *Journal of Molecular Catalysis A: Chemical*, vol. 123, pp. 155–161, Aug. 1997.

[114] G. I. Panov, V. I. Sobolev, K. A. Dubkov, V. N. Parmon, N. S. Ovanesyan, A. E. Shilov, and A. A. Shteinman, "Iron complexes in zeolites as a new model of methane monooxygenase," *Reaction Kinetics and Catalysis Letters*, vol. 61, pp. 251–258, July 1997.

[115] J.-H. Park, J.-H. Choung, I.-S. Nam, and S.-W. Ham, "N2o decomposition over wet- and solid-exchanged fe-zsm-5 catalysts," *Applied Catalysis B: Environmental*, vol. 78, no. 3, pp. 342–354, 2008.

[116] T. Zhang, X. Qin, Y. Peng, C. Wang, H. Chang, J. Chen, and J. Li, "Effect of fe precursors on the catalytic activity of fe/sapo-34 catalysts for n2o decomposition," *Catalysis Communications*, vol. 128, p. 105706, 2019.

[117] N. V. Beznis, B. M. Weckhuysen, and J. H. Bitter, "Partial oxidation of methane over co-ZSM-5: Tuning the oxygenate selectivity by altering the preparation route," *Catalysis Letters*, vol. 136, pp. 52–56, Nov. 2009.

[118] V. B. Kazansky and A. I. Serykh, "Unusual localization of zinc cations in MFI zeolites modified by different ways of preparation," *Physical Chemistry Chemical Physics*, vol. 6, no. 13, p. 3760, 2004.

[119] Y. Kuroda, T. Mori, H. Sugiyama, Y. Uozumi, K. Ikeda, A. Itadani, and M. Nagao, "On the possibility of AgZSM-5 zeolite being a partial oxidation catalyst for methane," *Journal of Colloid and Interface Science*, vol. 333, pp. 294–299, May 2009.

[120] D. K. Pappas, E. Borfecchia, M. Dyballa, I. A. Pankin, K. A. Lomachenko, A. Martini, M. Signorile, S. Teketel, B. Arstad, G. Berlier, C. Lamberti, S. Bordiga, U. Olsbye, K. P. Lillerud, S. Svelle, and P. Beato, "Methane to methanol: Structure–activity relationships for cu-CHA," *Journal of the American Chemical Society*, vol. 139, pp. 14961–14975, Oct. 2017.

[121] A. Oda, H. Torigoe, A. Itadani, T. Ohkubo, T. Yumura, H. Kobayashi, and Y. Kuroda, "Mechanism of ch4 activation on a monomeric zn2+-ion exchanged in mfi-type zeolite with a specific al arrangement: Similarity to the activation site for h2," *The Journal of Physical Chemistry C*, vol. 117, no. 38, pp. 19525–19534, 2013.

[122] Y. Mao and P. Hu, "Identification of the active sites and mechanism for partial methane oxidation to methanol over copper-exchanged CHA zeolites," *Science China Chemistry*, vol. 63, pp. 850–859, Mar. 2020.

[123] M. E. Rivera-Ramos and A. J. Hernández-Maldonado, "Adsorption of nsub2/sub and CHsub4/sub by ion-exchanged silicoaluminophosphate nanoporous sorbents: interaction with monovalent, divalent, and trivalent cations," *Industrial &amp Engineering Chemistry Research*, vol. 46, pp. 4991–5002, May 2007.

[124] K. Mirza, M. Ghadiri, M. Haghighi, and A. Afghan, "Hydrothermal synthesize of modified fe, ag and k-sapo-34 nanostructured catalysts used in methanol conversion to light olefins," *Microporous and Mesoporous Materials*, vol. 260, pp. 155–165, 2018.

[125] H. Huang, H. Wang, H. Zhu, S. Zhang, Q. Zhang, and C. Li, "Enhanced ethene to propene ratio over zn-modified SAPO-34 zeolites in methanol-to-olefin reaction," *Catalysis Science &amp Technology*, vol. 9, no. 9, pp. 2203–2210, 2019.

[126] D. R. Dubois, D. L. Obrzut, J. Liu, J. Thundimadathil, P. M. Adekkanattu, J. A. Guin, A. Punnoose, and M. S. Seehra, "Conversion of methanol to olefins over cobalt-, manganese- and nickel-incorporated SAPO-34 molecular sieves," *Fuel Processing Technology*, vol. 83, pp. 203–218, Sept. 2003.

[127] B. Tang, X.-H. Lu, D. Zhou, P. Tian, Z.-H. Niu, J.-L. Zhang, X. Chen, and Q.-H. Xia, "Co2-exchanged SAPO-5 and SAPO-34 as efficient heterogeneous catalysts for aerobic epoxidation of alkenes," *Catalysis Communications*, vol. 31, pp. 42–47, Jan. 2013.

[128] Y. Xu, W. Yu, H. Zhang, J. Xin, X. He, B. Liu, F. Jiang, and X. Liu, "Suppressing c–c bond dissociation for efficient ethane dehydrogenation over the isolated co(II) sites in SAPO-34," *ACS Catalysis*, vol. 11, pp. 13001–13019, Oct. 2021.

[129] P. Tian, Z. Liu, Z. Wu, L. Xu, and Y. He, "Characterization of metal-containing molecular sieves and their catalytic properties in the selective oxidation of cyclohexane," *Catalysis Today*, vol. 93-95, pp. 735–742, Sept. 2004.

[130] M. Kang, "Effect of cobalt incorporated into the framework of SAPO-34 (CoAPSO-34s) on NO removal," *Journal of Molecular Catalysis A: Chemical*, vol. 161, pp. 115–123, Nov. 2000.

[131] S. Andonova, S. Tamm, C. Montreuil, C. Lambert, and L. Olsson, "The effect of iron loading and hydrothermal aging on one-pot synthesized fe/SAPO-34

for ammonia SCR," *Applied Catalysis B: Environmental*, vol. 180, pp. 775–787, Jan. 2016.

[132] M. J. da Silva, "Synthesis of methanol from methane: Challenges and advances on the multi-step (syngas) and one-step routes (DMTM)," *Fuel Processing Technology*, vol. 145, pp. 42–61, May 2016.

[133] A. M. I. Bull, G.S. Koermer and S. Unverricht, "Catalysts, systems and methods utilizing non-zeolitic metal-containing molecular sieves having the cha crystal structure," 2009.

[134] K. Mathisen, M. Stockenhuber, and D. G. Nicholson, "In situ xas and ir studies on cu:sapo-5 and cu:sapo-11: the contributory role of monomeric linear copper(i) species in the selective catalytic reduction of nox by propene," *Phys. Chem. Chem. Phys.*, vol. 11, pp. 5476–5488, 2009.

[135] C. A. Schneider, W. S. Rasband, and K. W. Eliceiri, "NIH image to ImageJ: 25 years of image analysis," *Nature Methods*, vol. 9, pp. 671–675, June 2012.

[136] W. S. P.P. Knops-Gerrits, "Methane partial oxidation in new iron zeolite topologies," *in A. Corma, F.V. Melo, S. Mendioroz, J.L.G. Fierro*, 2000. Stud. Surf. Sci. Catal., Elsevier.

[137] K. Schlichte, T. Kratzke, and S. Kaskel, "Improved synthesis, thermal stability and catalytic properties of the metal-organic framework compound cu3(BTC)2," *Microporous and Mesoporous Materials*, vol. 73, pp. 81–88, Aug. 2004.

[138] R. A. Rakoczy and Y. Traa, "Nanocrystalline zeolite a: synthesis, ion exchange and dealumination," *Microporous and Mesoporous Materials*, vol. 60, pp. 69–78, June 2003.

[139] C. Wang, J. Wang, J. Wang, and M. Shen, "Promotional effect of ion-exchanged k on the low-temperature hydrothermal stability of cu/SAPO-34 and its synergic application with fe/beta catalysts," *Frontiers of Environmental Science &amp Engineering*, vol. 15, Sept. 2020.

[140] T. Doan, P. Dam, K. Nguyen, T. H. Vuong, M. T. Le, and T. H. Pham, "Copper-iron bimetal ion-exchanged sapo-34 for nh3-scr of nox," *Catalysts*, vol. 10, no. 3, p. 321, 2020.

[141] L. Huang, X. Wang, S. Yao, B. Jiang, X. Chen, and X. Wang, "Cu–mn bimetal ion-exchanged sapo-34 as an active scr catalyst for removal of nox from diesel engine exhausts," *Catalysis Communications*, vol. 81, pp. 54–57, 2016.

[142] F. Gao, E. D. Walter, N. M. Washton, J. Szanyi, and C. H. Peden, "Synthesis and evaluation of cu/SAPO-34 catalysts for NH3-SCR 2: Solid-state ion exchange and one-pot synthesis," *Applied Catalysis B: Environmental*, vol. 162, pp. 501–514, Jan. 2015.

[143] H. I. Hamoud, V. Valtchev, and M. Daturi, "Selective catalytic reduction

of NOx over cu- and fe-exchanged zeolites and their mechanical mixture," *Applied Catalysis B: Environmental*, vol. 250, pp. 419–428, Aug. 2019.

[144] ACS Materials, "SAPO-34." https://www.acsmaterial.com/sapo-34.html Accessed:10.09.22.

[145] M. Urrutxua, B. Pereda-Ayo, U. De-La-Torre, and J. R. Gonzalez-Velasco, "Evaluation of cu/sapo-34 catalysts prepared by solid-state and liquid ion-exchange methods for no x removal by nh3-scr," *ACS omega*, vol. 4, no. 12, pp. 14699–14713, 2019.

[146] J. Zhong, J. Han, Y. Wei, S. Xu, T. Sun, X. Guo, C. Song, and Z. Liu, "Enhancing ethylene selectivity in mto reaction by incorporating metal species in the cavity of sapo-34 catalysts," *Chinese Journal of Catalysis*, vol. 39, no. 11, pp. 1821–1831, 2018.

[147] Y. Zhang, Z. Ren, Y. Wang, Y. Deng, and J. Li, "Synthesis of small-sized SAPO-34 crystals with varying template combinations for the conversion of methanol to olefins," *Catalysts*, vol. 8, p. 570, Nov. 2018.

[148] X. Hu, M. Yang, D. Fan, G. Qi, J. Wang, J. Wang, T. Yu, W. Li, and M. Shen, "The role of pore diffusion in determining NH3 SCR active sites over cu/SAPO-34 catalysts," *Journal of Catalysis*, vol. 341, pp. 55–61, Sept. 2016.

[149] H. Yang, X. Liu, G. Lu, and Y. Wang, "Synthesis of SAPO-34 nanoplates via hydrothermal method," *Microporous and Mesoporous Materials*, vol. 225, pp. 144–153, May 2016.

[150] L. WU, Z. LIU, L. XIA, M. QIU, X. LIU, H. ZHU, and Y. SUN, "Effect of SAPO-34 molecular sieve morphology on methanol to olefins performance," *Chinese Journal of Catalysis*, vol. 34, pp. 1348–1356, July 2013.

[151] X. Xiang, Y. Cao, L. Sun, P. Wu, L. Cao, S. Xu, P. Tian, and Z. Liu, "Improving the low-temperature hydrothermal stability of cu-sapo-34 by the addition of ag for ammonia selective catalytic reduction of nox," *Applied Catalysis A: General*, vol. 551, pp. 79–87, 2018.

[152] J. Pérez-Ramírez, C. H. Christensen, K. Egeblad, C. H. Christensen, and J. C. Groen, "Hierarchical zeolites: enhanced utilisation of microporous crystals in catalysis by advances in materials design," *Chemical Society Reviews*, vol. 37, no. 11, p. 2530, 2008.

[153] M. Xu, J. Wang, T. Yu, J. Wang, and M. Shen, "New insight into cu/SAPO-34 preparation procedure: Impact of NH4-SAPO-34 on the structure and cu distribution in cu-SAPO-34 NH3-SCR catalysts," *Applied Catalysis B: Environmental*, vol. 220, pp. 161–170, Jan. 2018.

[154] T. Jiang and R. F. Lobo, "On the mechanism of ammonia scr over cu-and fe-containing zeolite catalysts," *Structure and Reactivity of Metals in Zeolite Materials*, pp. 155–178, 2018.

A Appendix

A.1 Additional data

A.1.1 Synthesis of the parent material conventional SAPO-34

The conventional SAPO-34 samples, used as parent material for ion exchange, were provided by Post.Doc. Daniel Ali in the inorganic research group at the Institute for Chemistry at NTNU, and were synthesised by Dr. Joakim Tafjord. For the synthesis of SAPO-34, a modified pocedure of a BASF patent[133] with tetraethylammonium hydroxide (TEAOH) as the structure directing agent (SDA) was used. First orthophosphoric acid (H_3PO_4, 85%, 8.7 g) was added to 41.9 g deionized water. Then aluminum isopropoxide (Al[OCH(CH3)2]3, 98%, 15.3 g) was slowly added, followed by continuous stirring. After the solution became homogeneous, AS-40 Ludox (SiO_2, 40% colloidal suspension in H_2O) was added, followed by the dropwise addition of the organic SDA, TEAOH (35%). After SDA addition, the suspension was stirred until homogeneous and then transferred to a stainless steel autoclave with a Teflon liner. By heating the autoclave to 190°C, hydrothermal synthesis was performed and crystallised for 72 hours. Subsequently the autoclave was placed in cold water to rapidly cool down the the product to room temperature. The solid product was then repeatedly washed and centrifuged with deionized water, before it was set to dry over night at 70°C. Last, the dried product was mortared and calcinated for 6 hours at 550°C to remove organic SDAs from the pores of the sample. All chemicals were provided by SigmaAldrich.

The parameters for the synthesis of conventional SAPO-34, used as parent material for ion-exchange in this masters project, is listed in the experimental section in Table 3.1.

A.1.2 Additional BET/BJH: Particle size distribution (PSD) and phase pure iron

Figure A.1 shows the particle size distribution (PSD) of all SAPO-34 samples.

Surface area measurments from nitrogen physisoprtion of the one phase pure Fe/S34-sample is presented in Table A.1.

Table A.1: Data from N_2 physisoprtion analysis of iron sample

Sample name	Surface area (m^2/g)			Pore volume (cm^3/g)		
	BET	Micro	External	Total	Micro	Meso
SAPO-34	510	486	25	0.28	0.25	0.03
0.1Fe/S34	64	8	56	0.09	0.004	0.08
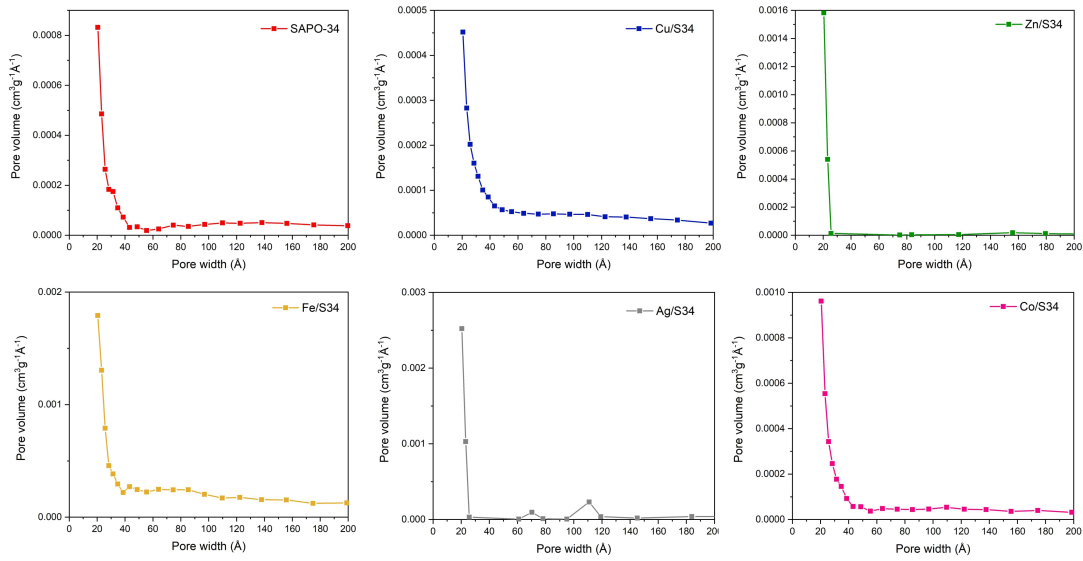
Figure A.1: Particle size distribution for SAPO-34 and Me/S34 (Me = Zn, Cu, Ag, Fe, Co) obtained from BJH analysis from nitrogen physisoprtion.

Figure A.2: Detailed data from ICP-MS.

A.1.3   Additional ICP-MS data

The detailed element data utilised to find metal content and Si/Al-ratio in all analysed samples are presented in Figure A.2 and Table A.2.

Table A.2: Elemental results in the form of wt.% of each element for all samples investigated with ICP-MS.

Sample name	Si	Al	P	Me
C-SAPO-34	4.080	16.999	15.728	-
Cu/SAPO-34	6.040	23.428	21.758	0.976
Zn/SAPO-34	3.822	14.849	12.960	0.405
Ag/SAPO-34	3.604	14.145	12.624	5.125
Co/SAPO-34	4.060	15.117	13.213	0.096

Further, graphical illustrations of the metal loadings and the Si/Al-ratios are presented in Figure A.3 and Figure A.4, respectively.
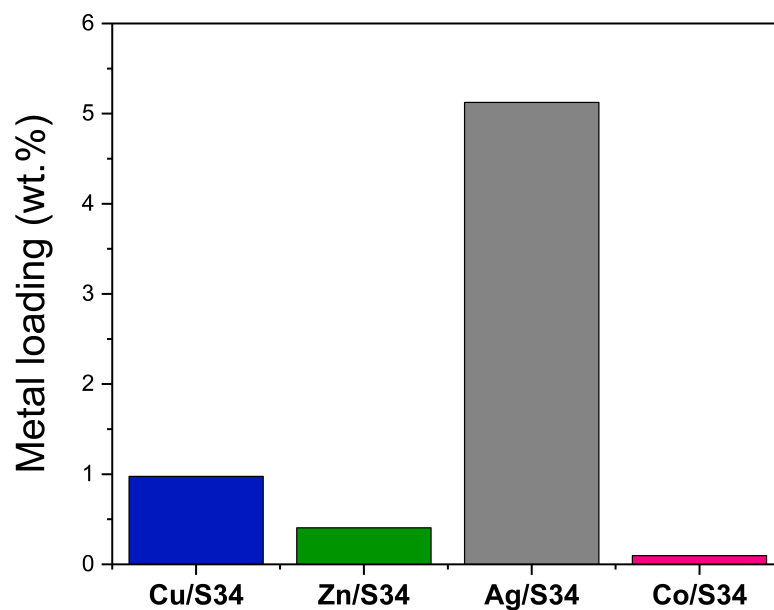
Figure A.3: The metal loadings obtained from elemental analysis in the form of wt.% metal for the different metal ion exchanged samples of SAPO-34.
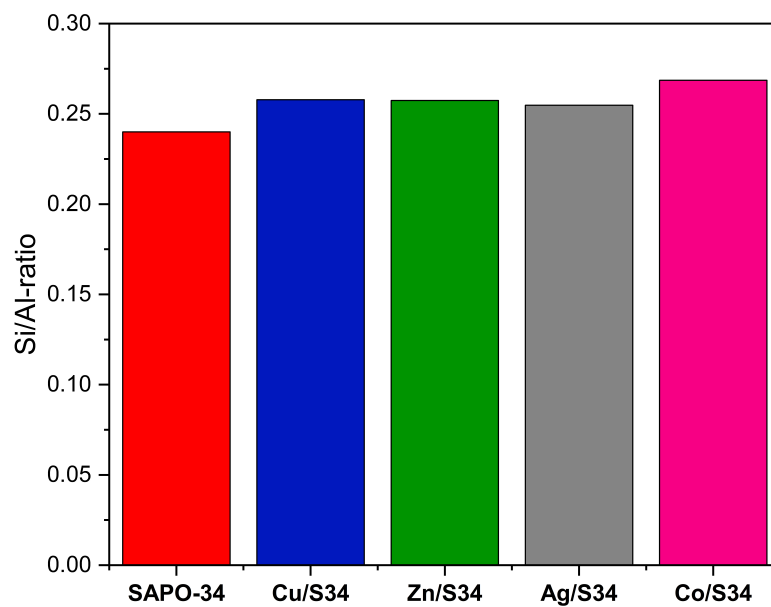
Figure A.4: The Si/Al-ratio of the Me/SAPO-34 samples with Cu, Co, Ag and Zn.

A.1.4   Additional SEM

In Figure A.5, SEM images with magnification 1.9k are shown.
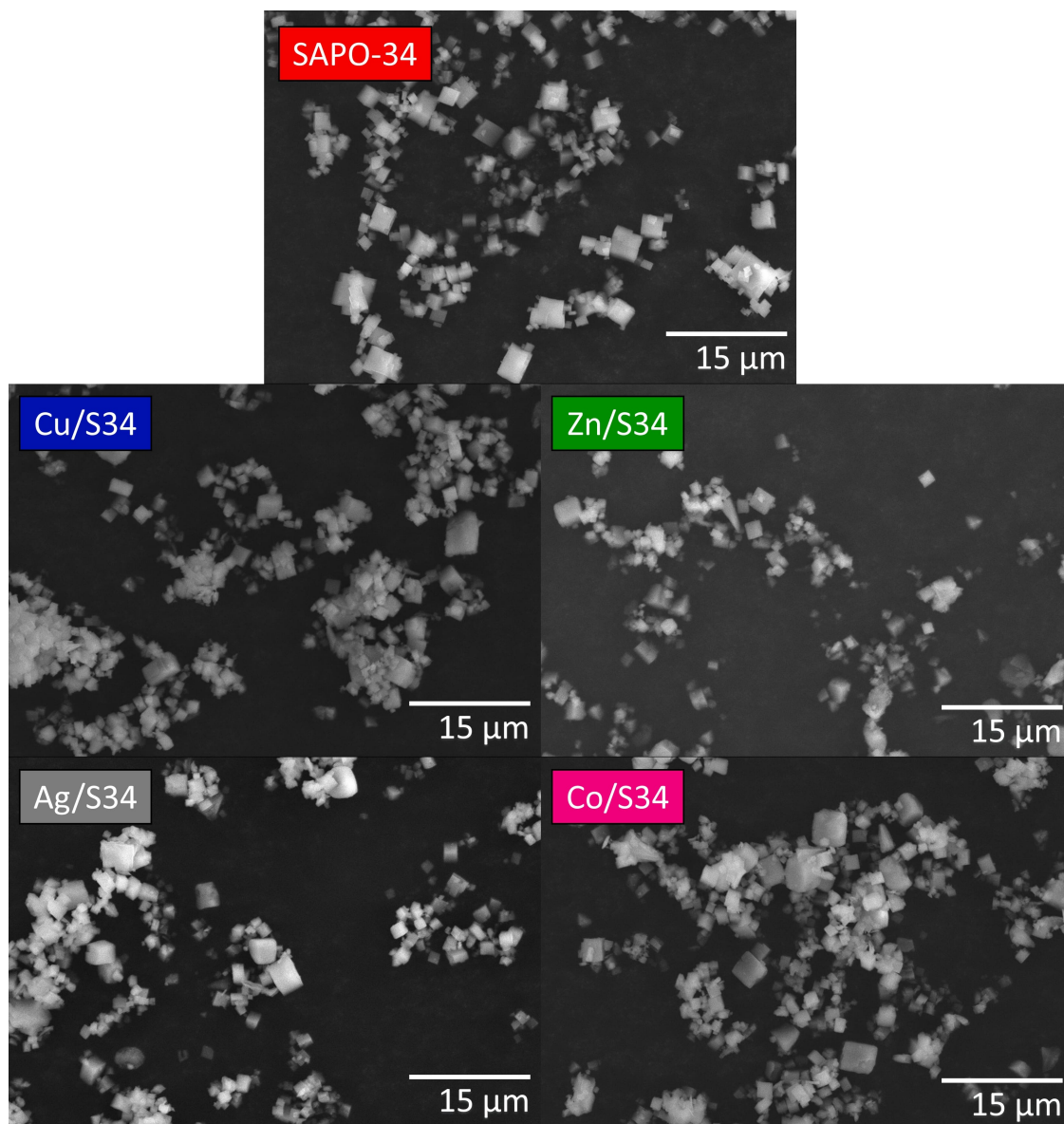
Figure A.5: SEM images of SAPO-34 and the metal ion exchanged samples, taken in SE mode with magnification 1.9k.

A.1.5   Pictures of samples

In **??** photographies of all samples are shown.
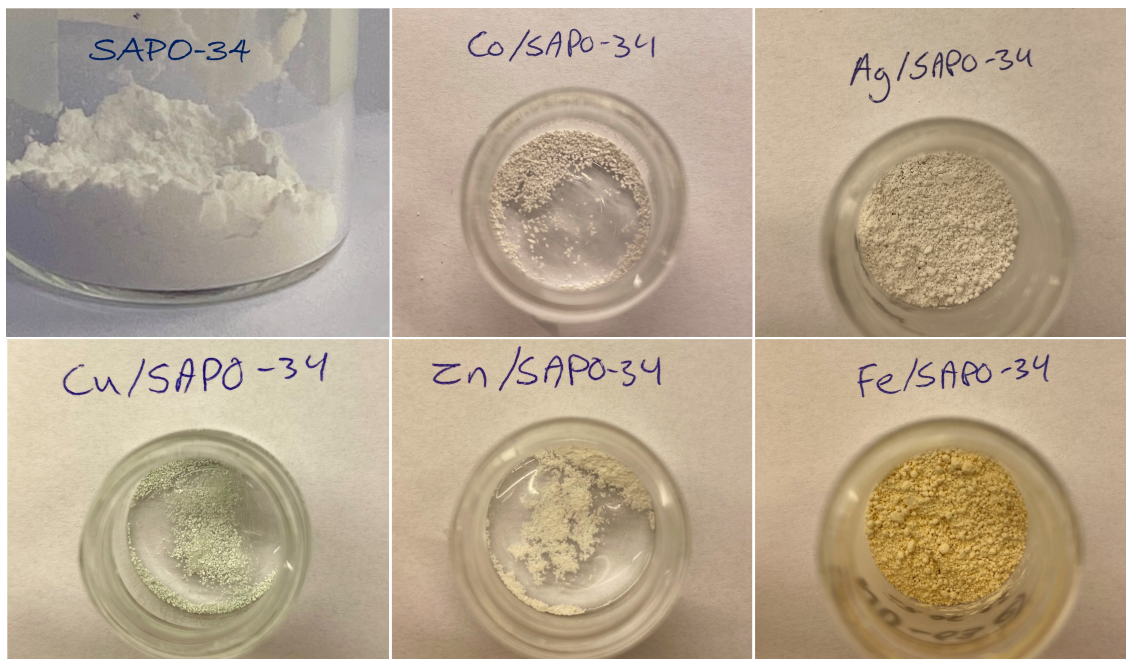
Figure A.6: Pictures of all samples.

A.1.6   Additional data from methane activation

The reaction conditions for the stepwise partial oxidation of methane to methanol is presented in Table A.3.

Table A.3: Reaction conditions for methane activation.

Activation gas, temp.	Reaction temp.	Flow rate	Sample mass	Particle size
O_2, 500°C	300°C	20 mL/min	50-100 mg	212-425 Mic.

Figure A.7 shows the integrated area from X=0.15 to X=1.25 of the normalised MeOH-signals for all catalytically tested samples, and Figure A.8 shows the methanol signals of the Me/S34-samples when subtracted the MeOH signal achieved of the plain SAPO-34.
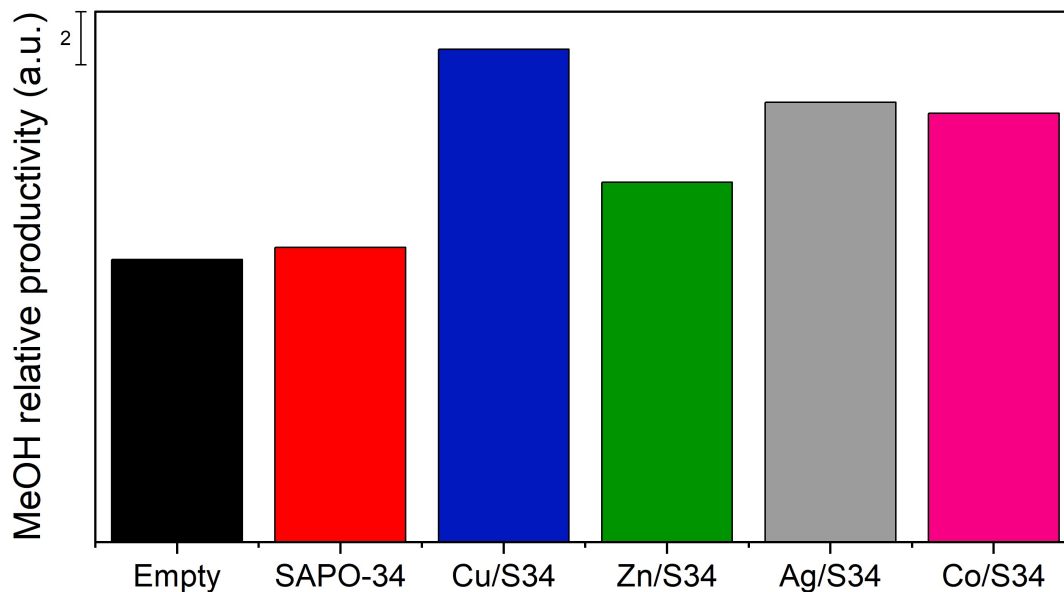
Figure A.7: The integrated area from X=0.15 to X=1.25 of the normalised MeOH-signals for the mother sample, the ion-exchanged samples and for the empty reactor run.
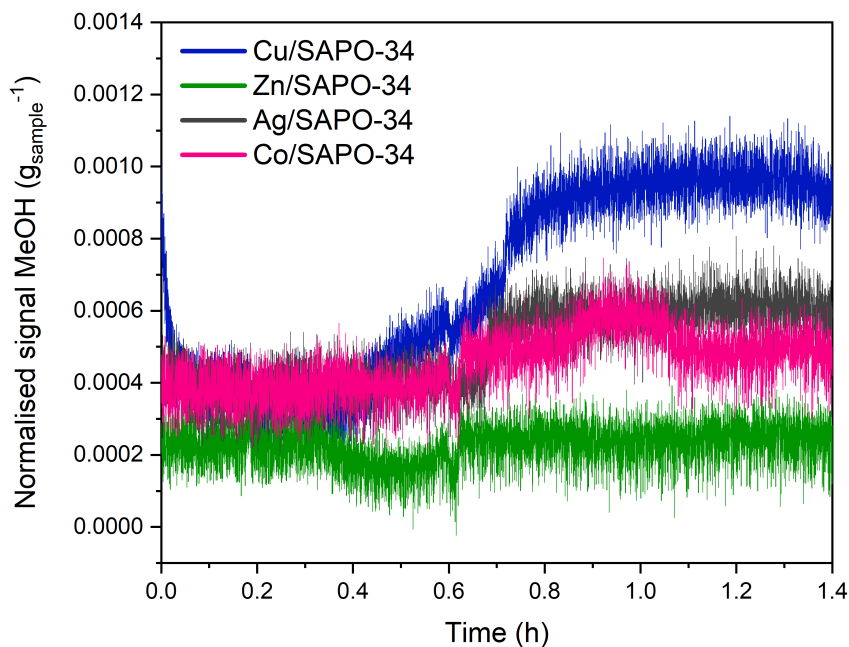
Figure A.8: Normalised MeOH-signal for the metal ion exchanged samples, the mother sample SAPO-34 and an empty reactor run. The signal is normalised with regard to the reference gas of argon, and is found by dividing the MeOH-signal with the Ar-signal. Last, the signal from the conventional sample is subtracted from the Me/SAPO-34 sample signals. In addition, the x-values (time) are offset.

Catalysis log

A log of the catalytic tests done for this project is presented in Table A.4.

Table A.4: Log of catalytic tests in this master project.

Sample	Number of experiments	Mass of samples [mg]
Empty reactor	3	-
SAPO-34	3	51.2, 100, 52.0
Cu/S34	3	74.3, 51.0, 51.2
Zn/S34	3	75.0, 100.2, 53.4
Co/S34	2	78.0, 50.4
Ag/S34	2	52.0, 50.1

A.2   Calculations

A.2.1   Ion exchange: Calculations of ion exchange solutions

Calculations of mass metal nitrate salt that were weighed out for making the respective ion exchange solutions with a concentration of 0.133 M are presented in Table A.5. The iron nitrate solutions with lower concentrations were made by diluting the original solution.

Table A.5: Salt solutions of destilled water and

Metal ion	Salt	Molar mass$_{salt}$ [g/mol]	Concentration(s) [M]
Cu^{2+}	$Cu(NO_3)_2 \times 3H_2O$	241.60	0.133
Zn^{2+}	$Zn(NO_3)_2 \times 6H_2O$	297.49	0.133
Co^{2+}	$Co(NO_3)_2 \times 6H_2O$	291.04	0.133
Fe^{2+}	$Fe(NO_3)_2 \times 9H_2O$	404.00	0.133, 0.06, 0.03, 0.01
Ag^+	$Ag(NO_3)$	169.87	0.133

A.2.2   XRD: Calculations of relative crystallinity

Calculation of relative crystallinity based on the sum of the reflections at $2\theta \approx 9.5$, 12.9 and 20.6 for the ion exchanged samples compared to that of the mother sample of SAPO-34 is shown in Figure A.9.

	A(X)	B(Y)	C(Y)	D(Y)	E(Y)	F(Y)
Long Name	XRD of	2Θ=9.5	2Θ=12.9	2Θ=20.6	Sum	Relative ins
Units						
Comments						
F(x)=					B+C+D	E/E28*100
28 SAPO-34		1988	590	539	3117	100
29 Cu/S34		692	292.5	328.75	1313.25	42.13186
30 Zn/S34		987	305	286	1578	50.6256
31 Ag/S34		784	254	227	1265	40.58389
32 Co/S34		938	344	285	1567	50.2727
33 Fe/S34		585	229	201	1015	32.56336
34 Fe/S34		143	136	108	387	12.41578

Figure A.9: Calculation of the relative crystallinity of the ion exchanged samples, relative of the mother sample, based on the sum of the important reflections at $2\theta \approx 9.5$, 12.9 and 20.6

A.2.3   SEM: Particle size calculations with ImageJ software

Particle size and particle size distribution was calculated for all samples using the ImageJ program for analysis of SEM images. The SEM images used are to be found in Figure A.5, and an example of the particle size distribution of the conventional SAPO-34 sample is presented in Figure A.10 as the other samples showed similar distributions.
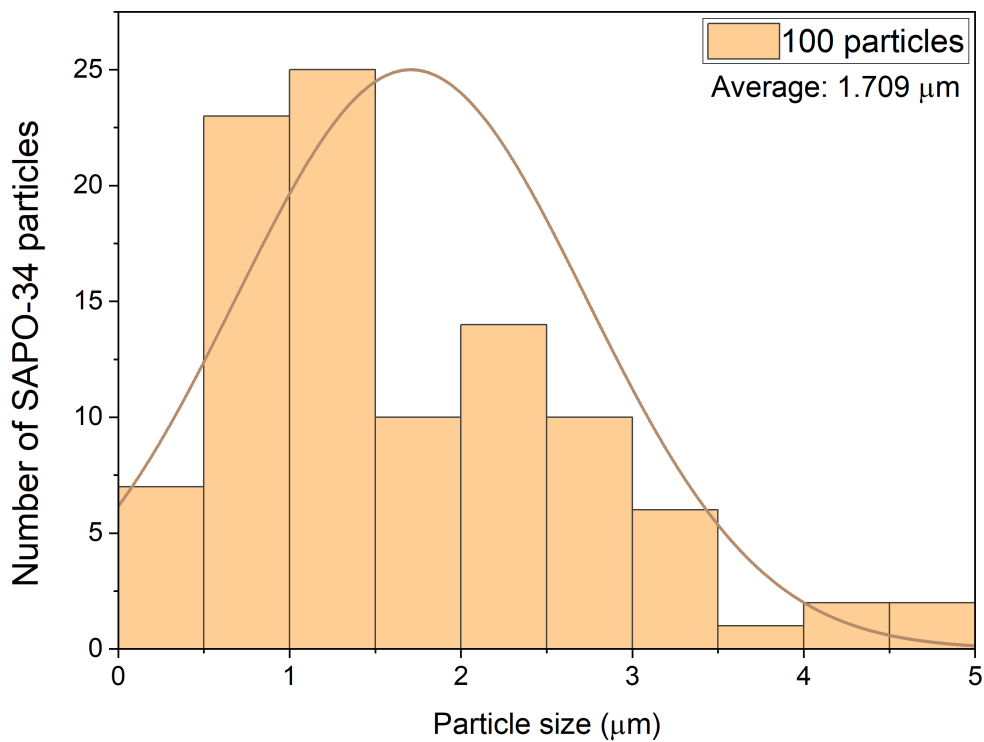
Figure A.10: Particle size distribution of SEM image (1.90k) of the conventional SAPO-34 sample.

A.3   Detailed risk evaluation for master project

Detaljert Risikorapport

			Status	Dato
ID	46659		Opprettet	17.02.2022
Risikoområde	Risikovurdering: Helse, miljø og sikkerhet (HMS)		Vurdering startet	17.02.2022
Opprettet av	Daniel Ali		Tiltak besluttet	
Ansvarlig	Karina Mathisen		Avsluttet	

Risikovurdering:

Master's project at E2-117: Ninni Maria Unneberg

Gyldig i perioden:

1/1/2022 - 12/31/2022

Sted:

3 - Gløshaugen / 360 - Realfagbygget / 1020 - Del E 2. etasje / E2-117

Mål / hensikt

The purpose of this risk assessment is to identify and evaluate the risks associated with a master's project at E2-117. Also, routines and measures are to be established to reduce the risk environment in compliance with the HSE-regulations.

The supervisor and the student must know the risk environment for the master's thesis and know about the existing measures and possible new measures that needs to be put into effect to reduce the risks for the master's thesis.

Bakgrunn

All activity at the department for chemistry needs to be identified and risk evaluated before the activity can be started.

Project description is attached this risk assessment.

Beskrivelse og avgrensninger

The risk assessment is performed in such a way that it focuses on the consequenses associated health and material assets. Consequences associated to environment and reputation will be assessed only in certain cases.

Each chemical will not be assessed here, but the safe work analysis (SWA) will elaborate the different risk associated to chemicals and gases in detail. These can also be found in EcoOnline.

Forutsetninger, antakelser og forenklinger

The student is responsible for knowing all necessary HSE-information that is relevant for the execution of the thesis i.e material safety data sheets, procedures from literature, user manuals for equipment etc. The risk assessment of the infrastructure must be known. The risk assessment of the laboratory is attached.

Vedlegg

Master project MeSAPO-34 - Ninni.docx

Referanser

Risk assessment of E2-117 (laboratory)(https://avvik.ntnu.no/Risk/EditRiskAssessment?id=12346&showActions=false&readOnlyMode=True)

Norges teknisk-naturvitenskapelige universitet (NTNU)	**Utskriftsdato:**	**Utskrift foretatt av:**	**Side:**
Unntatt offentlighet jf. Offentlighetsloven § 14	05.12.2022	Daniel Ali	1/17

X

Oppsummering, resultat og endelig vurdering

I oppsummeringen presenteres en oversikt over farer og uønskede hendelser, samt resultat for det enkelte konsekvensområdet.

Farekilde: **Inorganic synthesis**

Uønsket hendelse: **Work with chemicals**

Konsekvensområde: Helse   Risiko før tiltak: ⬤ Risiko etter tiltak: ⬤

Uønsket hendelse: **Work with carcinogenic and mutagenic chemicals.**

Konsekvensområde: Helse   Risiko før tiltak: ⬤ Risiko etter tiltak: ⬤

Uønsket hendelse: **Disposal of chemical waste.**

Konsekvensområde: Helse   Risiko før tiltak: ⬤ Risiko etter tiltak: ⬤

Uønsket hendelse: **Lack of preparation or attention of experiments.**

Konsekvensområde: Helse   Risiko før tiltak: ⬤ Risiko etter tiltak: ⬤
Materielle verdier   Risiko før tiltak: ⬤ Risiko etter tiltak: ⬤

Uønsket hendelse: **Overpressure in autoclave**

Konsekvensområde: Helse   Risiko før tiltak: ⬤ Risiko etter tiltak: ⬤
Materielle verdier   Risiko før tiltak: ⬤ Risiko etter tiltak: ⬤

Farekilde: **Working alone with masters thesis**

Uønsket hendelse: **Lack of assistance if an accident occurs.**

Konsekvensområde: Helse   Risiko før tiltak: ⬤ Risiko etter tiltak: ⬤

Farekilde: **Gas leakage during catalytic analysis**

Uønsket hendelse: **Gas leakage**

Konsekvensområde: Helse   Risiko før tiltak: ⬤ Risiko etter tiltak: ⬤

Norges teknisk-naturvitenskapelige universitet (NTNU)	**Utskriftsdato:**	**Utskrift foretatt av:**	**Side:**
Unntatt offentlighet jf. Offentlighetsloven § 14	05.12.2022	Daniel Ali	2/17

xi

Endelig vurdering

Involverte enheter og personer

En risikovurdering kan gjelde for en, eller flere enheter i organisasjonen. Denne oversikten presenterer involverte enheter og personell for gjeldende risikovurdering.

Enhet /-er risikovurderingen omfatter

- Institutt for kjemi

Deltakere

Daniel Ali

Muhammad Mohsin Azim

Ninni Maria Unneberg

Lesere

[Ingen registreringer]

Andre involverte/interessenter

[Ingen registreringer]

Følgende akseptkriterier er besluttet for risikoområdet Risikovurdering: Helse, miljø og sikkerhet (HMS):

Helse	**Materielle verdier**	**Omdømme**	**Ytre miljø**

Oversikt over eksisterende, relevante tiltak som er hensyntatt i risikovurderingen

I tabellen under presenteres eksisterende tiltak som er hensyntatt ved vurdering av sannsynlighet og konsekvens for aktuelle uønskede hendelser.

Farekilde	Uønsket hendelse	Tiltak hensyntatt ved vurdering
Inorganic synthesis	Work with chemicals	Disposal of chemical waste
	Work with chemicals	Mandatory use of personal protective equipment
	Work with chemicals	Concentrated and/or dangerous acids
	Work with chemicals	Experiments in fume cupboard
	Work with chemicals	Risk assessment of laboratory: E2-117
	Work with chemicals	Emergency equipment in the laboratories
	Work with chemicals	Guidelines for working alone.
	Work with chemicals	Material safety data sheet and substance register
	Work with chemicals	Risk assessment of chemicals.
	Work with chemicals	Disposal of chemical waste
	Work with chemicals	Storing of chemicals in the laboratory.
	Work with chemicals	Information sheets of produced substances.
	Work with chemicals	NTNU Laboratory and workshop handbook.
	Work with chemicals	Admittance controlled laboratory.
	Work with chemicals	Routines for cleaning day/week
	Work with chemicals	Safe work analysis - SWA
	Work with carcinogenic and mutagenic chemicals.	Experiments in fume cupboard
	Work with carcinogenic and mutagenic chemicals.	Risk assessment of laboratory: E2-117
	Work with carcinogenic and mutagenic chemicals.	Emergency equipment in the laboratories
	Work with carcinogenic and mutagenic chemicals.	Guidelines for working alone.
	Work with carcinogenic and mutagenic chemicals.	Material safety data sheet and substance register
	Work with carcinogenic and mutagenic chemicals.	Risk assessment of chemicals.
	Work with carcinogenic and mutagenic chemicals.	Disposal of chemical waste
	Work with carcinogenic and mutagenic chemicals.	Storing of chemicals in the laboratory.
	Work with carcinogenic and mutagenic chemicals.	Information sheets of produced substances.
	Work with carcinogenic and mutagenic chemicals.	Admittance controlled laboratory.
	Work with carcinogenic and mutagenic chemicals.	Safe work analysis - SWA
	Disposal of chemical waste.	Disposal of chemical waste

Norges teknisk-naturvitenskapelige universitet (NTNU)

Unntatt offentlighet jf. Offentlighetsloven § 14   **Utskriftsdato:** 05.12.2022   **Utskrift foretatt av:** Daniel Ali   **Side:** 5/17

Inorganic synthesis	Disposal of chemical waste.	Risk assessment of laboratory: E2-117
	Disposal of chemical waste.	Emergency equipment in the laboratories
	Disposal of chemical waste.	Material safety data sheet and substance register
	Disposal of chemical waste.	Risk assessment of chemicals.
	Disposal of chemical waste.	Disposal of chemical waste
	Disposal of chemical waste.	Admittance controlled laboratory.
	Disposal of chemical waste.	Routines for cleaning day/week
	Disposal of chemical waste.	Safe work analysis - SWA
	Lack of preparation or attention of experiments.	Disposal of chemical waste
	Lack of preparation or attention of experiments.	Mandatory use of personal protective equipment
	Lack of preparation or attention of experiments.	Concentrated and/or dangerous acids
	Lack of preparation or attention of experiments.	Experiments in fume cupboard
	Lack of preparation or attention of experiments.	Risk assessment of laboratory: E2-117
	Lack of preparation or attention of experiments.	Emergency equipment in the laboratories
	Lack of preparation or attention of experiments.	Guidelines for working alone.
	Lack of preparation or attention of experiments.	Material safety data sheet and substance register
	Lack of preparation or attention of experiments.	Risk assessment of chemicals.
	Lack of preparation or attention of experiments.	Disposal of chemical waste
	Lack of preparation or attention of experiments.	Storing of chemicals in the laboratory.
	Lack of preparation or attention of experiments.	Information sheets of produced substances.
	Lack of preparation or attention of experiments.	NTNU Laboratory and workshop handbook.
	Lack of preparation or attention of experiments.	Admittance controlled laboratory.
	Lack of preparation or attention of experiments.	Safe work analysis - SWA
	Lack of preparation or attention of experiments.	Gasdetectors/sniffer
	Lack of preparation or attention of experiments.	Safety valve on autoclaves
	Lack of preparation or attention of experiments.	Gas tanks
	Lack of preparation or attention of experiments.	Instruments - standard operating procedures/ Apparatus card
	Overpressure in autoclave	Risk assessment of laboratory: E2-117
	Overpressure in autoclave	Guidelines for working alone.
	Overpressure in autoclave	Safe work analysis - SWA
	Overpressure in autoclave	Safety valve on autoclaves

Norges teknisk-naturvitenskapelige universitet (NTNU)	**Utskriftsdato:**	**Utskrift foretatt av:**	**Side:**
Unntatt offentlighet jf. Offentlighetsloven § 14	05.12.2022	Daniel Ali	6/17

XV

Working alone with masters thesis	Lack of assistance if an accident occurs.	Disposal of chemical waste
	Lack of assistance if an accident occurs.	Mandatory use of personal protective equipment
	Lack of assistance if an accident occurs.	Concentrated and/or dangerous acids
	Lack of assistance if an accident occurs.	Experiments in fume cupboard
	Lack of assistance if an accident occurs.	Risk assessment of laboratory: E2-117
	Lack of assistance if an accident occurs.	Emergency equipment in the laboratories
	Lack of assistance if an accident occurs.	Guidelines for working alone.
	Lack of assistance if an accident occurs.	Material safety data sheet and substance register
	Lack of assistance if an accident occurs.	Risk assessment of chemicals.
	Lack of assistance if an accident occurs.	Disposal of chemical waste
	Lack of assistance if an accident occurs.	Storing of chemicals in the laboratory.
	Lack of assistance if an accident occurs.	Information sheets of produced substances.
	Lack of assistance if an accident occurs.	Admittance controlled laboratory.
	Lack of assistance if an accident occurs.	Safe work analysis - SWA
	Lack of assistance if an accident occurs.	Gasdetectors/sniffer
	Lack of assistance if an accident occurs.	Instruments - standard operating procedures/ Apparatus card
Gas leakage during catalytic analysis	Gas leakage	Mandatory use of personal protective equipment
	Gas leakage	Risk assessment of laboratory: E2-117
	Gas leakage	Guidelines for working alone.
	Gas leakage	Material safety data sheet and substance register
	Gas leakage	Risk assessment of chemicals.
	Gas leakage	Safe work analysis - SWA
	Gas leakage	Gas tanks

Eksisterende og relevante tiltak med beskrivelse:

Disposal of chemical waste

The chemicals waste is collected and stored in containers. The chemicals are sorted between chemical waste, halogenated organic chemical waste, non-halogenated chemical waste, inorganic chemical waste and powder. All chemical waste is considered as hazardous waste.

Mandatory use of personal protective equipment

It is mandatory to use personal protective equipment like eye goggles (when there is activity in the fume cupboards), lab coat (when there is activity in the fume cupboards) and shoes approved for laboratory use.

Concentrated and/or dangerous acids

A second person must be present when handling aqua regia, piranha solution or hydrofluoric acid.

For handling of hydrofluoric acid, an introductory course is mandatory for both user and supervisor.

Experiments in fume cupboard

Experiments concerning synthesis of inorganic materials/ wet chemistry must be performed in the fume cupboard.

Risk assessment of laboratory: E2-117

Risk assessment of laboratory E2-117 conducted of Karina Mathisen and Nina Brochs Klausen September 2016.

Emergency equipment in the laboratories

The laboratories are equipped with:
- Fire blanket.
- Fire extinguisher (CO2 and foam).
- Medicin cabinet.
- Emergency shower.
- Eyewasher on the sink.
- Eyewasher bottles (pH-neutral and isotonic saline)
- Absorption cloths for chemical spill.

Respiratory protective equipment is in the kitchen next to the laboratory.

Guidelines for working alone.

The faculty of natural sciences and technology has guidelines concerning working alone.

Activity that is accossiated with risks shall not be conducted alone. The activities must be classified to whether they are allowed to performed alone or not.

Material safety data sheet and substance register

The laboratories has a paper version (norwegian and english) of all the material safety data sheets used in the laboratory.

NTNU has EcoOnline as the digital substance register. All chemicals stored in the laboratort is registered in EcoOnline on the specific location.

EcoOnline Exposure is used to register the use substances that are carcinogenic and harmful for the reproductive system. Also the use of lead and lead containing substances, biological factors, ionising radiation, dust and asbestous fiber and harmful substances associated with mining.

Risk assessment of chemicals.

All chemicals for laboratory use are risk assessed for health risks in EcoOnline.

Disposal of chemical waste

The chemicals waste is collected and stored in containers. The chemicals are sorted between chemical waste, halogenated organic chemical waste, non-halogenated chemical waste, inorganic chemical waste and powder. All chemical waste is considered as hazardous waste.

Storing of chemicals in the laboratory.

All chemicals are stored in lockable cupboards for chemicals with ventilation, or in EX-approved fridge/freezer. The laboratory is equipped with admittance control with a badge and pin number.

Information sheets of produced substances.

All products are classified by an information sheet. Products to be stored must have be marked by the name of the chemical, chemical formula, concentration, amount, hazard pictograms, date and owner.

NTNU Laboratory and workshop handbook.

The laboratory must be equipped with the latest edition of the laboratory and workshop handbook.

Admittance controlled laboratory.

The laboratory has admittance control by card and pin-number. The persons who has access to the laboratory is people connected to the research group, technical staff, safety delegates and head of department.

Routines for cleaning day/week

The department has local guidelines for the undertaking of a cleaning day once per term.

Safe work analysis - SWA

All activities will be risk evaluated with the safe work analysis during the project.

They will be attached.

Gasdetectors/sniffer

A gasdetector is present in the relevant areas to prevent leakage of gases.

The sniffer is used to check setups and gas lines for leakage.

Safety valve on autoclaves

All autoclaves are to be used with safety valves to prevent excessive pressure build-up.

Gas tanks

Msut not be larger than 10 L and are fastened to wall according to regulations. Only approved regulators are to be used. All connections must be leak tested after assembly.

Instruments - standard operating procedures/ Apparatus card

Some instruments have their own standard operating procedures and apparatus card. Standard operating procedures are valid for three years. Apparatus cards are valid for one year. Information must be accessible in the lab.

Thermoresistant gloves

Used when handling high temperature oven and autoclaves coming out of the furnaces.

Dust mask

Always use a dust mask when handling fine powder outside the fume cupboard

Gas mask

Use a gas mask when working outside the fume cupboards with chemicals that are volatile and hazardous

Annual maintenance of fume cupboards

NTNU has a service agreement with an external company regarding the maintenance and the control of the fume cupboards. NTNU also has an annual internal control of the fume cupboards.

Norges teknisk-naturvitenskapelige universitet (NTNU)	**Utskriftsdato:**	**Utskrift foretatt av:**	**Side:**
Unntatt offentlighet jf. Offentlighetsloven § 14	05.12.2022	Daniel Ali	9/17

xviii

Risikoanalyse med vurdering av sannsynlighet og konsekvens

I denne delen av rapporten presenteres detaljer dokumentasjon av de farer, uønskede hendelser og årsaker som er vurdert. Innledningsvis oppsummeres farer med tilhørende uønskede hendelser som er tatt med i vurderingen.

Følgende farer og uønskede hendelser er vurdert i denne risikovurderingen:

- **Inorganic synthesis**
    - Work with chemicals
    - Work with carcinogenic and mutagenic chemicals.
    - Disposal of chemical waste.
    - Lack of preparation or attention of experiments.
    - Overpressure in autoclave
- **Working alone with masters thesis**
    - Lack of assistance if an accident occurs.
- **Gas leakage during catalytic analysis**
    - Gas leakage

Detaljert oversikt over farekilder og uønskede hendelser:

Farekilde: Inorganic synthesis

Uønsket hendelse: Work with chemicals

- -

Chemicals might have properties that are: corroding, poisonous, explosive, flammable, sensitizing and irritating. Chemicals might also be carcinogenic and may damage the DNA. The latter will be assessed in another event.

Sannsynlighet for hendelsen (felles for alle konsekvensområder):   **Svært sannsynlig (5)**

    Kommentar:

    Inorganic synthesis activity involves the use of chemicals with different hazards and must be evaluated in the SWA. This applies to acids / bases, organic amine and inhalation of fine silica powder.

Konsekvensområde: Helse   *Risiko:*

    Vurdert konsekvens: **Liten (1)**

        Kommentar: Our experience and previously reported events show that the level of injury is at Level 1: "Lesser damage requiring small treatment. Reversible damage. Short recovery time".

Uønsket hendelse: Work with carcinogenic and mutagenic chemicals.

- -

During the master's thesis there may be a possibility for the student will work with chemicals that qualifies the student to register in the EcoOnline Exposure.

Sannsynlighet for hendelsen (felles for alle konsekvensområder):   **Lite sannsynlig (2)**

    Kommentar:

    Specification will be given in the SWA

Konsekvensområde: Helse   *Risiko:*

    Vurdert konsekvens: **Liten (1)**

        Kommentar: In case of accident, only first aid measures will be required. Past experience and reported events indicate little consequence (1). Long-term impact can not be considered.

Norges teknisk-naturvitenskapelige universitet (NTNU)	**Utskriftsdato:**	**Utskrift foretatt av:**		**Side:**
Unntatt offentlighet jf. Offentlighetsloven § 14	05.12.2022	Daniel Ali		11/17

XX

Uønsket hendelse: Disposal of chemical waste.

- -

Wrong chemical waste handling might result in exposure of chemicals.

Sannsynlighet for hendelsen (felles for alle konsekvensområder):   **Ganske sannsynlig (4)**

    Kommentar:

    Transfer of waste to collection bins can lead to spillage. Spills can also occur when transporting the collection bins.

Konsekvensområde: Helse   *Risiko:*

    Vurdert konsekvens: **Liten (1)**

        Kommentar: In case of accident, only first aid measures will be required.
Past experience and reported events indicate little consequence (1). Long-term impact can not be considered.

Uønsket hendelse: Lack of preparation or attention of experiments.

- -

Lack of preparation or attention for experiments, may result in unexpected reactions.

Sannsynlighet for hendelsen (felles for alle konsekvensområder):   **Sannsynlig (3)**

    Kommentar:

    The students are generally well prepared when launching new projects where SWA is part of the preparation.

Konsekvensområde: Helse   *Risiko:*

    Vurdert konsekvens: **Middels (2)**

        Kommentar: In case of an accident, medical assistance may be required, e.g. spills on the eye.

Konsekvensområde: Materielle verdier   *Risiko:*

    Vurdert konsekvens: **Liten (1)**

        Kommentar: The damage in the laboratory will be limited to a fume cupboard.

Norges teknisk-naturvitenskapelige universitet (NTNU)   **Utskriftsdato:**   **Utskrift foretatt av:**   **Side:**

Unntatt offentlighet jf. Offentlighetsloven § 14   05.12.2022   Daniel Ali   12/17

Uønsket hendelse: Overpressure in autoclave

If the autoclaves are too full, overpressure may occur. Autoclaves are therefore never to be filled more than 2/3.

Sannsynlighet for hendelsen (felles for alle konsekvensområder):   **Svært lite sannsynlig (1)**

> *Kommentar:*
> [Ingen registreringer]

Konsekvensområde: Helse   *Risiko:*

> *Vurdert konsekvens:* **Middels (2)**
>
> > *Kommentar:* [Ingen registreringer]

Konsekvensområde: Materielle verdier   *Risiko:*

> *Vurdert konsekvens:* **Stor (3)**
>
> > *Kommentar:* [Ingen registreringer]

Farekilde: Working alone with masters thesis

Uønsket hendelse: Lack of assistance if an accident occurs.

Will not get help or can not alert co-workers if accident occurs.

Sannsynlighet for hendelsen (felles for alle konsekvensområder):   **Svært lite sannsynlig (1)**

Kommentar:

All work alone is limited in accordance with the Faculty's rules on family work. Any risky work should not take place whilst alone. SWA specifies the riskfilled work

Konsekvensområde: Helse   *Risiko:*

Vurdert konsekvens: **Stor (3)**

Kommentar: Accidents may require medical assistance

Norges teknisk-naturvitenskapelige universitet (NTNU)   **Utskriftsdato:**   **Utskrift foretatt av:**   **Side:**

Unntatt offentlighet jf. Offentlighetsloven § 14   05.12.2022   Daniel Ali   14/17

xxiv

Farekilde: Gas leakage during catalytic analysis

Catalytic analysis involves working with gases (FT-IR, GC-MS, NOx analyser)

Uønsket hendelse: Gas leakage

Working with gases may involve the following gases
- CO
- NO
- NO2
- Propen
- He

Sannsynlighet for hendelsen (felles for alle konsekvensområder):   **Lite sannsynlig (2)**

Kommentar:

All gas connections and lines must be checked before every experiment.

Konsekvensområde: Helse   *Risiko:*

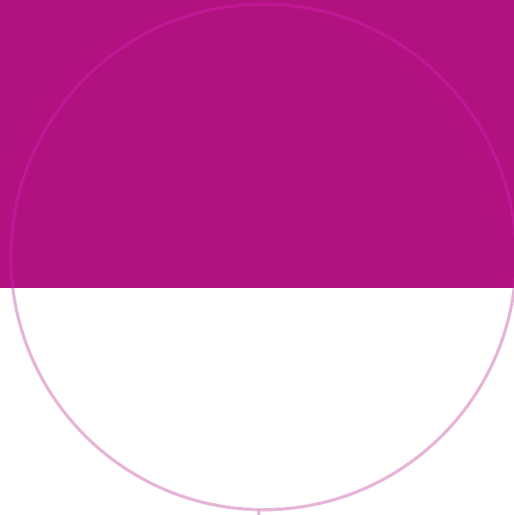*Vurdert konsekvens:* **Stor (3)**

Kommentar: [Ingen registreringer]

Oversikt over besluttede risikoreduserende tiltak:

Under presenteres en oversikt over risikoreduserende tiltak som skal bidra til å reduseres sannsynlighet og/eller konsekvens for uønskede hendelser.

Detaljert oversikt over besluttede risikoreduserende tiltak med beskrivelse:

Detaljert oversikt over vurdert risiko for hver farekilde/uønsket hendelse før og etter besluttede tiltak